ALTERATIONS IN TISSUE COMPOSITION AND NANOMECHANICAL PROPERTIES WITH AGEING, OSTEOPOROSIS, AND TREATMENT

A Dissertation

Presented to the Faculty of the Graduate School

of Cornell University

In Partial Fulfillment of the Requirements for the Degree of

Doctor of Philosophy

by

Jayme Carolynn Burket

January 2013

ALTERATIONS IN TISSUE COMPOSITION AND NANOMECHANICAL PROPERTIES WITH AGEING, OSTEOPOROSIS, AND TREATMENT

Jayme Carolynn Burket, Ph.D.

Cornell University 2013

Bone mineral density (BMD) is a macro-scale measurement used to diagnose osteoporosis and assess treatment efficacy, but it cannot capture nanoscale alterations within bone microstructures where fracture initiates. The objectives of this research were to determine variations in tissue properties within the microstructures of cortical and cancellous bone with aging, osteoporosis, and treatment, and examine their effects on microcrack resistance and mechanical function at higher length scales.

First, changes in tissue properties with the natural ageing process were examined in a baboon model for human ageing. Tissue stiffness and hardness followed trends in mineralization and aligned collagen content with animal age, increasing sharply during growth and remaining constant after sexual maturity.

Once this baseline for the natural ageing process was established, osteoporosis and antiresorptive treatment effects on bone tissue properties were examined in an ovine model for human osteoporosis. Zoledronate, from the most widely prescribed class of osteoporosis drugs (bisphosphonates), was compared with a treatment that acts through endogenous estrogen receptor pathways in bone, raloxifene (a selective estrogen receptor modulator, SERM). zoledronate was most effective in cancellous rather than cortical tissue and provided the greatest increases (relative to osteoporotic tissue) in stiffness, hardness, and mineralization at trabecular surfaces. In comparison, increases in these properties with raloxifene were similar throughout cancellous and cortical tissue. Both treatments improved the estimated bending stiffness of individual trabeculae, possibly providing some explanation for the large reductions in fracture risk with these drugs despite minimal changes in BMD. At higher length scales, zoledronate

improved bending stiffness and failure moment in whole bone tests.

Finally, microcracking resistance was assessed via a newly-developed experimental technique. The reduced resistance to crack elongation in cortical tissue from the osteoporosis model was largely corrected by raloxifene. These results suggest that bisphosphonate/SERM co-treatment treatment could possibly combine the best aspects of both drugs—the rapid improvement in strength with zoledronate and the improved microcrack resistance with raloxifene. The nanoscale alterations in bone tissue documented in this thesis provide a better understanding of normal and pathological bone function and may enable development of improved therapies for the prevention and treatment of osteoporosis.

BIOGRAPHICAL SKETCH

Jayme Carolynn Burket was born in San Antonio, Texas in 1983. She graduated from Sandra Day O'Connor High School in 2002 and attended the University of California at Berkeley. In May 2006 she completed her B.S. degree with Honors in Mechanical Engineering with a minor in Music. At U.C. Berkeley, Jayme sang with the University Chamber Chorus and earned a solo concert as part of the Berkeley Noon Concert Series. She was also a research assistant with the Lick Observatory Supernovae Search, where she discovered supernovae with the aid of a robotic telescope and eventually became the undergraduate team leader. In her senior year, Jayme served as treasurer for Pi Tau Sigma, the Mechanical Engineering honors society. During the summers before and after her senior year Jayme conducted research in biomechanics and corrosion inhibition at Southwest Research Institute and decided to apply to graduate school in biomedical mechanics. In 2006 she was accepted to the graduate program at Cornell University and a year later received the Graduate Research Fellowship from the National Science Foundation. She earned her M.S. degree in Mechanical Engineering in 2009 and her Ph.D. in the same field in 2012. While in graduate school, Jayme danced and taught ballet at the Ithaca Ballet Company and also became interested in triathlon, winning her age group in several local races and qualifying to compete in National Age Group Championships in 2011 and 2012. She also served as a TA and Head TA in 2010 and received the Ralph Bolgiano, Sr. Outstanding Teaching Assistant Award for her efforts. Throughout graduate school, Jayme led interactive outreach sessions at Cornell University and abroad at Weill Medical College, Clemson University, Tuskegee University, and Norfolk State University to interest underprivileged and underrepresented children in science and improve science education.

ACKNOWLEDGMENTS

The English poet Jon Donne wrote: "No man is an island," and this is certainly true of my graduate career. Many people supported me both professionally and otherwise during the past six years and without them my success would not be possible.

Most importantly I thank my committee chair, Dr. Marjolein van der Meulen for her incredible mentorship, patience, and exceptional technical guidance and inspiration. My committee members, Dr. Adele Boskey and Dr. Shefford Baker, also provided their expert knowledge and enthusiasm. Dr. Rebecca Williams and Dr. Elaine Farkas gave technical guidance on second harmonic generation microscopy methods, and Daniel Brooks performed the bulk and whole-bone mechanical testing of the ovine experiments. Dr. Yan Ma provided expert statistical advice for both the baboon and ovine studies. Dr. Stephen Doty and his lab at the Hospital for Special Surgery embedded and sectioned all of the samples for nanoindentation and Fourier transform infrared spectroscopy. Jennifer MacLeay and Lorena Havill conducted the animal handling components of the large animal studies. Ronnie Cooper and Lance Kuhn from Hysitron provided training and technical support for the nanoindentation instrument. John Grazul, John Hunt, Jon Shu, Philip Carubia, Shvaun Archer, Mila Spevak, and Kit Umbach all provided training and advice on instrument techniques. Marcia Sawyer and Judy Thoroughman not only gave key support for administrative tasks, but they were also great friends, sources of advice, and provided kind listening ears and a good laugh when needed.

This thesis work was funded by a National Science Foundation Graduate Research Fellowship and by NIH R01-AR041325, R01-AR053571 and P30-AR046121. NSF DMR - 0520404 supported the shared instrument facilities, and Hysitron, Inc. generously donated the nanoindentation instrument. An NIH NCRR base grant, P51-RR013987, supports the Southwest National Primate Research Center.

Many fellow students gave feedback on my research and provided support. Eve Donnelly, Maureen Lynch, Grace Kim, CJ Slyfield, Natalie Galley, Miki Kunitake, Frank Ko,

Garry Brock, and Joanna Hinks were key sounding boards and gave helpful technical and non-technical advice as well as friendship. All of the biomechanics faculty and students were extremely supportive and provided technical feedback on presentations and conference abstracts. Frank Havlak personally retrieved data and resuscitated my computer several times, most notably four days before my A exam.

The emotional support and much needed R&R provided by my friends and family outside of work were every bit as important as the technical support received. My mom, dad, sister, and Stas received excited or frustrated phone calls at all hours of the day and night and always lent a supportive ear. Stas especially has given me so much in terms of his patience, love, laughter, and especially his last 40-day countdown (texted to my phone every morning) leading up to my B-exam. My roommate and good friend Sarah Thebaud provided advice, camaraderie, and quite a few evenings of key stress relief (i.e. dancing around the living room to 80's music). My students and friends at the Ithaca Ballet Company and fellow members of the Ithaca Triathlon Club have been extremely supportive and helped me blow off steam one pirouette or swim/bike/run mile at a time. Finally, my adopted family: Kenton, Larissa, and Harrison (and the puppies, cats, and frogs), truly made the last two years of graduate school the most memorable, and I have gained close friends that I will cherish for life.

TABLE OF CONTENTS

LIST OF FIGURES

LIST OF TABLES

CHAPTER 1
INTRODUCTION

Ageing and age-related skeletal diseases such as osteoporosis lead to fragility fractures that compromise the skeleton's ability to provide structural support for the body. One in three women and one in five men over the age of fifty will experience an osteoporotic fracture in their lifetime [1–3]. Fragility fractures lead to increased morbidity and mortality, and the associated economic burden is over $17 billion dollars annually in the United States, alone [4].

1.1 Osteoporosis Diagnosis and Bone Mineral Density

Osteoporosis is diagnosed by measuring bone mineral density (BMD) with a dual-energy x-ray absorptiometry (DEXA) scan. Patients with BMD between 1 and 2.5 standard deviations below the mean for a young, healthy adult (T-score of -1 to -2.5) are diagnosed as osteopenic, or having low bone density. Patients with BMD more than 2.5 standard deviations below the young adult mean (T-score < -2.5) or who are osteopenic and have fragility fracture are diagnosed as osteoporotic. Patients with BMD more than 2.5 standard deviations below the young adult mean with a fragility fracture(s) present are deemed severely osteoporotic [5].

Bone is a hierarchical composite material with factors from the sub-nanoscale through the scale of the whole bone contributing to fracture risk (Figure 1). BMD measures the quantity of bone and the overall level of mineralization at the apparent (bulk tissue) level, but cannot resolve alterations in properties at smaller length scales. Failure in bone initiates at these smaller length scales and depends on tissue micro-architecture, nanoscale properties of mineral and matrix constituents, and spatial distributions of mineral and matrix properties within bone structures [6–17]. Discrepancies between BMD and fracture risk highlight the importance of considering property alterations below the apparent level: 1) BMD alone is relatively insensitive to first fracture risk. Clinically, large overlaps in BMD exist between groups of patients with and without fractures, and patients with identical BMD t-scores have different fracture outcomes

[8,18–20]. Fractured and non-fractured patients show differences in tissue composition and organization at the micro- and nanoscales [6,21–23]. 2) Antiresorptive treatments for osteoporosis provide large reductions in fracture risk (30-50%) despite only minor changes in BMD (0-8%) [11,24,25]. Tissue from treated patients shows micro and nanoscale alterations in mineral and matrix properties, heterogeneity, microdamage, and tissue architecture [26–34]. 3) Previous fluoride treatments for osteoporosis increased BMD but did not reduce fractures. Abnormal mineral formation and mineralization defects caused by fluoride treatment impair mechanical function [35–40].

Clearly, contributions from all hierarchical length scales in bone must be considered to fully understand mechanisms of bone fragility and successfully develop and evaluate new therapies. Most studies to date focus on apparent or whole bone length scales; therefore, micro

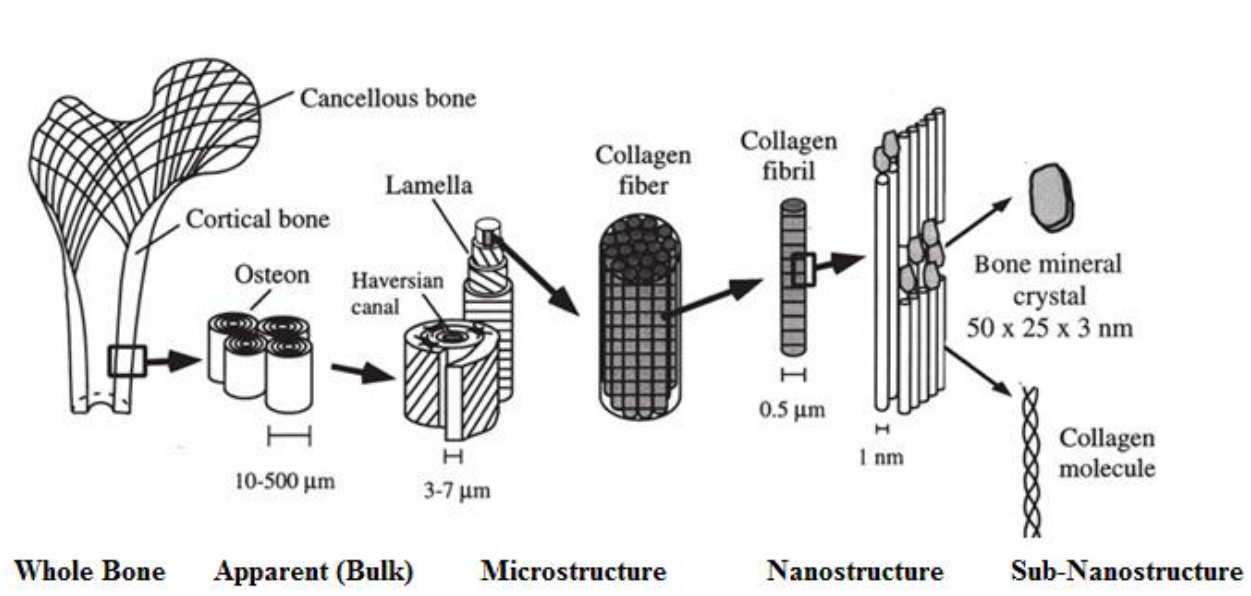

Figure 1.1 *Hierarchical structure of bone across multiple length scales. Figure adapted from* [45].

and nanoscale alterations in tissue composition and organization with ageing, disease, and treatment must be documented and related to alterations visible at these higher length scales.

1.2 Bone Composition and Microstructure

The organization within bone extends across multiple length scales (Figure 1). The tissue itself

is a mineral-platelet-reinforced composite comprised of 65% mineral, 35% organic matrix, cells, and water [41–43]. The mineral phase is an impure form of hydroxyapatite, $Ca_{10}(PO_4)_6(OH)_2$ with incorporated ions such as carbonate, citrate, magnesium, fluoride, and strontium. The organic matrix is roughly 90% Type I collagen and 10% noncollagenous proteins and serves as the template for mineralization [41,44]. Sub nanoscale triple-helical collagen molecules assemble together in highly ordered, staggered arrays to form fibrils. These arrays are stabilized by collagen cross-links. Plate-shaped crystals nucleate in gap zones between collagen molecules and extend into overlapped regions between molecules. The mineral crystals orient with their long axis (c-axis) parallel to the longitudinal axis of the fibrils [41,42,44,45]. These fibrils bundle together to form collagen fibers, which in turn form layers called lamellae.

The healthy human skeleton contains two distinct tissue microarchitectures: a dense architecture called cortical bone, and a more porous structure called cancellous bone. Cortical bone forms the exterior shell of the skeleton and is prevalent in the midshafts of long bones. Cancellous bone is interior to the cortical shell and is found primarily in vertebrae and at the ends of long bones [41,44]. In both cortical and cancellous bone, highly-aligned, mineralized collagen fibers form layers called lamellae. Lamellae in cortical bone form concentric cylinders around longitudinal blood vessels and create the basic structural unit called the osteon [41,44]. The collagen orientation between successive lamellae in cortical bone is thought to rotate in a plywood-like fashion [46–49]. The structure of cancellous bone is less dense than cortical bone and consists of rod and plate-like struts called trabeculae. Lamellae form roughly parallel to the long axes of the individual struts [41,44]. The alignment of collagen within cancellous lamellae is less documented, though evidence suggests that the collagen fibers are preferentially oriented along the longitudinal axes of trabeculae [50]. Between lamellae in both cortical and cancellous bone are transition zones called interlamellar regions. These regions appear to have less aligned or less dense collagen and are less mineralized than the lamellae, though the exact nature of interlamellar regions is still unclear and somewhat controversial [51,52].

1.3 Modeling and Remodeling

As a living, biological material, bone continuously adapts to surrounding conditions. Through modeling and remodeling, bone responds to changes in the loading environment, repairs microdamage, and maintains ion homeostasis within the body [41,44]. Due to the constant turnover of bone tissue, a single bone will contain tissue of varying ages. The variety of tissue ages within bone structures leads to microscale and sub microscale heterogeneity in both composition and mechanical properties, and specific spatial distributions of these properties within bone structures [53–63].

The modeling and remodeling processes are performed by bone cells: osteoclasts are responsible for the resorption (removal) of bone tissue, while osteoblasts lay down unmineralized osteoid (predominantly collagen) that then undergoes mineralization. Osteocytes (osteoblasts that become embedded in the bone matrix) are also involved in modeling and remodeling by serving as a sensory network that detects strain and possibly microdamage in bone tissue and then acts together with bone lining cells to direct the timing and location of modeling and remodeling events [41,44,64].

Modeling in human bone occurs predominantly during growth prior to skeletal maturity but can also occur in response to mechanical stimulation throughout life. In modeling, osteoclasts and osteoblasts are decoupled and resorption and formation can occur independently and on different bone surfaces [41,44]. During growth, formation primarily adds bone to the periosteal (outer) surfaces while resorption removes bone (more slowly) from the endosteal (inner) surfaces. The modeling process is also responsible for shaping the ends of long bones.

The remodeling process maintains the bone structure—replacing immature (primary) bone in infancy and older, damaged bone throughout life. Remodeling removes microdamage, replaces dead or over-mineralized bone, and maintains mineral homeostasis in the body. During remodeling, osteoclasts and osteoblasts are closely coupled through signaling factors and resorption and formation are spatially related and occur in a cyclic manner [41,44,65].

1.3.1 Remodeling in Cortical Bone

The osteonal structure of cortical bone forms as a result of the remodeling process, which takes place along canals containing blood vessels running longitudinally through the bone (Figure 2). Osteoclasts tunnel along these blood vessels, called Haversian canals, and resorb cylindrical volumes of bone. Osteoblasts follow and deposit layers of unmineralized bone matrix called osteoid to refill the volume, starting at the periphery and finishing at the center blood vessel. The resorption phase is relatively short in comparison to the formation phase and lasts one to two weeks. The resorption cavity is refilled and the surface near the blood vessel again becomes quiescent two to four months after the process began [41,44,66]. The resulting osteon contains a natural gradient of increasing tissue age from center to periphery because of the way the cylindrical volume was filled back in from periphery to center [59].

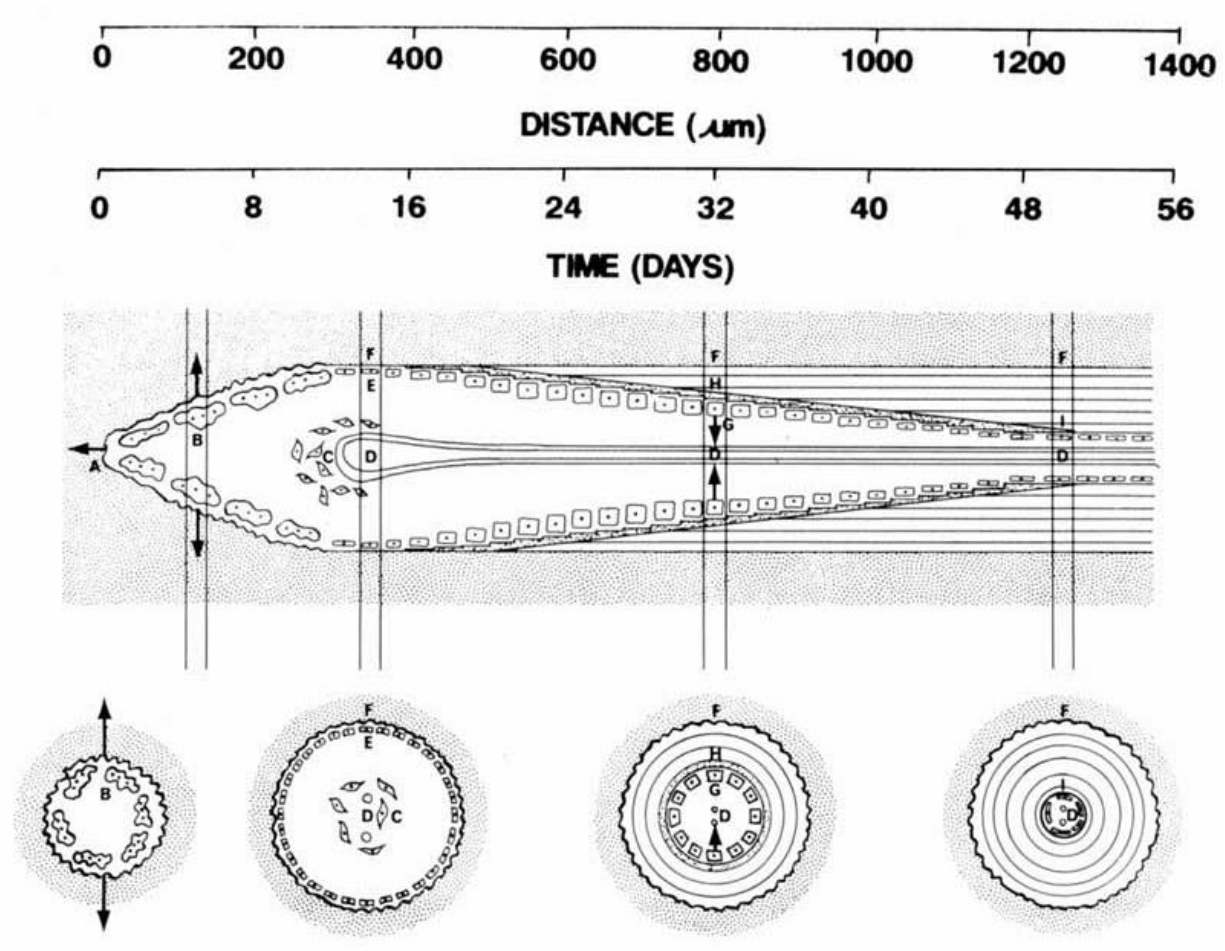

Figure 1.2 *Diagram of the Haversian remodeling process with the distance and time scale measured from the tip of the cutting cone (A). The remodeling event in this figure is traveling from right to left. (B) Osteoclasts resorb existing bone. (C) Dividing precursors of osteoclasts and osteoblasts. (D) Capillary loop. (E) Mononuclear cells lining the reversal zone from resorbing to forming. (F) Cement line separating new from old bone. (G) Osteoblasts forming layers of new bone. (H) Osteoid. (I) Cells lining the Haversian canal after remodeling process is completed. Figure adapted from* [66].

1.3.2 Remodeling in Cancellous Bone

Cancellous bone is more metabolically active than cortical bone due to the high surface-to-volume ratio and proximity to blood and marrow [41,44]. The basic structural unit is the trabecular packet, an irregularly-shaped volume of bone that is removed and replaced from the trabecula during the remodeling process (Figure 3). Remodeling units in cancellous bone travel along surfaces of trabeculae. Osteocytes remove a wedge-shaped volume of bone and are followed by osteoblasts that refill the space with osteoid [41,44,66]. Like in cortical bone, the remodeling process in cancellous bone creates a natural gradient in tissue age. The youngest tissue is at the surfaces of trabeculae where the osteoblasts finished refilling the resorption cavity.

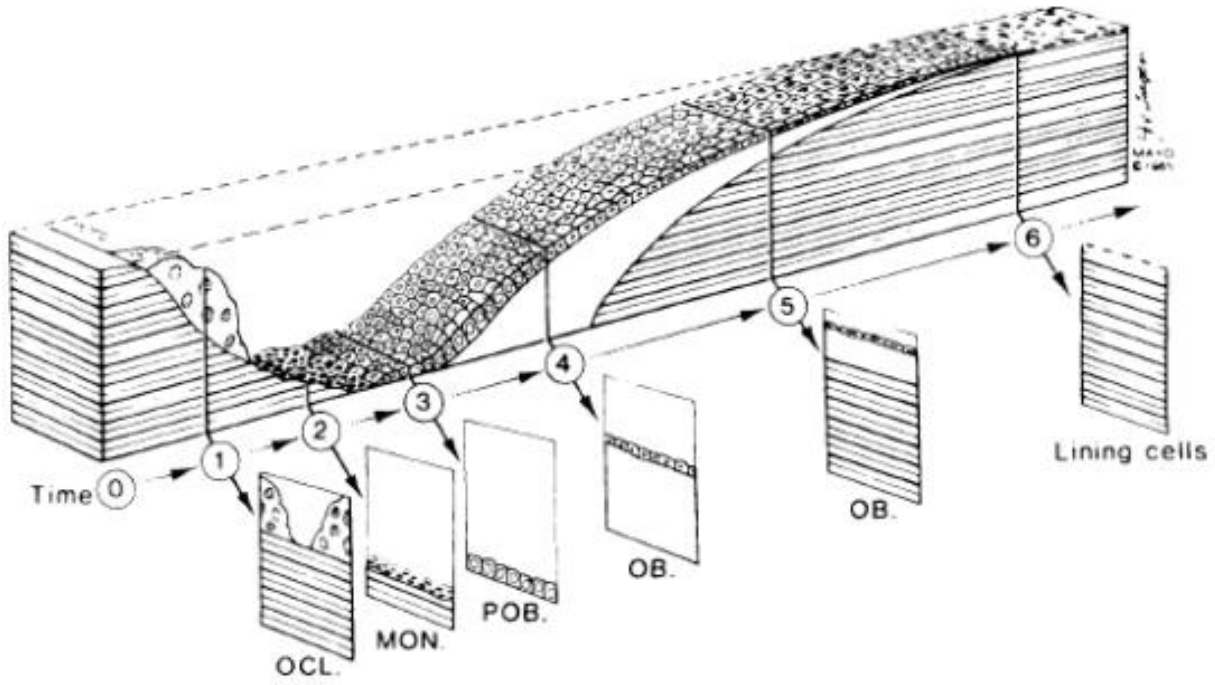

Figure 1.3 *Diagram of the trabecular remodeling process. The remodeling event is traveling from right to left in this figure. Time points one and two show resorption by osteoclasts; time point three shows reversal; time points four and five show formation by osteoblasts, and time point 6 shows the completion of remodeling with the new surface covered with lining cells. Figure adapted from* [66].

1.3.3 The Mineralization Process and Mineral Heterogeneity

The mineralization process progresses in two phases once the unmineralized osteoid is laid down by osteoblasts. In the first 5-10 days after formation the tissue rapidly accrues up to 70% of final mineralization in the phase called primary mineralization. The rate of mineral accrual subsequently slows in the secondary mineralization phase [41,66–69]. Levels of mineral content follow the spatial variations in tissue age due to the time-dependency of the mineralization process. Consequently, newly formed osteons in cortical bone are less mineralized than the older interstitial tissue between osteons [53]. The osteons themselves contain an increasing gradient in mineralization following the gradient in tissue age from center to periphery [21,70]. In cancellous bone, newly formed trabecular packets are less mineralized than older, more mature packets. Newer tissue at the surface is less mineralized than older tissue nearer the center of the trabeculae [56,71,72].

1.4 Apparent Level Structure-Mechanical Function Relationships

Mechanical testing of machined bulk tissue specimens demonstrates that the collagen matrix in bone primarily provides toughness while the mineral-platelet reinforcement provides stiffness. Degradation of bone's collagen matrix with irradiation while leaving the mineral phase intact substantially reduces work to fracture and impact energy but has little effect on stiffness (Figure 4) [73,74]. Conversely, progressive decalcification to remove mineral without disrupting the collagen matrix decreases stiffness while leaving post-yield behavior unchanged (Figure 4) [75]. Though bone mineral dominates elastic behavior, more highly-mineralized bone supports less strain at failure [42]. The collagen matrix is crucial for post-yield toughness and gives the bone composite an order of magnitude greater failure strain than that provided by the mineral alone [42,74,76].

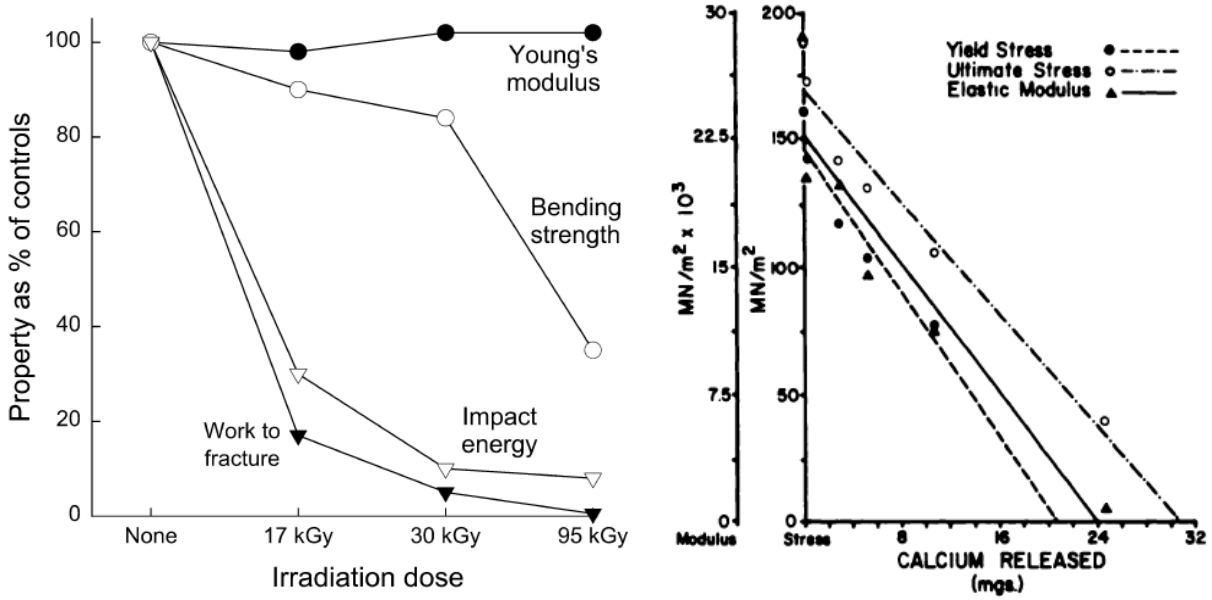

Figure 1.4 (Left) *The effect of irradiation on four mechanical properties of human compact bone. Irradiation degrades collagen while having little impact on mineral. Samples with degraded collagen had decreased work to fracture (decreased toughness) and decreased impact energy, yet had little change in Young's modulus (stiffness). Figure from* [74]. ***(Right)*** *Yield stress, ultimate stress, and elastic modulus vs. the amount of calcium removed in bovine tensile bone specimens.* R^2 *values range from 0.94 to 0.98. Figure from* [175].

1.4.1 Effects of Heterogeneity and Spatial Variations on Nanomechanical Function

More recently, nanoscale mechanical tests paired with compositional analyses show that tissue stiffness and hardness follow trends in mineralization [56,59,62,68,77,78]. These nanomechanical properties also increase with greater aligned collagen content [79]. Nanoscale spatial distributions and biological heterogeneity in tissue composition cause similar nanomechanical property variations in bone tissue [62]. Tissue stiffness and hardness increase rapidly in the first days after formation with the process of primary mineralization and then level off in older tissue with the slower progression of secondary mineralization [67,68]. Osteons in human cortical bone have lower stiffness and hardness than older, more mineralized interstitial tissue [53,54,62,80]. Similarly, newer trabecular packets have lower stiffness and hardness than older trabecular packets within human cancellous bone [56,63,72]. In both cortical and cancellous tissue, nanomechanical properties fluctuate between lamellar and interlamellar regions. Lamellar tissue has greater stiffness and hardness than interlamellar tissue due to greater mineral and aligned collagen content [53,54,62,79,80]. Fracture toughness below the

apparent level is difficult to measure experimentally, and consequently has not been correlated with these variations in nanoscale tissue composition and mechanical properties.

1.4.2 Effects of Nanoscale Tissue Variations on Macro-Scale Mechanical Function

The contribution of nanoscale mechanical property variations to changes in macro-scale mechanical function and fracture risk remains largely unclear. Modeling studies in cortical bone suggest nanoscale mechanical heterogeneity (especially in inelastic properties) promotes energy dissipation in the bulk tissue [15,16]. Transverse cracks arrest or deflect at interfaces between osteons and the interstitial tissue between osteons, trapping cracks at the cement lines and providing a mechanism for slowing crack growth and increasing fracture toughness [81–83]. A conflicting view is that cortical bone microstructure exists primarily for the improved ability to remodel and remove microdamage. Proponents of this theory suggest the Haversian microstructure actually reduces resistance to fatigue relative to a more uniform structure [84,85]. Nonetheless, variations between osteonal and interstitial properties affect microcrack propagation and direction [86]. Increasing ratios of interstitial to osteonal hardness correlate experimentally with decreased longitudinal fracture toughness [87].

Failure of cancellous bone results from the microdamage and failure of individual trabecular struts [88–90]. Struts transverse to the primary loading direction fracture first due to shear stresses induced from a cantilever-type mode of bending. Struts aligned in the primary loading direction subsequently fail by buckling. Both transverse and longitudinal trabeculae dissipate energy by accumulating microscopic internal matrix damage prior to failure [88–90]. Modeling of heterogeneity in trabecular bone demonstrates that the regions of lower stiffness at surfaces alter distributions of stress and strain within trabeculae and may result in greater stress magnitudes when compared to a simplified homogeneous model [12].

1.5 Ageing and Osteoporosis

The primary cause of osteoporosis is a loss of estrogen with ageing [91,92], though other factors such as disuse, estrogen-independent age-related mechanisms (such as hyperparathyroidism, oxidative stress in bone cells), certain drugs, also contribute to bone loss [91,93]. Osteoporosis is more prevalent in women because they have lower bone mass than men and experience precipitous bone loss at menopause with the abrupt loss of estrogen (Figure 5) [92]. Estrogen regulates both the rate of bone turnover and the balance between resorption and formation in the remodeling cycle [93–95]. A negative balance develops when estrogen is lost and less bone is formed than resorbed in each remodeling cycle. Coupled with an increased activation frequency of remodeling cycles, this imbalance causes the rapid drop in bone mass associated with high-turnover or postmenopausal type I osteoporosis in women.

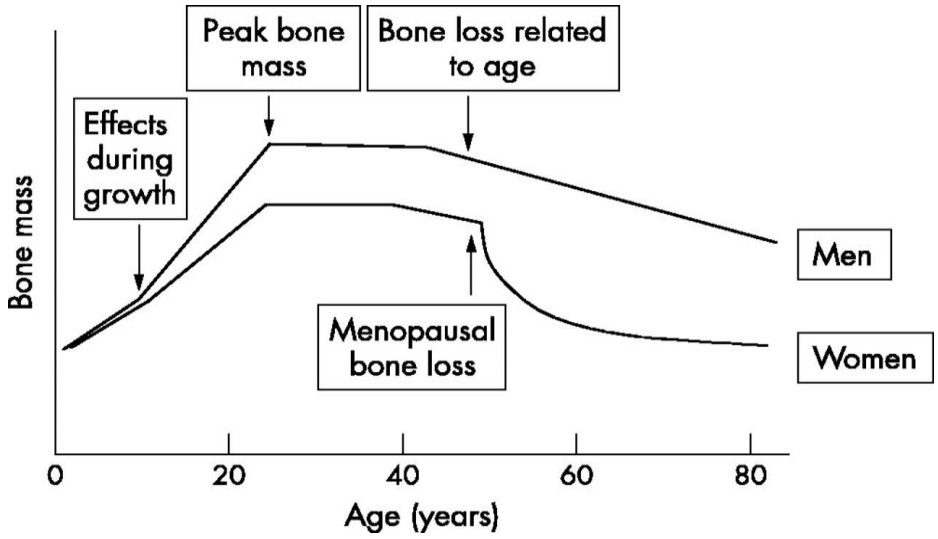

Figure 1.5 *Schematic showing bone mass with age in humans. Women experience a precipitous drop in bone mass at menopause resulting from the abrupt loss of estrogen* [97].

Estrogen's action in bone is complex and mediated by a host of factors that directly and indirectly affect bone remodeling cells [93,96–99]. With estrogen loss, the rate of remodeling increases, osteoclastogenesis increases and apoptosis decreases, and osteoblastogenesis and osteoblast apoptosis increase. Hence, greater numbers of osteoclasts with prolonged activity resorb larger than normal volumes of bone in each remodeling cycle. Concomitantly, increased

numbers of osteoblasts are unable to keep up with resorption due to decreased lifespan and consequently a negative balance develops.

1.6 Osteoporosis Treatment

Current treatments for osteoporosis employ two strategies for combating increased turnover and the loss of bone mass with estrogen withdrawal [25,100–105]. To date, most treatments are antiresorptive and target osteoclasts. These drugs inhibit the total amount of bone turnover, including both resorption and formation. In contrast, new anabolic agents employ an alternative approach and increase only bone formation. Effects of treatments can differ between skeletal sites, cortical and cancellous bone, and patient populations [106,107]. Drugs are approved by the Food and Drug Administration (FDA), and can be approved for prevention and/or treatment of osteoporosis [5]. For approval to prevent osteoporosis, i.e. to prevent the decline in bone mass with menopause, treatments must improve BMD but not necessarily reduce fracture risk in a population without osteoporosis. For approval to treat postmenopausal osteoporosis, i.e. to correct the loss of bone once it has already initiated, treatments must significantly reduce fracture risk among postmenopausal women.

Calcium and vitamin D are crucial in preventing and treating osteoporosis in addition to pharmaceutical interventions [100,105]. Vitamin D is essential for calcium absorption from the gut. Deficient levels of vitamin D and/or calcium cause hyperparathyroidism—excessive secretion of parathyroid hormone (PTH) from the parathyroid glands due to hypocalcaemia—and osteomalacia—poorly mineralized bone. Consequently, bone resorption increases to compensate for the calcium deficiency by removing calcium from the bone [108,109]. Vitamin D and calcium supplements are most effective in elderly populations who often do not receive adequate vitamin D from diet and sunlight exposure [100,110–112]. Supplementation is less effective or ineffective in populations with adequate intake and populations with less-deficient levels [113]. These studies suggest that deficiencies should be corrected, but calcium and vitamin D are not

sufficient to treat osteoporosis [100,105]. Adequate calcium and vitamin D levels also maximize the effectiveness of pharmaceutical treatments [114].

1.6.1 Antiresorptive Agents

Antiresorptive drugs are divided into several subclasses, each acting through different mechanisms to decrease bone turnover and reduce fracture risk. These subclasses include hormone replacement therapies (HRT: estrogen, estrogen + progestin), selective estrogen receptor modulators (SERMs: tamoxifen and raloxifene), bisphosphonates (alendronate, zoledronate, risedronate, ibandronate, etc.), non-steroidal hormones (calcitonin), and antibodies (denosumab). Hormone replacement therapies are approved only for prevention of osteoporosis. Raloxifene and the bisphosphonates are approved for both prevention and treatment, and the non-steroidal hormones are approved for treatment only [115].

1.6.1.1 Hormone Replacement Therapy

HRT has fallen out of favor due to a controversial benefit/risk profile [116,117]. Women who have had a hysterectomy can receive estrogen alone, while women with an intact uterus receive estrogen and progestin in a combined cyclic regimen [100]. These therapies increase the risk for deep vein thrombosis and pulmonary embolism, and there is some evidence that long term treatment may increase cancer risk (breast, endometrial, and ovarian) [100,105,107,118].

HRT increases BMD and reduce fracture risk by simply replacing the estrogen that is lost with menopause (see section 1.5). BMD increases 5-10% in early, late, and elderly postmenopausal populations, with the most marked reductions in women who began therapy within five years after menopause [100,105]. Estrogen reduces vertebral, non-vertebral, and hip fractures by roughly 30% compared with placebo [100,105,107,118]. The addition of progestin does not alter the bone effects of estrogen [105,118]. Unfortunately, bone loss resumes after treatment cessation and progresses at the same rate as prior to treatment [100,105,107,119–121]. Within five years of treatment withdrawal, the reduction in fracture risk is lost regardless of

treatment duration [119–121]. The long term benefit/risk profile and bone loss post-treatment raise questions about treatment efficacy and whether HRT benefits outweigh the risks.

1.6.1.2 Selective Estrogen Receptor Modulators (SERMs)

SERMs have an advantage over HRT because they exhibit tissue-specific agonist-antagonist activity. Thus, they can mimic the effects of estrogen in bone (see section 1.5) and reduce bone turnover, but not stimulate tissues in which the effects of estrogen are undesirable (endometrium, breast). The two SERM treatments most investigated for osteoporosis treatment are tamoxifen and raloxifene. Only raloxifene has obtained FDA approval because tamoxifen is a weak agonist for bone and increases cancer risk by stimulating the endometrium [100,122]. Raloxifene is a stronger agonist in bone, reduces the risk for breast cancer, and does not increase the risks for cardiovascular events, uterine bleeding, or endometrial cancer like HRT [100,118,122]. Similar to HRT, raloxifene can increase the risk for venous thrombosis and may also increase hot flashes [100,122].

SERMs act through endogenous estrogen pathways to reduce bone turnover and fracture risk. These drugs bind to estrogen receptors (ER-α and ER-β) and act through estrogen response elements (EREs) and coregulator proteins. The effects of raloxifene on bone turnover and fracture risk are relatively well documented. Raloxifene prevents bone loss at all skeletal sites (vertebral, hip, and non-vertebral) and reduces bone turnover markers to premenopausal levels in early postmenopausal women [100,122]. Vertebral fractures are reduced by 30-50%, depending on dosage, but hip or non-vertebral fractures are not significantly decreased [100,122]. Despite the marked reduction in vertebral fracture risk, three years of raloxifene treatment increased BMD by only 2% in the spine and proximal femur [122]. Like HRT, bone loss resumes after raloxifene treatment cessation[123].

1.6.1.3 Bisphosphonates

Bisphosphonates are the largest and most studied class of drugs and act as the first line of treatment for postmenopausal osteoporosis. The first generation of bisphosphonates does not contain nitrogen, has limited potency, and is not approved by the FDA. Newer, nitrogen-containing bisphosphonates are much more potent and several have FDA approval for prevention and treatment: alendronate, risedronate, ibandronate, and zoledronate [114,124–126]. The safety profile of bisphosphonates is better than that of HRT. The most common side effects are mild gastrointestinal irritation that can become severe in some patients [100,105,107,124]. Intravenously administered zoledronate and ibandronate produce no gastrointestinal effects. In rare cases, bisphosphonates have been associated with osteonecrosis of the jaw; however, most of these patients were treated with high doses for cancer [93]. Bisphosphonates stay metabolically active in the body for decades after administration and bone turnover markers remain reduced for at least five years after treatment cessation [93,127]. Rare cases of atypical femoral fractures with long-term bisphosphonate treatment have been reported, although the precise mechanisms behind this phenomenon are yet unknown [124,128]. Recent concerns have arisen that long-term bisphosphonate treatment may result in over-suppression of bone turnover and impairment of the skeleton's ability to repair microdamage [106,114,124].

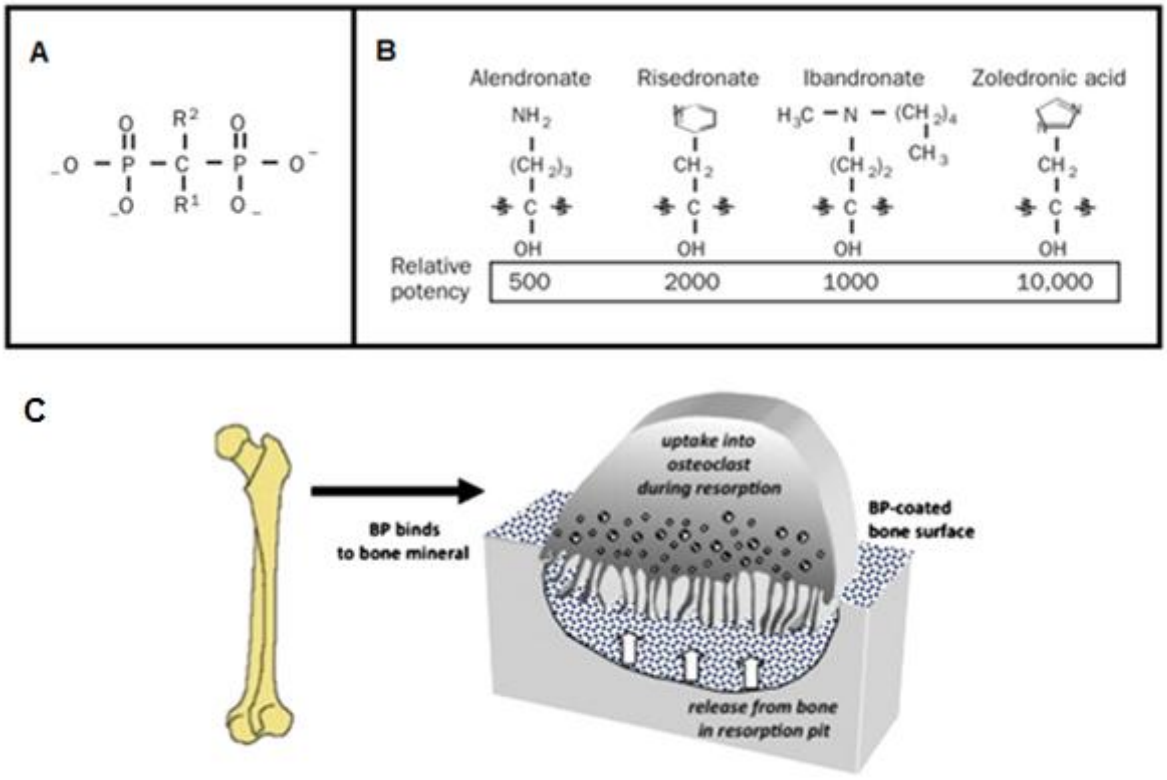

Figure 1.6 *(A) Bisphosphonate chemical structure showing R^2 side chains. (B) Side chain structure of nitrogen-containing bisphosphonates and their associated potency* [114] *. (C) Bisphosphonates bind to bone mineral and are taken up by osteoclasts during resorption* [176].

The chemical structure of nitrogen-containing bisphosphonates dictates skeletal uptake and retention and determines the relative potency of the various compounds (Figure 6) [114,125]. Flanking phosphate groups on either side of the central carbon atom provide a high affinity for bone mineral and allow binding to hydroxyapatite crystals. The R^2 side-chain determines potency. Bisphosphonates preferentially bind to bone mineral at sites of active bone remodeling (Figure 6) [114]. When endocytosed by osteoclasts during resorption, bisphosphonates prevent osteoclast fiber assembly and membrane ruffling and osteoclast apoptosis ensues [114,126]. Simultaneously, the activation frequency of new remodeling units formed by osteoclasts is reduced and the rate of turnover decreases [114,126]. With less frequent bone turnover, the duration of secondary mineralization is extended and a greater percentage of bone tissue reaches high levels of mineralization [26,114,129,130]. In addition to

endocytosis by osteoclasts, a low level of bisphosphonates is continuously released from the bone and activates survival kinases that promote osteoblast survival [131]. Consequently bone formation is increased despite the overall reduction in bone remodeling. This produces a slight increase in BMD, from 0-8% [25,132].

All approved bisphosphonates except for ibandronate provide marked fracture reduction at vertebral, hip, and non-vertebral skeletal sites [107,114]. Ibandronate reduces vertebral fractures but has not substantially reduced fractures at other sites. Reductions in fracture rates are similar between alendronate, risedronate, and zoledronate: 40-65% in vertebral, 30-55% in hip, and 20-60% in non-vertebral fractures in large population studies [93,118]. Out of these, alendronate and zoledronate produce the greatest increases in BMD (Figure 7) [107,124]. Fractures are reduced in osteopenic and osteoporotic women and those with or without vertebral fractures [93,124]. Alendronate, the most studied bisphosphonate (and indeed the most studied osteoporosis drug), continues to reduce bone turnover at least five years after cessation of treatment [124]. Alendronate and zoledronate have a more prolonged effect after treatment withdrawal than risedronate and ibandronate [124] likely due to their higher affinity for bone mineral.

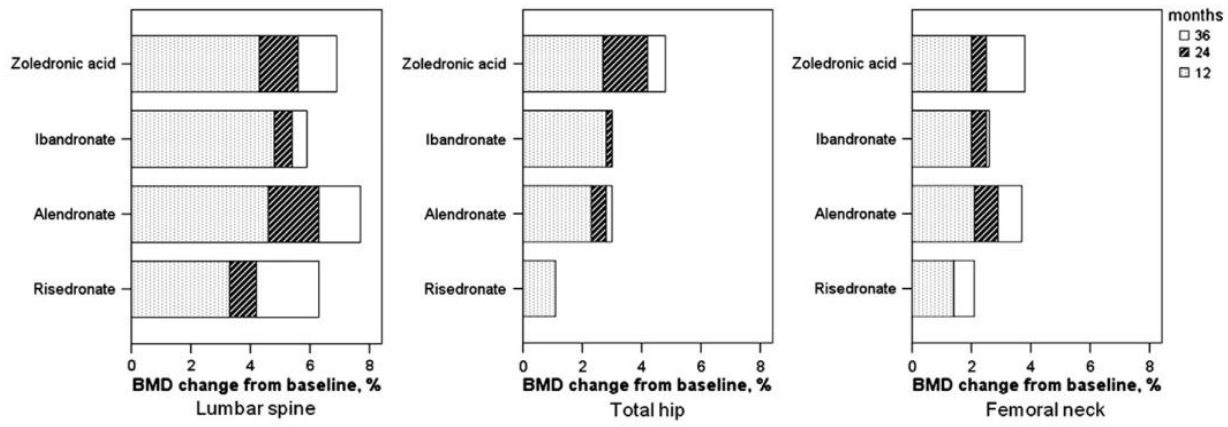

Figure 1.7 *Improvement in BMD with approved bisphosphonate treatments for the lumbar spine, total hip, and femoral neck.. Different colors on the bars show effects of different treatment durations. alendronate and zoledronate provide the greatest increases in BMD. These data also illustrate the variation in treatment effects between different skeletal sites* [124].

1.6.1.4 Calcitonin

Though approved by the FDA, the use of calcitonin for treating postmenopausal osteoporosis has been limited by cost and poor tolerance. Side effects were common with subcutaneous and intravenous injection and included nausea, flushing, and diarrhea [100,105,133]. Tolerance improved with the development of an intranasal delivery system; however, some patients still develop neutralizing antibodies that render calcitonin ineffective [105]. Furthermore, calcitonin is much less potent than other treatments, reduces vertebral but not non-vertebral fractures, and is less effective at preventing cortical than cancellous bone loss [100,105,107,118]. Calcitonin is a second or third line drug for patients who cannot tolerate bisphosphonates [133].

Calcitonin is a amino-acid peptide hormone produced by thyroid C cells that binds to calcitonin receptors on osteoclasts and rapidly inhibits osteoclast activity [100,105,133–135]. Osteoclasts lose their ruffled border and motility, and the proton pump and excretion of lysosomal enzymes are inhibited [135,136]. The resulting reduction in vertebral fractures is about 30%, with little effect on BMD [107,118].

1.6.1.5 Denosumab

Denosumab is a promising new treatment for osteoporosis recently approved by the FDA for patients at high risk for fracture [106]. Indications for treatment are osteoporosis with either a history of osteoporotic fracture, multiple risk factors for fracture, or intolerance to other treatments. The safety profile through three years of use is excellent [137]. Concerns to be studied are the long-term effects both on the immune system and due to osteoclast suppression [106].

Denosumab is a fully human monoclonal antibody to RANKL. RANKL is produced by osteoblasts and is a local factor that regulates osteoclast differentiation. By binding to RANKL and preventing binding with RANK (receptor activator of nuclear factor-κβ) receptors on cells of the osteoclast lineage, denosumab reduces osteoclastogenesis, osteoclast activity, and hence bone resorption [137–139].

Denosumab reduces turnover to a greater degree than bisphosphonate treatment and reduces vertebral, hip and non-vertebral fractures [106]. Vertebral fractures were reduced by 68%, hip fractures by 40%, and non-vertebral fractures by 20% in large clinical trials [140,141]. Forearm BMD also increases with denosumab, demonstrating potency in both cortical and cancellous bone [137]. In contrast, bisphosphonates do not affect forearm BMD. Denosumab is not incorporated into bone tissue like the bisphosphonates and is cleared rapidly after treatment withdrawal [106,141]. Thus, improvements in bone turnover markers and BMD are lost when treatment is stopped. However, reintroduction of denosumab again reduces turnover markers and increases BMD [137].

1.6.2 Anabolic Agents

Only one anabolic agent, teriparatide (hPTH [1-34]), is currently approved by the FDA for treatment of postmenopausal osteoporosis. While the antiresorptive treatments decrease bone turnover (both resorption and formation), anabolic treatments increase bone turnover and stimulate osteoblasts more than osteoclasts. With each remodeling cycle resorption spaces are overfilled causing a net increase in bone mass [106,142–144]. Anabolic treatments may even decouple osteoblasts and osteoclasts and stimulate formation directly without requiring prior bone resorption [143]. Trabecular thickness and connectivity increase with anabolic treatments; in contrast, antiresorptive treatments only stabilize and preserve trabecular architecture [143,144].

Clinical trials were performed with both recombinant human parathyroid hormone (rhPTH [1-84]) and synthetic human parathyroid hormone (teriparatide, hPTH [1-34]). The FDA rejected rhPTH [1-84] due to side effects of hypercalcemia and hypercalcinuria (high levels of calcium in the blood and urine, respectively) and clinical trials were abandoned due to development of osteosarcoma (malignant bone tumors) in rats [100,141,142]. The rates of osteosarcoma were dose and duration dependent [143]. Teriparatide gained FDA approval, but only for treatment of patients at high risk for fracture or who did not respond to other treatments.

Treatment duration is approved only to 24 months due to the safety concerns, and the expense of teriparatide is relatively high compared to other osteoporosis treatments [100].

Endogenous human PTH is an 84-amino acid peptide secreted from the parathyroid glands. The intact peptide and its fragments (including teriparatide) are key endocrine regulators of calcium homeostasis and act as either anabolic or catabolic agents in bone, depending on the manner of administration [144,145]. Continuously high levels of PTH in pathologic conditions such as primary hyperparathyroidism or chronic renal disease result in bone loss, whereas intermittent administration builds bone mass. The anabolic response of teriparatide is mediated through a host of factors. Teriparatide acts through PTH/PTHrP receptors found in osteoblasts, osteocytes, and bone lining cells [96,145,146]. With teriparatide, osteoblastogenesis increases and osteoblast apoptosis is prevented [145,146]. With more osteoblasts that live longer, remodeling sites are over-filled and there is a net gain in bone. In addition, bone lining cells revert to an active osteoblast phenotype and modeling is renewed at key sites such as the periosteum [145]. Through these effects on cells in the osteoblastic lineage, intermittent PTH administration rapidly increases the level of bone formation [145,147]. Eventually, the increase in formation is followed by a delayed and smaller increase in bone resorption. This delay creates the "anabolic window"—the time period in which anabolic treatment is most effective [145,147].

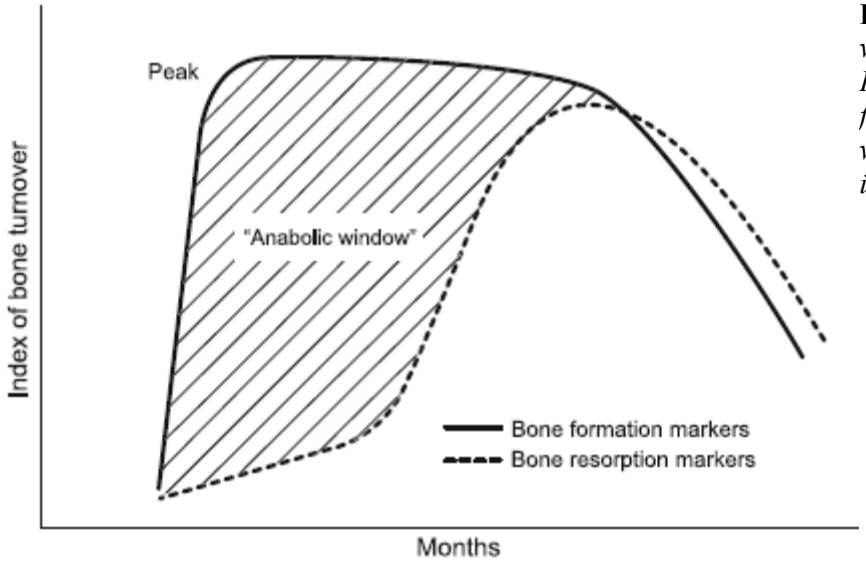

Figure 1.8 *The anabolic window created by intermittent PTH administration. Bone formation is rapidly increased while the increase in resorption is delayed* [106].

Teriparatide markedly reduces both vertebral and hip fracture risk. Vertebral fractures are reduced by over 60% and non-vertebral by over 50% [118]. Remarkably, moderate to severe fractures are reduced by 90% [145]. The average increase in BMD with 1-3 years of treatment is 10-14%, due to improvements in the trabecular compartment [143,144]. Both trabecular thickness and connectivity increase with treatment [143,144]. In contrast, cortical BMD is not improved or decreases slightly due to increased endocortical remodeling [143]. Though the resulting increase in cortical porosity initially raised concern, increased cortical diameter and thickness due to periosteal apposition appear to compensate biomechanically [143].

Improvements in BMD and fracture risk are greater with teriparatide than with Alendronate, but BMD gains are lost when teriparatide is withdrawn [142,143]. Micro-computed tomography-based models also show greater increases in vertebral strength with teriparatide than with alendronate relative to controls [148]. Combination therapies with antiresorptive treatments are being studied as a way to preserve improvements in BMD and fracture risk. Combination treatment with either HRT or raloxifene improves BMD in postmenopausal women over mono-therapy, and combination treatment with denosumab performed similarly in rats [142,144,147]. Treatment with alendronate subsequently to teriparatide provides additional gains in BMD [143,145,147]. In contrast, pre-treating with bisphosphonates blunted the effects of teriparatide [93,142,143,145,147].

1.6.3 Treatments in Development

Antiresorptive and anabolic drugs in the development pipeline show promise for future prevention and treatment for postmenopausal osteoporosis. Several new SERMs—bazedoxifene, lasofoxifene, ospemifene—are in stage III clinical trials [141]. Bazedoxifene shows similar effectiveness as raloxifene at reducing vertebral fractures. The strontium salt, strontium ranelate is also in stage III clinical trials and is already approved in Europe. Strontium substitutes for calcium ions in bone mineral and exerts a combined anabolic and antiresorptive effect, rebalancing bone turnover in favor of formation [100,101,105,106,149,150]. The reduction in

fractures with strontium ranelate is more modest than that with bisphosphonate treatment. Vertebral fractures are reduced by roughly 40% and non-vertebral fractures by 15% [150].

1.7 Apparent Level Mechanical Effects of Osteoporosis and Treatment

To date, apparent level and nanoscale characterization of bone with osteoporosis and treatments has been limited and has focused on effects in cancellous tissue because fragility fractures occur in predominantly cancellous locations. However, the cortical shell becomes increasingly important for load bearing and fracture resistance with the preferential loss of cancellous bone with osteoporosis [40,91,151–153]. Treatment differences may also exist between cortical and cancellous tissue [154]. Thus, in the future cortical tissue should also be considered when evaluating osteoporosis and the success of potential therapies.

At the apparent level, micro-CT based modeling of bone from patients with and without fragility fractures shows that patients with fractures have a cancellous architecture that is overadapted to the primary loading axis [155,156]. Patients with fractures have decreased transverse stiffness but no change in stiffness or strength in the primary loading direction compared to patients without fractures [155,156]. With SERM treatment, cancellous and cortical bone had increased primary stiffness, strength, and toughness in a canine model relative to healthy control animals [157]. Bisphosphonates also increase cancellous stiffness in the primary loading direction relative to untreated, healthy canines [23].

1.8 Nanoscale Compositional and Mechanical Effects of Osteoporosis and Treatment

Increased turnover and imbalances in the remodeling cycle with osteoporosis result in nanoscale compositional and mechanical alterations in bone tissue. To date, studies of nanoscale property changes with osteoporosis have produced mixed results because of small sample sizes [58,154,155,158–160]. In cancellous bone, osteoporosis reduces the overall heterogeneity of both tissue mineralization and mineral crystallinity within trabeculae [58,155,159,160]. Patients with fragility fractures demonstrated increased mineralization and mineral crystallinity compared

to those without fracture [21]. Increased mineralization is beneficial for strength and stiffness up to a point, but excessive mineralization can lead to brittleness [21]. Decreased work to fracture with ageing correlates with decreased work to fracture of the collagen network and increased pentosidine cross-links formed during nonenzymatic glycation [161]. Collagen maturity was also elevated in fractured patients and the spatial distribution of collagen maturity within trabeculae was markedly altered [21,22].

Few studies have characterized alterations in nanoscale tissue material properties with treatments, and even fewer have correlated treatment-induced changes in composition with the resulting effects on tissue nanomechanical function and crack resistance. Most of these studies only examined changes in cancellous tissue. Additionally, most tissue-level studies have been performed with bisphosphonates, since these drugs have been around the longest and are the most widely used for treatment of post-menopausal osteoporosis.

The reduction in turnover with bisphosphonates results in fewer new remodeling packets with lower levels of mineralization and a greater proportion of the bone reaches mature mineralization levels. Human bone tissue treated with alendronate has increased mineralization and reduced mineral heterogeneity relative to osteoporotic bone [34,129,162]. The same has been shown in animal models with zoledronate treatment [26,72,163,164]. Alendronate and risedronate increased cancellous and cortical tissue mineralization and collagen crosslinking maturity and decreased mineral heterogeneity in canine studies [26,27]. Treatment effects in these animals differed slightly between cancellous and cortical tissue. With bisphosphonates, collagen structure was altered through increased nonenzymatic (mature) crosslinks and increased isomerization [27]. Interestingly, in these same animals the SERM, raloxifene, did not alter collagen structure.

Increasing evidence from animal models suggests that changes in tissue composition with osteoporosis and treatments results in alterations in tissue mechanical function and crack resistance. Nanoscale tissue stiffness followed increased tissue mineralization in cancellous tissue from ovariectomized ewes treated with bisphosphonates [72]. Cancellous tissue treated

with alendronate and risedronate had increased numbers of microcracks and increased crack density compared to untreated tissue in the aforementioned canine studies [31]. Cortical tissue from the ribs of these dogs had greater crack length [165]. Increased microdamage correlated positively with increasing dose and treatment duration in these studies [31,165]. Interestingly, the treated vertebrae and ribs had similar strength as those from untreated animals when normalized by BMD, but had reduced energy absorption and toughness [31,165]. These studies provide remarkable insight into micro- and nanoscale alterations with bisphosphonate treatment; however, the canine model does have some limitations. Animals were not osteopenic or osteoporotic and were estrogen replete. Additionally, the rib is not load-bearing and may behave differently than load-bearing sites.

Raloxifene treatment in canines also altered mechanical function with evidence pointing towards changes in tissue material properties as a factor. Raloxifene enhanced vertebral strength independent of a change in BMD [30], suggesting that alterations in tissue properties might be a factor. However, unlike bisphosphonates, raloxifene did not alter collagen structure in these animals [27]. In vertebral cortical bone of the rat, raloxifene increased both indentation modulus and hardness relative to OVX [166].

Like the antiresorptive treatments, the anabolic agent, teriparatide, has been shown to alter tissue material properties and crack resistance. Teriparatide treatment for 24 months decreased crack length in iliac crest biopsies from treatment naïve patients and decreased crack density, crack surface density, and crack length in patients previously treated with alendronate [167]. In rats, teriparatide increased nanoscale tissue hardness relative to OVX in vertebral cortical bone [166].

1.9 Thesis Aims

Alterations in macro-scale measures of BMD and fracture risk with ageing, osteoporosis, and approved treatments are well-established; however, changes in BMD account for only a small proportion of the changes in fracture risk. Micro- and nanoscale alterations in bone material

composition and organization play an important role in the mechanical function of the skeleton and may explain some of the discrepancy between BMD and fracture risk. Nanoscale alterations with ageing, osteoporosis, and treatments are not well documented and understanding these alterations will improve our ability to predict fracture and develop successful treatment.

1.9.1 Aim 1: Establish a Baseline for Nanoscale Material Alterations with Ageing

Nanoscale material variations with the natural ageing process in healthy bone tissue must first be established to understand changes leading to age-related and osteoporotic fragility fractures. Previous studies of human bone tissue produced conflicting results with tissue age and patient age due to the limited age ranges of subjects studied and small sample sizes [53,60,62,70,168,169]. Therefore, the first objective of this thesis was to establish a baseline for the age-related compositional and nanomechanical alterations that occur in bone tissue with the natural ageing process. Part of this aim was to correlate the changes in tissue composition with their resulting nanomechanical effects. Understanding these relationships improved our understanding of normal bone function.

The first experiment of this thesis work addressed the first aim by examining nanoscale tissue composition and nanomechanical properties in the osteons of a primate model for human ageing. Human bone is difficult to obtain and data regarding health and treatment are often unreliable. Baboons contain the same Haversian microstructure and remodeling process as human bone and females follow a very similar ageing process that includes menopause, reproductive senescence, and eventually skeletal fragility with ageing [170]. The baboons for this experiment were from a closely-monitored colony with reliable data regarding health and treatment and were not used for any other study; therefore, they should provide an accurate baseline for changes with the natural ageing process. Material changes with tissue age were studied in these animals by characterizing tissue along radial lines following the gradient in tissue age across osteons. Changes with animal age were investigated by examining osteons in bones from animals with ages spanning the entire baboon lifetime—from birth through skeletal

maturity and old age. These results were presented at the Materials Research Society and Orthopaedic Research Society annual meetings and have been published in the Journal of Biomechanics [171].

1.9.2 Aim 2: Determine Nanoscale Alterations with Osteoporosis and Treatment

Once the natural age-related variations in nanoscale tissue composition and mechanical function were established, pathological alterations with osteoporosis and treatments could be observed. Altered or imbalanced remodeling with osteoporosis and treatments can affect nanoscale composition and mechanical properties and spatial distributions of these properties within bone structures [22], yet few studies have documented changes at this length scale. The second aim of this thesis was, therefore, to examine nanoscale material changes with osteoporosis and different treatments. Correlating nanoscale tissue composition and nanomechanical function in this aim and relating changes at the nanoscale to changes at higher length scales provided a better understanding of pathological bone function and may eventually enable researchers to improve upon current therapies for skeletal disease.

A large, multi-level experiment was designed to address Aims 2 and 3 of this thesis. In this experiment, nanoscale material properties were examined and correlated within cancellous and cortical bone from an ovine model for postmenopausal osteoporosis. Spatial distributions of properties were characterized across individual trabecular struts in cancellous bone and individual osteons in cortical bone. Alterations in cortical and cancellous tissue were compared because both are important for fracture resistance and treatment can produce different effects in different tissue types; however, few studies have examined cortical bone and there is a small population of patients on long-term bisphosphonate treatment that have experienced atypical cortical fractures [128]. In these same animals, bulk and whole bone mineral and mechanical properties are examined to determine how changes in nanoscale properties translate to changes at higher length scales. Like the baboon model from Experiment 1, mature ovine bone contains a Haversian microstructure similar to human bone and health and treatment status can be closely

monitored and controlled [172–174]. The dietary metabolic acidosis model (MA) in ewes produces similar changes as postmenopausal osteoporosis and reduces both BMD and whole bone strength [173,174].

The first treatment chosen for this experiment was a bisphosphonate because this class of drug is most widely prescribed and most studied. In addition, bisphosphonates are the only treatments to date whose effects are maintained after withdrawal [127]. Alendronate was the original bisphosphonate chosen for this experiment because it is the most widely used and oldest of the nitrogen-containing bisphosphonates [115]. Alendronate (and zoledronate) also provides the greatest change in BMD and fracture risk of the bisphosphonates and prevents fracture at vertebral, hip, and non-vertebral sites [124]. Due to problems administering alendronate through cannulae in the ewes, the bisphosphonate was switched to zoledronate. Zoledronate has a similar potency to alendronate and can be given intravenously, eliminating the need for cannular administration.

The SERM, raloxifene, was chosen as the treatment for comparison. Raloxifene is the most potent and only FDA-approved SERM. Zoledronate and raloxifene are both antiresorptive drugs that act through distinctly different mechanisms. Both provide similar reductions in fracture risk in the vertebrae [107]. In addition, raloxifene acts through the natural estrogen pathways in bone, making it an ideal choice for comparison [99].

1.9.3 Aim 3: Examine Micro-Cracking With Osteoporosis and Treatment

Failure of bone initiates at the tissue-level with damage and micro-cracks. Bisphosphonate treatment has been linked with increased microcracking [31,33,165], and concern has arisen that over-supression of bone turnover with treatment may eventually lead to increased propensity for microcracking and the accumulation of damage. Fracture resistance is difficult to measure at these small length scales and no one has yet examined relationships between changes in nanoscale tissue material properties and changes in microcracking resistance with osteoporosis and treatment. Therefore, the third aim of this thesis was to develop a method to induce

microscale cracks in bone tissue and to examine differences in cracking with osteoporosis and different treatments.

Aim 3 was addressed by part of the large, multi-level ovine experiment outlined in Aim 2. A sharp tip connected to a microindentation instrument was used to create micro-cracking in the same cortical specimens previously used to characterize nanoscale material properties. Differences in the propensity for micro-cracking and micro-crack behavior are examined with osteoporosis, zoledronate, and raloxifene. Differences between newer osteonal tissue and older interstitial tissue were also compared.

BIBLIOGRAPHY

[1] Melton LJ, Atkinson EJ, O'Connor MK, O'Fallon M, Riggs L. Bone Density and Fracture Risk in Men. Journal of Bone and Mineral Research 1998;13:1915-1923.

[2] Melton LJ, Chrischilles E, Cooper C. Perspective. How many women have osteoporosis? Journal of Bone and Mineral Research 1992;7:1005.

[3] Kanis JA, Johnell O, Oden A, Sernbo I, Dawson A, de Laet C. International Long-Term Risk of Osteoporotic Fracture in Malmo. Bone 2000;11:669-674.

[4] Burge R, Dawson-hughes B, Solomon DH, Wong JB, King A, Tosteson A. Incidence and Economic Burden of Osteoporosis-Related Fractures in the United States, 2005–2025. Journal of Bone and Mineral Research 2007;22.

[5] WHO. Assessment of fracture risk and its application to screening for postmenopausal osteoporosis. WHO Technical Report Series 843. 1994.

[6] Sornay-rendu E, Boutroy S, Munoz F, Delmas PD. Alterations of Cortical and Trabecular Architecture Are Associated With Fractures in Postmenopausal Women, Partially Independent of Decreased BMD Measured by DXA: The OFELY Study. Journal of Bone and Mineral Research 2007;22:425-433.

[7] van der Meulen MC, Jepsen KJ, Mikić B. Understanding bone strength: size isn't everything. Bone 2001;29:101-4.

[8] Marshall D, Johnell O, Wedel H. Meta-analysis of how well measures of bone mineral density predict occurrence of osteoporotic fractures. British Medical Journal 1996;312:1254-1259.

[9] Viguet-Carrin S, Garnero P, Delmas PD. The role of collagen in bone strength. Osteoporosis International 2006;17:319-336.

[10] Garnero P. Biomarkers for osteoporosis management: utility in diagnosis, fracture risk prediction and therapy monitoring. Molecular Diagnosis Therapy 2008;12:157-170.

[11] Delmas PD, Seeman E. Changes in bone mineral density explain little of the reduction in vertebral or nonvertebral fracture risk with anti-resorptive therapy. Bone 2004;34:599-604.

[12] Renders GAP, Mulder L, van Ruijven LJ, Langenbach GEJ, van Eijden TMGJ. Mineral heterogeneity affects predictions of intratrabecular stress and strain. Journal of Biomechanics 2011;44:402-7.

[13] Cioffi I, Van Ruijven LJ, Renders GAP, Farella M, Michelotti A, Van Eijden TMGJ. Regional variations in mineralization and strain distributions in the cortex of the human mandibular condyle. Bone 2007;41:1051-1058.

[14] Renders GAP, Mulder L, Langenbach GEJ, Van Ruijven LJ, Van Eijden TMGJ. Biomechanical effect of mineral heterogeneity in trabecular bone. Journal of Biomechanics 2008;41:2793-2798.

[15] Tai K, Dao M, Suresh S, Palazoglu A, Ortiz C. Nanoscale heterogeneity promotes energy dissipation in bone. Nature Materials 2007;6:454-462.

[16] Yao H, Dao M, Carnelli D, Tai K, Ortiz C. Size-dependent heterogeneity benefits the mechanical performance of bone. Journal of the Mechanics and Physics of Solids 2011;59:64-74.

[17] Garnero P, Sornay-Rendu E, Chapuy MC, Delmas PD. Increased bone turnover in late postmenopausal women is a major determinant of osteoporosis. Journal of Bone and Mineral Research 1996;11:337-349.

[18] Ross PD, Davis JW, Vogel JM, Wasnich RD. A Critical Review of Bone Mass and the Risk of Fractures in Osteoporosis. Calcified Tissue International 1990;46:149-161.

[19] Kanis JA, Borgstrom F, De Laet C, Johansson H, Johnell O, Jonsson B, et al. Assessment of fracture risk. Osteoporosis International 2005;16:581-9.

[20] Faulkner KG. Bone matters: are density increases necessary to reduce fracture risk? Journal of Bone and Mineral Research 2000;15:183-7.

[21] Gourion-Arsiquaud S, Faibish D, Myers E, Spevak L, Compston J, Hodsman A, et al. Use of FTIR Spectroscopic Imaging to Identify Parameters Associated With Fragility Fracture. Journal of Bone and Mineral Research 2009;24:1565-1571.

[22] Paschalis EP, Shane E, Lyritis G, Skarantavos G, Mendelsohn R, Boskey AL. Bone fragility and collagen cross-links. Journal of Bone and Mineral Research 2004;19:2000-4.

[23] Day JS, Ding M, Bednarz P, van der Linden JC, Mashiba T, Hirano T, et al. Bisphosphonate treatment affects trabecular bone apparent modulus through micro-architecture rather than matrix properties. Journal of Orthopaedic Research 2004;22:465-71.

[24] Ettinger B, Black DM, Mitlak BH, Knickerbocker RK, Nickelsen T, Genant HK, et al. Reduction of vertebral fracture risk in postmenopausal women with osteoporosis treated with raloxifene: results from a 3-year randomized clinical trial. The Journal of the American Medical Association 1999;282:637-45.

[25] Cummings SR, Karpf DB, Harris F, Genant HK, Ensrud K, LaCroix AZ, et al. Improvement in spine bone density and reduction in risk of vertebral fractures during treatment with antiresorptive drugs. The American Journal of Medicine 2002;112:281-289.

[26] Gourion-Arsiquaud S, Allen MR, Burr DB, Vashishth D, Tang SY, Boskey AL. Bisphosphonate treatment modifies canine bone mineral and matrix properties and their heterogeneity. Bone 2010;46:666-672.

[27] Allen MR, Gineyts E, Leeming DJ, Burr DB, Delmas PD. Bisphosphonates alter trabecular bone collagen cross-linking and isomerization in beagle dog vertebra. Osteoporosis International 2008;19:329-337.

[28] Saito M. Effects of SERMs on bone health. Effects of raloxifene and bisphosphonate on bone quality in osteoporosis: collagen cross-links, mineralization, and bone strength. Clinical Calcium 2010;20:345-354.

[29] Saito M. Assessment of bone quality. Effects of bisphosphonates, raloxifene, alfacalcidol, and menatetrenone on bone quality: collagen cross-links, mineralization, and microdamage. Clinical Calcium 2008;18:364-372.

[30] Allen MR, Iwata K, Sato M, Burr DB. Raloxifene enhances vertebral mechanical properties independent of bone density. Bone 2006;39:1130-5.

[31] Allen MR, Iwata K, Phipps R, Burr DB. Alterations in canine vertebral bone turnover, microdamage accumulation, and biomechanical properties following 1-year treatment with clinical treatment doses of risedronate or alendronate. Bone 2006;39:872-9.

[32] Mashiba T, Mori S, Burr DB, Komatsubara S, Cao Y, Manabe T, et al. The effects of suppressed bone remodeling by bisphosphonates on microdamage accumulation and degree of mineralization in the cortical bone of dog rib. Journal of Bone and Mineral Metabolism 2005;23 Suppl:36-42.

[33] Allen MR, Burr DB. Bisphosphonate effects on bone turnover, microdamage, and mechanical properties: What we think we know and what we know that we don't know. Bone 2011;49:56-65.

[34] Roschger P, Rinnerthaler S, Yates J, Rodan GA, Fratzl P, Klaushofer K. Alendronate increases degree and uniformity of mineralization in cancellous bone and decreases the porosity in cortical bone of osteoporotic women. Bone 2001;29:185-191.

[35] Lundy MW, Stauffer M, Wergedal JE, Baylink DJ, Featherstone JDB, Hodgson SF, et al. Histomorphometric analysis of iliac crest bone biopsies in placebo-treated versus fluoride-treated subjects. Osteoporosis International 1995;5:115-129.

[36] Boivin G, Duriez J, Chapuy MC, Flautre B, Hardouin P, Meunier PJ. Relationship between bone fluoride content and histological evidence of calcification defects in osteoporotic women treated long term with sodium fluoride. Osteoporosis International 1993;3:204-208.

[37] Sogaard CH, Mosekilde L, Richards A. Marked decrease in trabecular bone quality after five years of sodium fluoride therapy--assessed by biomechanical testing of iliac crest bone biopsies in osteoporotic patients. Bone 1994;15:393-9.

[38] Aaron JE, de Vernejoul MC, Kanis JA. The effect of sodium fluoride on trabecular architecture. Bone 1991;12:307-10.

[39] Haguenauer D, Welch V, Shea B, Tugwell P, Adachi JD, Wells G. Fluoride for the Treatment of Postmenopausal Osteoporotic Fractures : A Meta-Analysis. Osteoporosis International 2000;11:727-738.

[40] Rico H. The Therapy of Osteoporosis and the Importance of Cortical Bone. Calcified Tissue International 1997;61:431-432.

[41] Cowin SC. Bone Mechanics Handbook. Second Edi. United States: CRC Press LLC. 2001.

[42] Fratzl P, Gupta HS, Paschalis EP, Roschger P. Structure and mechanical quality of the collagen-mineral nano-composite in bone. Journal of Materials Chemistry 2004;14:2115.

[43] Weiner S, Wagner HD. The Material Bone: Structure-Mechanical Function Relations. Annual Review of Materials Science 1998;28:271-298.

[44] Bilezikian JP, Raisz LG, Rodan GA. Principles of Bone Biology. United States: Academic Press. 1996.

[45] Rho JY, Kuhn-Spearing L, Zioupos P. Mechanical properties and the hierarchical structure of bone. Medical Engineering & Physics 1998;20:92-102.

[46] Giraud-Guille MM. Twisted plywood architecture of collagen fibrils in human compact bone osteons. Calcified Tissue International 1988;42:167-80.

[47] Weiner S, Arad T, Sabanay I, Traub W. Rotated plywood structure of primary lamellar bone in the rat: orientations of the collagen fibril arrays. Bone 1997;20:509-14.

[48] Wagermaier W, Gupta HS, Gourrier A, Paris O, Roschger P, Burghammer M, et al. Scanning texture analysis of lamellar bone using microbeam synchrotron X-ray radiation. Journal of Applied Crystallography 2007;40:115-120.

[49] Wagermaier W, Gupta HS, Gourrier A, Burghammer M, Roschger P, Fratzl P. Spiral twisting of fiber orientation inside bone lamellae. Biointerphases 2006;1:1.

[50] Jaschouz D, Paris O, Roschger P, Hwang H-S, Fratzl P. Pole figure analysis of mineral nanoparticle orientation in individual trabecula of human vertebral bone. Journal of Applied Crystallography 2003;36:494-498.

[51] Boyde A, Hordell MH. Scanning electron microscopy of lamellar bone. Zeitschrift für Zellforschung und mikroskopische Anatomie 1969;93:213-31.

[52] Ziv V, Sabanay I, Arad T, Traub W, Weiner S. Transitional structures in lamellar bone. Microscopy Research and Technique 1996;33:203-13.

[53] Rho JY, Zioupos P, Currey JD, Pharr GM. Microstructural elasticity and regional heterogeneity in human femoral bone of various ages examined by nano-indentation. Journal of Biomechanics 2002;35:189-198.

[54] Zysset PK, Guo XE, Hoffler CE, Moore KE, Goldstein SA. Elastic modulus and hardness of cortical and trabecular bone lamellae measured by nanoindentation in the human femur. Journal of Biomechanics 1999;32:1005-1012.

[55] Hoffler CE, Moore KE, Kozloff K, Zysset PK, Brown MB, Goldstein SA. Heterogeneity of bone lamellar-level elastic moduli. Bone 2000;26:603-609.

[56] Smith LJ, Schirer JP, Fazzalari NL. The role of mineral content in determining the micromechanical properties of discrete trabecular bone remodeling packets. Journal of Biomechanics 2010;43:3144-9.

[57] Ruffoni D, Fratzl P, Roschger P, Klaushofer K, Weinkamer R. The bone mineralization density distribution as a fingerprint of the mineralization process. Bone 2007;40:1308-1319.

[58] Roschger P, Paschalis EP, Fratzl P, Klaushofer K. Bone mineralization density distribution in health and disease. Bone 2008;42:456-466.

[59] Gourion-arsiquaud S, Burket JC, Havill LM, Dicarlo E, Doty SB, Mendelsohn R, et al. Spatial Variation in Osteonal Bone Properties Relative to Tissue and Animal Age. Journal of Bone and Mineral Research 2009;24:1271-1281.

[60] Paschalis EP, Betts F, DiCarlo E, Mendelsohn R, Boskey AL. FTIR microspectroscopic analysis of normal human cortical and trabecular bone. Calcified Tissue International 1997;61:480-486.

[61] Paschalis EP, Mendelsohn R. Variations in the individual thick lamellar properties within osteons by nanodentation. Bone 2000;26:545-6.

[62] Gupta HS, Stachewicz U, Wagermaier W. Mechanical modulation at the lamellar level in osteonal bone. Scanning Electron Microscopy 2006;12:1913-1921.

[63] Brennan O, Kennedy OD, Lee TC, Rackard SM, O'Brien FJ. Biomechanical properties across trabeculae from the proximal femur of normal and ovariectomised sheep. Journal of Biomechanics 2009;42:498-503.

[64] Martin RB. Toward a unifying theory of bone remodeling. Bone 2000;26:1-6.

[65] Hadjidakis DJ, Androulakis II. Bone remodeling. Annals of the New York Academy of Sciences 2006;1092:385-96.

[66] Parfitt a M. Osteonal and hemi-osteonal remodeling: the spatial and temporal framework for signal traffic in adult human bone. Journal of Cellular Biochemistry 1994;55:273-86.

[67] Miller LM, Little W, Schirmer A, Sheik F, Busa B, Judex S. Accretion of Bone Quantity and Quality in the Developing Mouse Skeleton. Journal of Bone and Mineral Research 2007;22.

[68] Donnelly E, Boskey AL, Baker SP, van der Meulen MCH. Effects of tissue age on bone tissue material composition and nanomechanical properties in the rat cortex. Journal of Biomedical Materials Research A 2010;92:1048-56.

[69] Grynpas M. Calcified Tissue Age and Disease-Related Changes in the Mineral of Bone. Bone 1993;53.

[70] Paschalis EP, DiCarlo E, Betts F, Sherman P, Mendelsohn R, Boskey a L. FTIR microspectroscopic analysis of human osteonal bone. Calcified Tissue International 1996;59:480-7.

[71] Willems NMBK, Mulder L, Langenbach GEJ, Grünheid T, Zentner A, Van Eijden TMGJ. Age-related changes in microarchitecture and mineralization of cancellous bone in the porcine mandibular condyle. Journal of Structural Biology 2007;158:421-427.

[72] Brennan O, Kennedy OD, Lee TC, Rackard SM, O'Brien FJ, McNamara LM. The effects of estrogen deficiency and bisphosphonate treatment on tissue mineralisation and stiffness in an ovine model of osteoporosis. Journal of Biomechanics 2011;44:386-90.

[73] Currey JD, Foreman J, Laketic I, Mitchell J, Pegg DE, Reilly GC. Effects of ionization radiation on the mechanical properties of human bone. Journal of Orthopaedic Research 1997;15:111-117.

[74] Currey JD. Role of collagen and other organics in the mechanical properties of bone. Osteoporosis International 2003;14 Suppl 5:S29-36.

[75] Burstein AH, Zika JM, Heiple KG, Klein L. Contribution of collagen and mineral to the elastic-plastic properties of bone. Journal of Bone and Joint Surgery 1975;57-A.

[76] Wainwright SA, Biggs WD, Currey JD, Gosline JM. Mechanical Design in Organisms. Princeton: Princeton University Press. 1982

[77] Donnelly E, Chen DX, Boskey AL, Baker SP, van der Meulen MCH. Contribution of mineral to bone structural behavior and tissue mechanical properties. Calcified Tissue International 2010;87:450-460.

[78] Mulder L, Koolstra JH, Den Toonder JMJ, Van Eijden TMGJ. Relationship between tissue stiffness and degree of mineralization of developing trabecular bone. Journal of Biomedical Materials Research Part A 2008;84:508-515.

[79] Donnelly E, Baker SP, Boskey AL, van der Meulen MCH. Quasistatic and dynamic nanomechanical properties of cancellous bone tissue relate to collagen content and organization. Journal of Biomedical Materials Research A 2006;21.

[80] Rho JY, Tsui TY, Pharr GM. Elastic properties of human cortical and trabecular lamellar bone measured by nanoindentation. Biomaterials 1997;18:1325-1330.

[81] O'Brien FJO, Taylor D, Lee TC. The effect of bone microstructure on the initiation and growth of microcrack. Journal of Orthopaedic Research 2005;23.

[82] Saha S, Hayes WC. Relations between tensile impact properties and microstructure of compact bone. Calcified Tissue Research 1977;24:65-72.

[83] Hiller LP, Stover SM, Gibson VA, Gibeling JC, Prater CS, Hazelwood SJ, et al. Osteon pullout in the equine third metacarpal bone: effects of ex vivo fatigue. Journal of Orthopaedic Research 2003;21:481-8.

[84] Zioupos P, Gresle M, Winwood K. Fatigue strength of human cortical bone: age, physical, and material heterogeneity effects. Journal of biomedical materials research. Part A 2008;86:627-36.

[85] Carter DR, Hayes WC, Schurman DJ. Fatigue Life of Compact Bone-II. Effects of Microstructure and Density. Journal of Biomechanics 1976;9:211-218.

[86] Guo XE, Liang LC, Goldstein SA. Micromechanics of Osteonal Cortical Bone Fracture. Transactions of the ASME 1998;120:112-117.

[87] Phelps JB, Hubbard GB, Wang X, Agrawal CM. Microstructural heterogeneity and the fracture toughness of bone. Journal of Biomedical Materials Research 2000;51:735-741.

[88] Fyhrie DP, Schaffler MB. Failure mechanisms in human vertebral cancellous bone. Bone 1994;15:105-9.

[89] Michel MC, E GX-D, J GL, A MT, Hayes WC. Compressive Fatigue Behavior of Bovine Trabecular Bone. Journal of Biomechanics 1993;26:453-463.

[90] Thurner PJ, Wyss P, Voide R, Stauber M, Stampanoni M, Sennhauser U, et al. Time-lapsed investigation of three-dimensional failure and damage accumulation in trabecular bone using synchrotron light. Bone 2006;39:289-99.

[91] Khosla S, Melton LJ, Riggs BL. The unitary model for estrogen deficiency and the pathogenesis of osteoporosis: is a revision needed. Journal of Bone and Mineral Research 2011;26:441-51.

[92] Riggs BL, Khosla S, Melton LJ. A unitary model for involutional osteoporosis: estrogen deficiency causes both type I and type II osteoporosis in postmenopausal women and contributes to bone loss in aging men. Journal of Bone and Mineral Research 1998;13:763-73.

[93] Sambrook P, Cooper C. Osteoporosis. Lancet 2006;367:2010-8.

[94] Pacifici R. Estrogen, cytokines, and pathogenesis of postmenopausal osteoporosis. Journal of Bone and Mineral Research 1996;11:1043-51.

[95] Azuma K, Inoue S. Selective estrogen receptor modulators: mechanisms of action and their tissue selectivity. Clinical Calcium 2004;14:12-26.

[96] Manolagas SC. Birth and death of bone cells: basic regulatory mechanisms and implications for the pathogenesis and treatment of osteoporosis. Endocrine Reviews 2000;21:115-137.

[97] Dogan E, Posaci C. Monitoring hormone replacement therapy by biochemical markers of bone metabolism in menopausal women. Postgraduate Medical Journal 2002;78:727-31.

[98] Glasebrook AL, Short LL, Cole LW, Sato M, Bryant HU. Regulation of serum IL-6 by raloxifene in an ovariectomized rat model. Bone 1996;19 Suppl:995.

[99] Bryant HU, D P. Mechanism of Action and Preclinical Profle of Raloxifene , a Selective Estrogen Receptor Modulator. Reviews in Endocrine & Metabolic Disorders 2001;2:129-138.

[100] Delmas PD. Treatment of postmenopausal osteoporosis. The Lancet 2002;359:2018-2026.

[101] Altkorn D, Vokes T. Treatment of postmenopausal osteoporosis. The Journal of the American Medical Association 2001;285:1415-8.

[102] Reginster J-Y. Treatment of postmenopausal osteoporosis. British Medical Journal 2005;330:1449.

[103] Lewiecki EM. Prevention and treatment of postmenopausal osteoporosis. Obstetrics and gynecology clinics of North America 2008;35:301-315, ix.

[104] Cranney A. Treatment of postmenopausal osteoporosis. British Medical Journal 2007;327:355-356.

[105] Eastell R. Treatment of postmenopausal osteoporosis. The New England Journal of Medicine 1998;March:736-746.

[106] Gallacher SJ, Dixon T. Impact of treatments for postmenopausal osteoporosis (bisphosphonates, parathyroid hormone, strontium ranelate, and denosumab) on bone quality: a systematic review. Calcified Tissue International 2010;87:469-84.

[107] MacLean C, Newberry S, Maglione M, McMahon M, Ranganath V, Suttorp M, et al. Systematic Review : Comparative Effectiveness of Treatments to Prevent Fractures in Men and Women with Low Bone Density or Osteoporosis. Annals of Internal Medicine 2008;148:197-213.

[108] Lips P. Vitamin D deficiency and secondary hyperparathyroidism in the elderly: consequences for bone loss and fractures and therapeutic implications. Endocrine Reviews 2001;22:477-501.

[109] Bell TD, Demay MB, Burnett-Bowie SM. The biology and pathology of vitamin D control in bone. Journal of Cellular Biochemistry 2010;111:7-13.

[110] Chapuy MC, Arlot ME, Duboeuf F, Brun J, Crouzet B, Arnaud S, et al. Vitamin D3 and Calcium to Prevent Hip Fractures in Elderly Women. New England Journal of Medicine 1992:1637-1642.

[111] Recker RR, Hinders S, Davies KM, Heaney RP, Stegman MR, Lappe JM, et al. Correcting calcium nutritional deficiency prevents spine fractures in elderly women. Journal of Bone and Mineral Research 1996;11:1961-6.

[112] Chapuy M, Arlot ME, Delmas PD, Meunier PJ, Strang J, Griffiths P, et al. Effect of calcium and cholecalciferol treatment for three years on hip fractures in elderly women. British Medical Journal 1994;308:1081-1082.

[113] Lips P, Graafmans WC, Ooms ME, Bezemer PD, Bouter LM. Vitamin D supplementation and fracture incidence in elderly persons. A randomized, placebo-controlled clinical trial. Annals of internal medicine 1996;124:400-6.

[114] Drake MT, Clarke BL, Khosla S. Bisphosphonates: mechanism of action and role in clinical practice. Mayo Clinic Proceedings 2008;83:1032-45.

[115] FDA. U.S. Food and Drug Administration Drug Labels. Drugs@FDA 2012. Available: http://www.accessdata.fda.gov/scripts/cder/drugsatfda/. Accessed 24 Mar 2012.

[116] WHO. WHO Pharmaceuticals Newsletter 2002, No. 3. 2002.

[117] Nelson HD, Humphrey LL, Nygren P, Teutsch SM, Allan JD. Postmenopausal Hormone Replacement Therapy. 2012;288.

[118] Greenblatt D. Treatment of postmenopausal osteoporosis. Pharmacotherapy 2005;25:574-84.

[119] Cauley JA, Seeley DG, Ensrud K, Ettinger B, Black D, Cummings SR. Estrogen replacement therapy and fractures in older women. Study of Osteoporotic Fractures Research Group. Annals of Internal Medicine 1995;122:9-16.

[120] Felson DT, Zhang Y, Hannan MT, Kiel DP, Wilson PWF, Anderson JJ. The effect of postmenopausal estrogen therapy on bone density in elderly women. The New England Journal of Medicine 1993;329.

[121] Christiansen C, Transb IB. Bone mass in postmenopausal women after withdrawal of oestrogen/gestagen replacement therapy. The Lancet 1981;1:459-461.

[122] Riggs BL, Hartmann LC. Selective estrogen-receptor modulators -- mechanisms of action and application to clinical practice. Journal of Medicine Cincinnati 2003;348.

[123] Neele SJM, Evertz R, De Valk-De Roo G, Roos JC, Netelenbos JC. Effect of 1 year of discontinuation of raloxifene or estrogen therapy on bone mineral density after 5 years of treatment in healthy postmenopausal women. Bone 2002;30:599-603.

[124] Eastell R, Walsh JS, Watts NB, Siris E. Bisphosphonates for postmenopausal osteoporosis. Bone 2011;49:82-8.

[125] Ebetino FH, Hogan A-ML, Sun S, Tsoumpra MK, Duan X, Triffitt JT, et al. The relationship between the chemistry and biological activity of the bisphosphonates. Bone 2011;49:20-33.

[126] Rogers MJ, Crockett JC, Coxon FP, Mönkkönen J. Biochemical and molecular mechanisms of action of bisphosphonates. Bone 2010;49:34-41.

[127] Ensrud KE, Barrett-Connor EL, Schwartz A, Santora AC, Bauer DC, Suryawanshi S, et al. Randomized trial of effect of alendronate continuation versus discontinuation in women with low BMD: results from the Fracture Intervention Trial long-term extension. Journal of Bone and Mineral Research 2004;19:1259-69.

[128] Shane E, Burr D, Ebeling PR, Abrahamsen B, Adler R a, Brown TD, et al. Atypical subtrochanteric and diaphyseal femoral fractures: report of a task force of the American Society for Bone and Mineral Research. Journal of Bone and Mineral Research 2010;25:2267-94.

[129] Boivin G, Meunier PJ. Effects of bisphosphonates on matrix mineralization. Journal of Musculoskeletal Neuronal Interactions 2002;2:538-543.

[130] Boivin G, Chavassieux PM, Santora AC, Yates J, Meunier PJ. Alendronate increases bone strength by increasing the mean degree of mineralization of bone tissue in osteoporotic women. Bone 2000;27:687-694.

[131] Bellido T, Plotkin LI. Novel actions of bisphosphonates in bone: Preservation of osteoblast and osteocyte viability. Bone 2011;49:50-5.

[132] Sambrook PN, Geusens P, Ribot C, Solimano JA, Ferrer-Barriendos J, Gaines K, et al. Alendronate produces greater effects than raloxifene on bone density and bone turnover in postmenopausal women with low bone density: results of EFFECT (Efficacy of FOSAMAX versus EVISTA Comparison Trial) International. Journal of Internal Medicine 2004;255:503-511.

[133] Kirk JK, Hepfinger C. Calcitonin. Clinical Reviews in Bone and Mineral Metabolism 2005;3:39-49.

[134] Pondel M. Calcitonin and calcitonin receptors: bone and beyond. International Journal of Experimental Pathology 2000;81:405-22.

[135] Stepan JJ, Alenfeld F, Boivin G, Feyen JHM, Lakatos P. Mechanisms of action of antiresorptive therapies of postmenopausal osteoporosis. Endocrine Regulations 2003;37:225-38.

[136] Zaidi M, Moonga BS, Abe E. Calcitonin and bone formation : a knockout full of surprises. Journal of Clinical Investigation 2002;110:1769-1771.

[137] Miller PD. Denosumab: anti-RANKL antibody. Current Osteoporosis Reports 2009;7:18-22.

[138] Roodman GD. Regulation of osteoclast differentiation. Annals of the New York Academy of Sciences 2006;1068:100-9.

[139] Lewiecki EM. Drug evaluation RANK ligand inhibition with denosumab for the management of osteoporosis. Expert Opinion on Biological Therapy 2006;6:1041-1050.

[140] Iqbal J, Sun L, Zaidi M. Denosumab for the treatment of osteoporosis. Current Osteoporosis Reports 2010;8:163-7.

[141] Salari Sharif P, Abdollahi M, Larijani B. Current, new and future treatments of osteoporosis. Rheumatology International 2011;31:289-300.

[142] File E, Deal C. Clinical update on teriparatide. Current Rheumatology Reports 2009;11:169-76.

[143] Hodsman AB, Bauer DC, Dempster DW, Dian L, Hanley DA, Harris ST, et al. Parathyroid hormone and teriparatide for the treatment of osteoporosis: a review of the evidence and suggested guidelines for its use. Endocrine Reviews 2005;26:688-703.

[144] Quattrocchi E, Kourlas H. Teriparatide : A Review. Clinical Therapeutics 2004;26.

[145] Poole KES, Reeve J. Parathyroid hormone - a bone anabolic and catabolic agent. Current Opinion in Pharmacology 2005;5:612-7.

[146] Datta NS, Abou-Samra AB. PTH and PTHrP signaling in osteoblasts. Cellular Signaling 2009;21:1245-54.

[147] Bilezikian JP. Combination anabolic and antiresorptive therapy for osteoporosis: opening the anabolic window. Current Osteoporosis Reports 2008;6:24-30.

[148] Keaveny TM, Donley DW, Hoffmann PF, Mitlak BH, Glass EV, Martin JAS. Effects of Teriparatide and Alendronate on Vertebral Strength as Assessed by Finite Element Modeling of QCT Scans in Women With Osteoporosis. Journal of Bone and Mineral Research 2007;22.

[149] Riggs BL, Parfitt AM. Drugs used to treat osteoporosis: the critical need for a uniform nomenclature based on their action on bone remodeling. Journal of Bone and Mineral Research 2005;20:177-84.

[150] Deeks ED, Dhillon S. Strontium Ranelate. Drugs 2010;70:733-759.

[151] Christiansen BA, Kopperdahl DL, Kiel DP, Keaveny TM, Bouxsein ML. Mechanical contributions of the cortical and trabecular compartments contribute to differences in age-related changes in vertebral body strength in men and women assessed by QCT-based finite element analysis. Journal of Bone and Mineral Research 2010;26:974-983.

[152] Riggs BL, Melton LJ, Robb R A, Camp JJ, Atkinson EJ, Peterson JM, et al. Population-based study of age and sex differences in bone volumetric density, size, geometry, and structure at different skeletal sites. Journal of Bone and Mineral Research 2004;19:1945-54.

[153] Eswaran S, Gupta A, Adams M, Keaveny T. Cortical and trabecular load sharing in the human vertebral body. Journal of Bone and Mineral Research 2006;21:307-314.

[154] Paschalis EP, Betts F, DiCarlo E, Mendelsohn R, Boskey AL. FTIR microspectroscopic analysis of human iliac crest biopsies from untreated osteoporotic bone. Calcified Tissue International 1997;61:487-92.

[155] Homminga J, McCreadie BR, Ciarelli TE, Weinans H, Goldstein SA, Huiskes R. Cancellous bone mechanical properties from normals and patients with hip fractures differ on the structure level, not on the bone hard tissue level. Bone 2002;30:759-764.

[156] Homminga J, Van-Rietbergen B, Lochmüller EM, Weinans H, Eckstein F, Huiskes R. The osteoporotic vertebral structure is well adapted to the loads of daily life, but not to infrequent "error" loads. Bone 2004;34:510-516.

[157] Allen MR, Hogan HA, Hobbs WA, Koivuniemi AS, Koivuniemi MC, Burr DB. Raloxifene enhances material-level mechanical properties of femoral cortical and trabecular bone. Endocrinology 2007;148:3908-13.

[158] Boskey AL, DiCarlo E, Paschalis E, West P, Mendelsohn R. Comparison of mineral quality and quantity in iliac crest biopsies from high- and low-turnover osteoporosis: an FT-IR microspectroscopic investigation. Osteoporosis International 2005;16:2031-2038.

[159] McCreadie BR, Morris MD, Chen T-C, Sudhaker Rao D, Finney WF, Widjaja E, et al. Bone tissue compositional differences in women with and without osteoporotic fracture. Bone 2006;39:1190-1195.

[160] Gadeleta SJ, Boskey AL, Paschalis E, Carlson C, Menschik F, Baldini T, et al. A physical, chemical, and mechanical study of lumbar vertebrae from normal, ovariectomized, and nandrolone decanoate-treated cynomolgus monkeys (Macaca fascicularis). Bone 2000;27:541-50.

[161] Wang X, Shen X, Li X, Agrawal CM. Age-related changes in the collagen network and toughness of bone. Bone 2002;31:1-7.

[162] Boskey AL, Spevak L, Weinstein RS. Spectroscopic markers of bone quality in alendronate-treated postmenopausal women. Osteoporosis International 2009;20:793-800.

[163] Fuchs RK, Faillace ME, Allen MR, Phipps RJ, Miller LM, Burr DB. Bisphosphonates do not alter the rate of secondary mineralization. Bone 2011;49.

[164] Roschger P, Fratzl P, Klaushofer K, Rodan G. Mineralization of cancellous bone after alendronate and sodium fluoride treatment: a quantitative backscattered electron imaging study on minipig ribs. Bone 1997;20:393-397.

[165] Allen MR, Reinwald S, Burr DB. Alendronate reduces bone toughness of ribs without significantly increasing microdamage accumulation in dogs following 3 years of daily treatment. Calcified Tissue International 2008;82:354-60.

[166] Brennan TC, Rizzoli R, Ammann P. Selective Modification of Bone Quality by PTH, Pamidronate, or Raloxifene. Journal of Bone and Mineral Research. 2009;24:800-808.

[167] Sipos A, Dobnig H, Stepan JJ, Burr DB, Li J, Michalska D. Teriparatide Reduces Bone Microdamage Accumulation in Postmenopausal Women Previously Treated With Alendronate*. Journal of Bone and Mineral Research 2009;24:1998-2006.

[168] Akkus O, Polyakova-Akkus A, Adar F, Schaffler MB. Aging of microstructural compartments in human compact bone. Journal of Bone and Mineral Research 2003;18:1012-1019.

[169] Rho JY, Roy ME, Tsui TY, Pharr GM. Elastic properties of microstructural components of human bone tissue as measured by nanoindentation. Journal of biomedical materials research 1999;45:48-54.

[170] Havill LM, Mahaney MC, Czerwinski SA, Carey KD, Rice K, Rogers J. Bone mineral density reference standards in adult baboons (Papio hamadryas) by sex and age. Bone 2003;33:877-888.

[171] Burket JC, Gourion-Arsiquaud S, Havill LM, Baker SP, Boskey AL, van der Meulen MCH. Microstructure and nanomechanical properties in osteons relate to tissue and animal age. Journal of Biomechanics 2011;44:277-84.

[172] MacLeay JM, Olson JD, Enns RM, Les CM, Toth CA, Wheeler DL, et al. Dietary-induced metabolic acidosis decreases bone mineral density in mature ovariectomized ewes. Calcified Tissue International 2004;75:431-437.

[173] Macleay JM, Olson JD, Turner AS. Effect of dietary-induced metabolic acidosis and ovariectomy on bone mineral density and markers of bone turnover. Journal of Bone and Mineral Metabolism 2004;22:561-568.

[174] Macleay JM, Sullivan E, Jackinsky S, Les C, Turner A. Ovine modeling of dietary induced metabolic acidosis and bone loss. International Congress Series 2007;1297:282-285.

[175] Burstein AH, Zika JM, Heiple KG, Klein L. Contribution of collagen and mineral to the elastic-plastic properties of bone. The Journal of Bone and Joint Surgery 1975;57:956-961.

[176] Russell RGG. Bisphosphonates: The first 40years. Bone 2011;49:2-19.

CHAPTER 2

MICROSTRUCTURE AND NANOMECHANICAL PROPERTIES IN OSTEONS RELATE TO TISSUE AND ANIMAL AGE*

2.1 Introduction

The incidence of osteoporotic fracture increases dramatically with ageing [1,2]. Measures of bone mass and architecture alone are inadequate for predicting age-related fracture risk [3–5]. Tissue-level material properties are a missing component in our knowledge of ageing and bone fragility, but are clearly critical to understanding skeletal mechanical integrity. Nano-scale variability of the elastic modulus in healthy bone hinders crack propagation and acts as a toughening mechanism [6,7]. In addition, osteoporosis alters the nano-scale heterogeneity of the material properties and composition of bone tissue [8–10].

To understand the skeletal changes leading to osteoporosis and age-related fracture, one must first understand the natural variations that occur in healthy bone tissue with ageing [11]. Due to the remodeling process, bones from a single animal contain tissue of varying ages; thus, tissue age within a given animal is not the same as the animal's age. In primates, the Haversian remodeling process creates a natural gradient in tissue age across the osteon [12]. In this process, osteoclasts travel along the Haversian canal and resorb a cylindrical volume of bone surrounding the blood vessel. Osteoblasts follow the osteoclasts and form layers of bone to refill the resorbed cylinder, starting at the periphery and finishing at the center near the blood vessel 2 to 4 months after the process was initiated [13]. Hence, in a section transverse to the Haversian canal, osteons appear as concentric ring-like structures, with the newest tissue located at the center nearest to the blood vessel, and the oldest tissue located at the periphery of the osteon.

Tissue-level variations in composition and mechanical properties with either tissue or animal age have been studied individually, producing mixed results [14–19]. As a consequence,

* Burket JC, Gourion-Arsiquaud S, Havill LM, Baker SP, Boskey AL, van der Meulen MCH. Microstructure and nanomechanical properties relate to tissue and animal age. Journal of Biomechanics 2011; 44(2): 277-284.

relationships between these properties and ageing in humans are still unclear. Even fewer studies have related tissue composition to mechanical function [20–22]. Furthermore, material variations have only been examined over limited age ranges [14,18,19,23]. As tissue composition plays a crucial role in determining mechanical function, understanding these relationships will improve our understanding of normal and pathological bone function and may enable us to improve upon current therapies for skeletal diseases such as osteoporosis. In rodent models, tissue composition and mechanical properties varied systematically with tissue age in newly formed tissue [21,22]; however, cortical microstructure and skeletal ageing processes of rodents differ markedly from those of humans.

The present study utilized the natural gradient in relative tissue age across osteons in female baboons to study tissue age and animal age-related variations in tissue composition and mechanical properties over the entire lifespan of the animal. Baboon bone is an excellent model for human bone because baboons have a similar Haversian microstructure resulting from secondary remodeling and also experience a similar ageing process, including increased skeletal fragility [24,25]. The maximum lifespan of a baboon is approximately 1/3 that of the human, with sexual maturity occurring around five years of age [26,27]. This lifespan is sufficiently long to elicit reproductive senescence and menopause, accompanied by changes in hormone levels that are important in bone metabolism and loss [24,28,29].

The goals of this study were to characterize changes in nanomechanical properties and tissue composition with both tissue age (relative and animal age over the entire lifespan of the baboon, and to examine relationships between tissue composition and mechanical properties. In a previous study of the baboon samples utilized here, preliminary analyses with Raman spectroscopy and more extensive analyses with Fourier transform infrared spectroscopic imaging (FTIRI) showed variations in compositional parameters with both tissue and animal age [12]. However, variations in mechanical parameters were examined only with tissue age in one age group (13 years old). We hypothesized that tissue mechanical properties would vary with

changes in mineral and aligned collagen content as a function of both tissue and animal age in a non-human primate model.

2.2 Materials and Methods

2.2.1 Samples and Specimen Preparation.

Femoral bone samples were obtained from twelve female baboons examined previously [12], aged 0.28 to 32.45 years, representing the majority of the baboon lifespan [27]. All animals were housed outdoors in group housing at Southwest National Primate Research Center/Southwest Foundation for Biomedical Research (SNPRC/SFBR, San Antonio, TX) and had no evidence of metabolic bone disease. The Institutional Animal Care and Use Committee approved all procedures at SNPRC/SFBR, and no animals were euthanized specifically for this study.

After necropsy, the femurs were wrapped in saline soaked gauze and stored at -20º C. The femurs were fixed, dehydrated, and embedded in polymethlymethacrylate [30]. Transverse sections from the midshaft were polished anhydrously to achieve a root mean square surface roughness less than 15 nm on a 5 μm x 5 μm AFM scan (Dimension 3100, Veeco Metrology Group) [31].

Three osteons per sample were selected for characterization by nanoindentation, Raman spectroscopy and SHG, and three radial lines were characterized within each osteon (Figure 2.1). To sample a consistent anatomical area between samples, osteons were selected from the postero-lateral quadrant of the femurs, within 2 mm of the endosteal surface (Figure 2.1). The osteons did not have widened Haversian canals and lamella near the canals were well-formed and not eroded, suggesting that these osteons were not remodeling at the time of animal death.

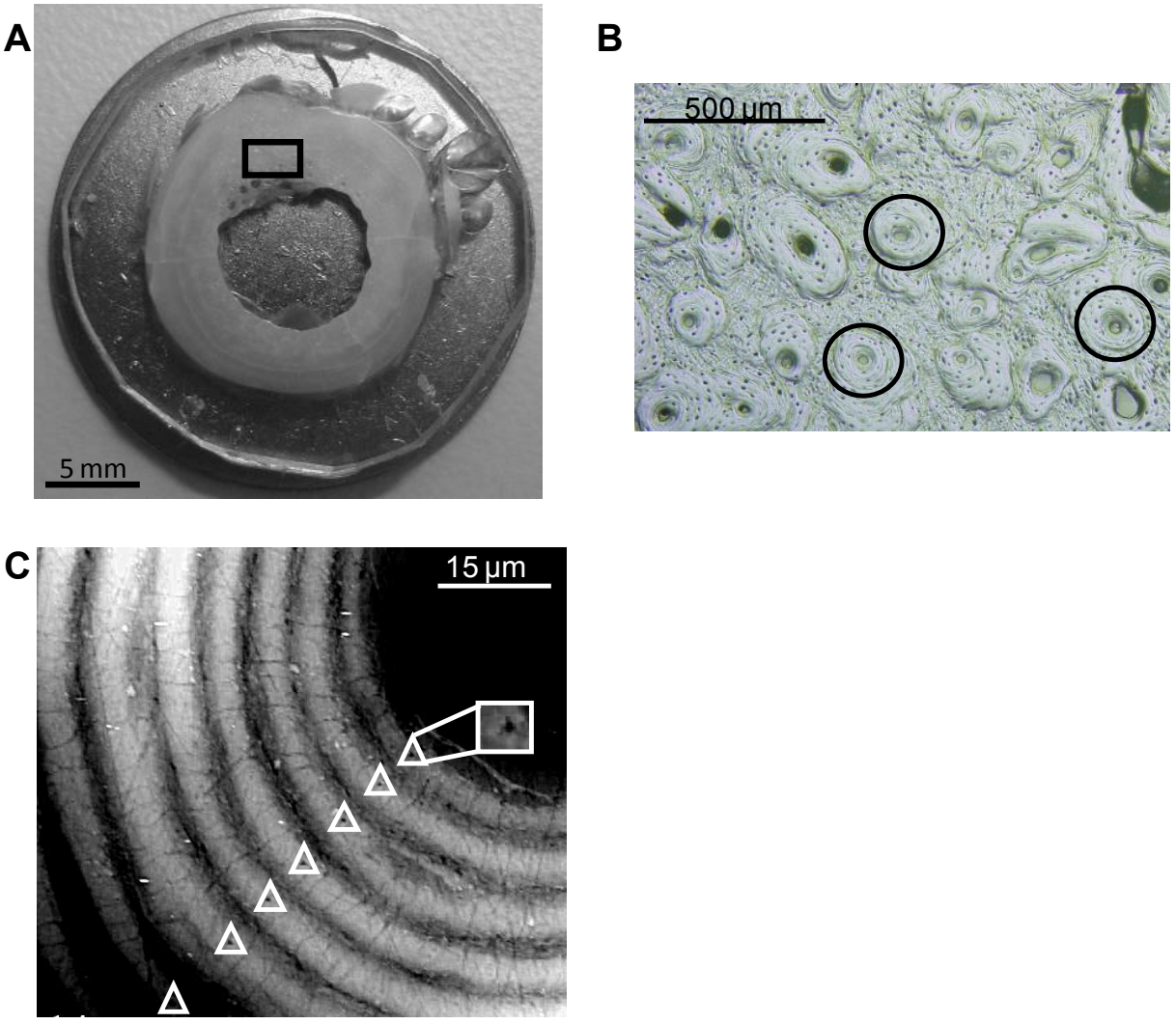

Figure 2.1 *(A) Cross section of a baboon femur embedded in polymethlymethacrylate showing the area chosen for characterization. (B) Light microscopy image of the area boxed in part (A) with specific osteons chosen for characterization circled. (C) Atomic force microscopy image of a quadrant of one of the osteons showing one radial line that was characterized with nanoindentation, Raman spectroscopy, and second harmonic generation. The residual indentations are visible in the white triangles. The insert shows a magnified view of a residual indentation.*

2.2.2 Nanoindentation.

Nanoindentation was used to probe the tissue nanomechanical properties. As nanoindentation tests volumes of material at a length scale less than that of individual microstructural features in bone, this technique avoids confounding factors such as microstructure and porosity that affect tissue properties at larger length scales [32,33]. A 20 μm x 20 μm surface topography scan was made with the scanning nanoindenter (TriboIndenter, Hysitron, Inc.) prior to each indentation to place them at the center of lamellae, ensuring that comparable material was sampled between measurements (Figure 2.1) [31,34]. Each osteon contained between 5 and 15 lamellae that were characterized along 3 radial lines, resulting in 15 to 45 indentations per osteon (~ 45 to 135 per animal). The tip was loaded into the sample at a rate of 50 μN/s, held at a maximum load of 700 μN for 10 s, and then unloaded at a rate of 50 μN/s [31,34], resulting in ~150 nm deep indentations. The indentation modulus and hardness were calculated from the unloading portion of the load-displacement curve [35].

2.2.3 Raman Spectroscopy

Raman spectroscopy was used to characterize the tissue composition. Spectra were collected using a near-infrared, 785 nm laser focused through a 50x, 0.75 numerical aperture air objective (InVia microRaman, Renishaw), producing 2 μm diameter beam. Peak heights were identified after subtracting background fluorescence using WiRE^{TM} V2.0 software (Renishaw). Spectra were taken on 5 lamellae spaced across the radii of the osteons, resulting in 15 measurements per osteon (45 per animal). Spectra were acquired along the same radial lines characterized with nanoindentation and centered on lamellae when visible to match the nanoindentation locations as closely as possible.

Three bone parameters were calculated: mineral-to-matrix ratio, carbonate-to-phosphate ratio, and crystallinity [12,14,23,36–38]. Mineral-to-matrix ratio, a measure of the degree of mineralization of the tissue, was calculated as the ratio of the phosphate υ1 (~965 cm^{-1}) to the

CH_2 wag (~1450 cm^{-1}) peaks [23]. The CH_2 wag peak was used due to noise around the Amide I peak. Carbonate-to-phosphate ratio, a measure of the level of carbonate substitution into the hydroxyapatite crystal lattice, was calculated as the ratio of the carbonate υ1 (~1070 cm^{-1}) to the phosphate υ1 peak [37]. Crystallinity, a measure of crystal size and perfection, was estimated as the reciprocal of the full width at half maximum of the phosphate υ1 peak (FWHM) [36]. For this measure, a sharper phosphate υ1 peak (smaller FWHM) indicates greater mineral crystal size and perfection.

2.2.4 Second Harmonic Generation Microscopy (SHG).

SHG microscopy utilizes nonlinear scattering of photons from aligned collagen fibers within bone to create a map of aligned collagen content. These measurements distinguish whether the collagen contained in the plane of measurement, in this case the transverse plane, is aligned within that plane. The aligned collagen within the plane is proportional to the square root of SHG intensity [39–43]. A 2.5 W Ti:Sapphire (Mai Tai Deep See, Spectra Physics), with a pulse rate of 80 MHz at 780 nm was focused onto the samples with a 25x, 1.05 numerical aperture water objective (Olympus). SHG photons were collected in epi mode and optically filtered to remove backscattered incident light. In-plane and out-of-plane focal volume dimensions (FWHM) were approximately 497 nm and 1500 nm, respectively. SHG images of the three osteons analyzed with Raman spectroscopy and nanoindentation were taken as the Kalman average of 3 scans.

The three radial lines per osteon characterized with nanoindentation and Raman spectroscopy were located on the SHG images. For each pixel along the radial lines, the square root of the SHG intensity was averaged for a window 1 pixel wide and 4 pixels high (497 nm x 1988 nm, Image J, National Institutes of Health). For each lamella, maxima corresponding to lamellar aligned collagen and minima corresponding to interlamellar aligned collagen were recorded. Each osteon contained between 5 and 15 lamella, hence 15 to 45 maxima and minima

were recorded per osteon (~45 to 135 per animal). The relative degree of aligned collagen for each lamellae was calculated as the peak height ratio of lamellar to interlamellar aligned collagen [31,34,44]. To isolate the contributors to changes in peak height ratio, lamellar and interlamellar values were determined individually and normalized by the mean aligned collagen content of the osteon to correct for intensity variations.

2.2.5 Data Analysis

All statistical testing for variations with animal and tissue age were performed on the raw, unaveraged data using linear models (JMP 7.0, SAS Institute, Inc.), with animal age (0.28-32.45 years, n=12 animals), osteon (1–3, nested variable), radial line (1–3, nested variable), and distance from the center of the osteon (0-80 μm, representative of tissue age) as factors. First, multi-factor ANOVAs tested whether relationships between parameters and animal age or tissue age depended on maturity (young, 0–5 years old, or mature, >5 years old) [27]. If maturity was not significant, a multi-factor ANOVA was performed on the combined data. If maturity was significant, separate multifactor ANOVAs were run for young and mature data. P-values less than 0.05 were considered significant.

To correlate nanomechanical properties with compositional measures, the mean values of the outcome measures were calculated for each baboon. Single-factor ANOVAs tested for the individual effect of each compositional measure on indentation modulus and hardness. Then, multi-factor ANOVAs determined the combination of compositional parameters with greatest predictive power for indentation modulus and hardness. A change of 0.05 in the coefficient of variation (R^2) was considered an improved model fit.

To visualize the tissue age data, results for a single animal were averaged by binning in 6 μm increments across the 3 radii of the 3 sampled osteons. Specifically, the mean distance from the center of the osteon and mean parameter values were calculated for each 6 μm bin of the indentation modulus and Raman data.

2.3 Results

Sexual maturity (age≤5 years) significantly influenced indentation modulus but tissue age did not. Indentation modulus increased steeply with animal age across young, sexually immature animals and increased gradually across sexually mature animals (Figure 2.2). The magnitude of the increases were 1.85 GPa, or about 6.6%, per year across young animals ($p<0.0001$, ages 0.28 to 2.81 years, n=6), and only 0.08 GPa, or 0.2% per year, across sexually mature animals ($p=0.0058$, ages 6.21 to 32.45 years, n=6) (Table 2.1). Indentation modulus did not vary with tissue age across the osteon (Figure 2.2).

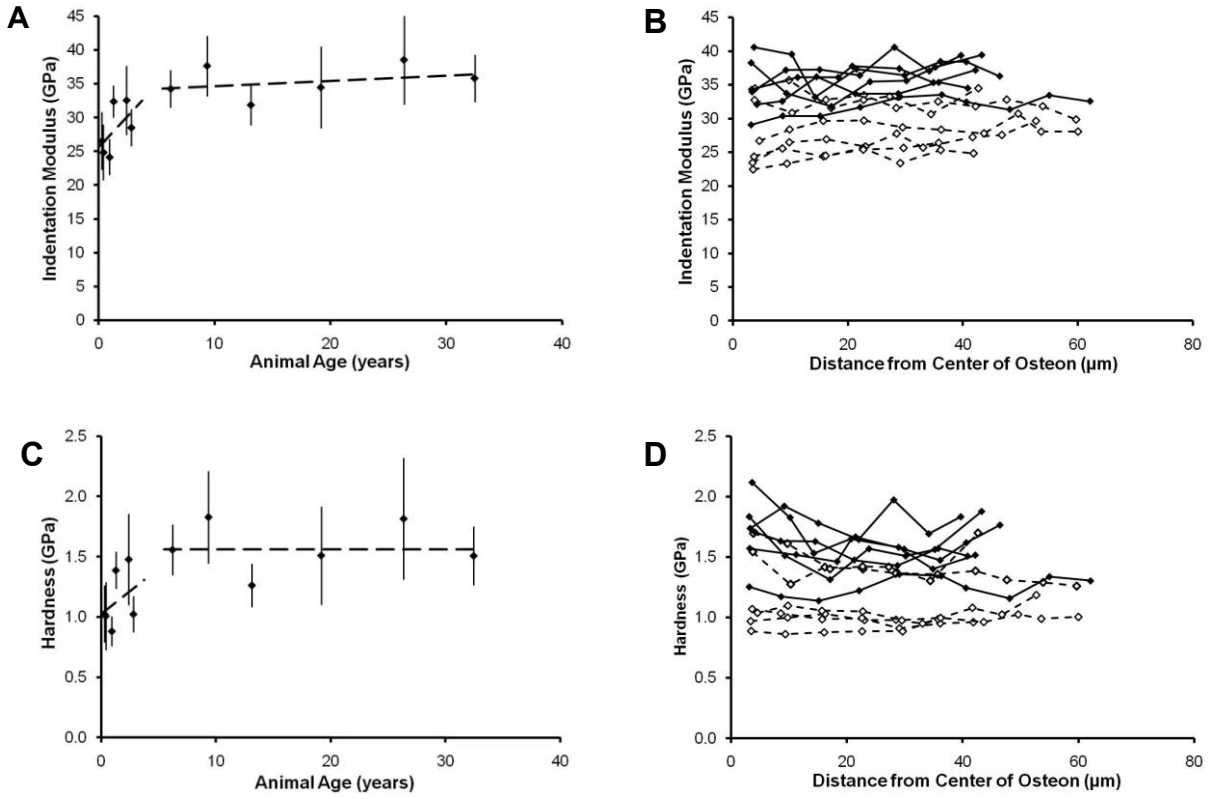

Figure 2.2 *Nanoindentation results versus animal and tissue age (A) Indentation modulus and (C) hardness increased with animal age in the young animals and were constant after sexual maturity. Each point in (A) and (C) represents the mean ± SD of all measurements for a single animal (means ± SD used only for visual representation). The dashed lines are from the ANOVA models for young and mature animals, which were performed on the raw, unaveraged data (45-135 measurements per animal). (B) Indentation modulus and (D) hardness were constant with tissue age. Increasing distance from the center of the osteon corresponds with increasing tissue age. Open symbols with dashed lines represent young animals and solid symbols with solid lines represent mature animals.*

Table 2.1 *Significant variations of mechanical and compositional measures with animal and tissue age. Ranges reported for percent change across the osteon reflect variable osteon size. NS = not significant, p ≥ 0.05; young = 0 – 5 years; mature > 5 years.*

	Animal Age (% Change Per Year)		Tissue Age (% Change Across Osteon)	
	Young	Mature	Young	Mature
Indentation Modulus	6.6	0.20	NS	
Hardness	6.8	NS	NS	-9 to -18
Mineral:Matrix	12	NS	NS	
Carbonate:Phosphate	6.7	NS	6 to 12	
Crystallinity	0.08		3 to 6	1.2 to 2.4
Peak Height Ratio	4.6	0.45	6 to 12	

Hardness was significantly influenced by both sexual maturity and tissue age (Figure 2.2). Hardness increased steeply across young animals but showed no correlation with animal age in sexually mature animals (Figure 2.2). In young animals, hardness increased 0.08 GPa, or about 6.8%, per year ($p<0.0001$, Table 2.1). Hardness did not vary with tissue age across the osteon radii in young animals, but decreased with tissue age in mature animals, decreasing by 0.3% per micron for a total decrease of 9-18% across the osteon radii ($p=0.0008$).

Mineral-to-matrix ratio was affected by animal age but not tissue age. Mineral-to-matrix ratio increased by 0.88, or about 12%, per year across young animals ($p<0.0001$), but was independent of age in mature animals (Table 2.1, Figure 2.3). Mineral-to-matrix ratio was not correlated with tissue age across the osteon radii.

Carbonate-to-phosphate ratio was affected by both animal age and tissue age. Carbonate-to-phosphate ratio increased by 0.01, or 6.7%, per year across young animals ($p<0.0001$) and was independent of animal age after sexual maturity (Table 2.1, Figure 2.3). Carbonate-to-phosphate ratio increased with tissue age across the osteon radii in both young and mature animals, increasing by 0.2% per micron ($p<0.0001$).

Crystallinity varied with both animal age and tissue age. Crystallinity increased by 0.08% per year with animal age regardless of maturity ($p<0.0001$, Table 2.1, Figure 2.3), while

the increase in crystallinity with tissue age was greater in young than in mature animals. In young animals, crystallinity increased by 0.1% per micron or 3-6% total across the osteon radii ($p<0.0001$). In mature animals, the magnitude of the increase with tissue age was less than half that which occurred in young animals, 0.04% per micron or 1.2-2.4% total across the osteon radii ($p<0.0001$).

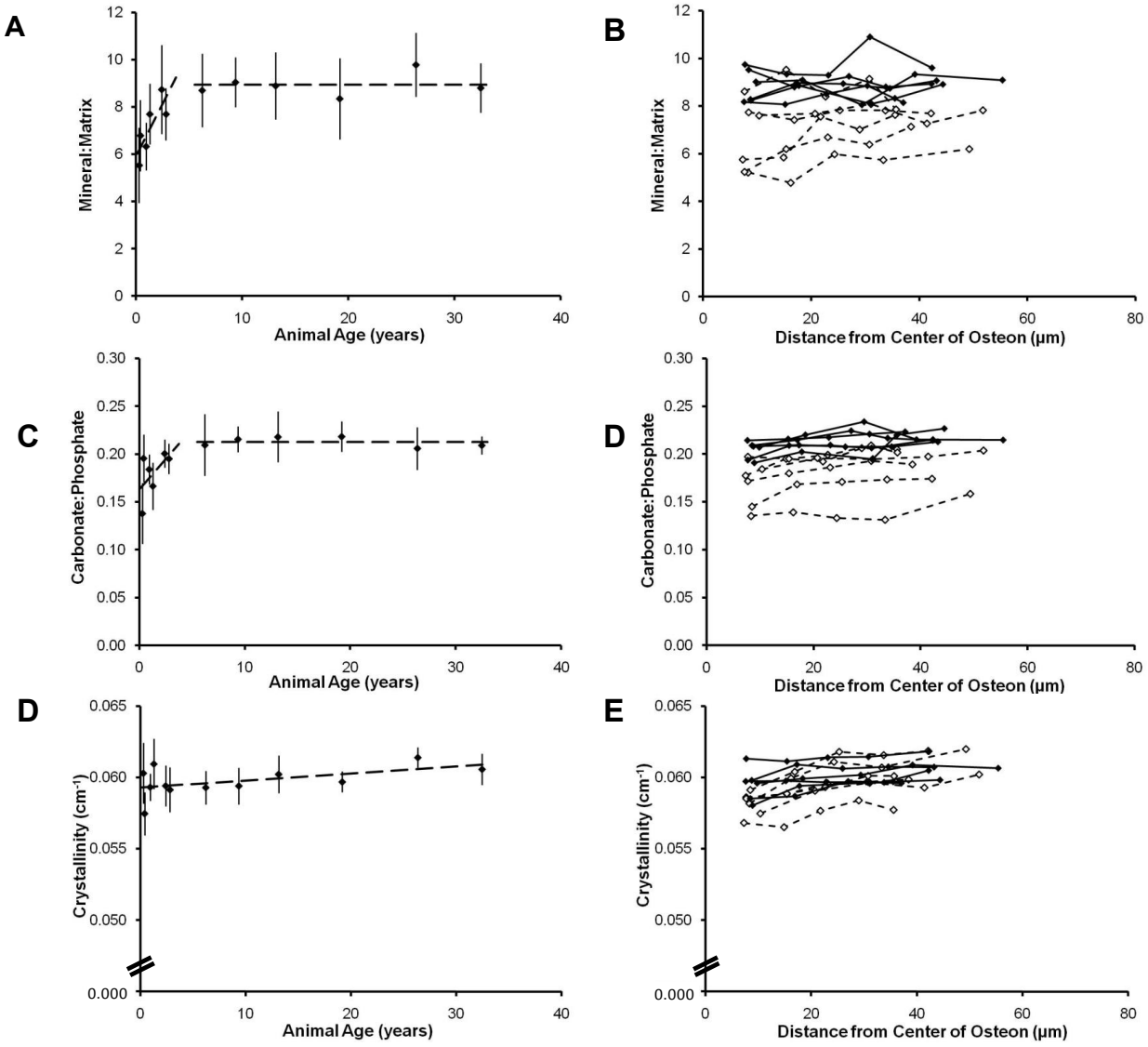

Figure 2.3 *Raman spectroscopy results versus animal and tissue age. (A) Mineral-to-matrix ratio and (C) carbonate substitution both increased in the young animals and were constant after sexual maturity, whereas (E) crystallinity increased with animal age independent of maturity. Each point in (A), (C), and (E) represents the mean ± SD of all measurements for a single animal (means ± SD used only for visual representation). The dashed lines are from the ANOVA models, which were performed on the raw, unaveraged data (45 measurements per animal) (B) Mineral to matrix ratio showed no change with tissue age, whereas (D) carbonate substitution increased with animal age, independent of maturity, and (F) crystallinity increased with tissue age faster in young than in mature animals. Increasing distance from the center of the osteon corresponds with increasing tissue age. Open symbols with dashed lines represent young animals and solid symbols with solid lines represent mature animals.*

Aligned collagen content varied with tissue and animal age (Figure 2.4). The peak height ratio of lamellar to interlamellar aligned collagen increased by 4.6% per year with animal age in young animals, and by 0.45% per year in mature animals ($p<0.0001$) (Table 2.1). This increase with animal age was due to both increased lamellar aligned collagen (+2.7% per year in young animals, and +0.22% per year in mature animals) and decreased interlamellar aligned collagen with animal age (-1.5% per year in young animals, -0.20% per year in mature animals). With tissue age, collagen peak height ratio increased by 0.19% per micron, for a total increase of 6 to 12% across the osteon radii, regardless of animal age ($p<0.0001$). This increase was primarily due to increased lamellar aligned collagen (+0.30% per micron in all animals).

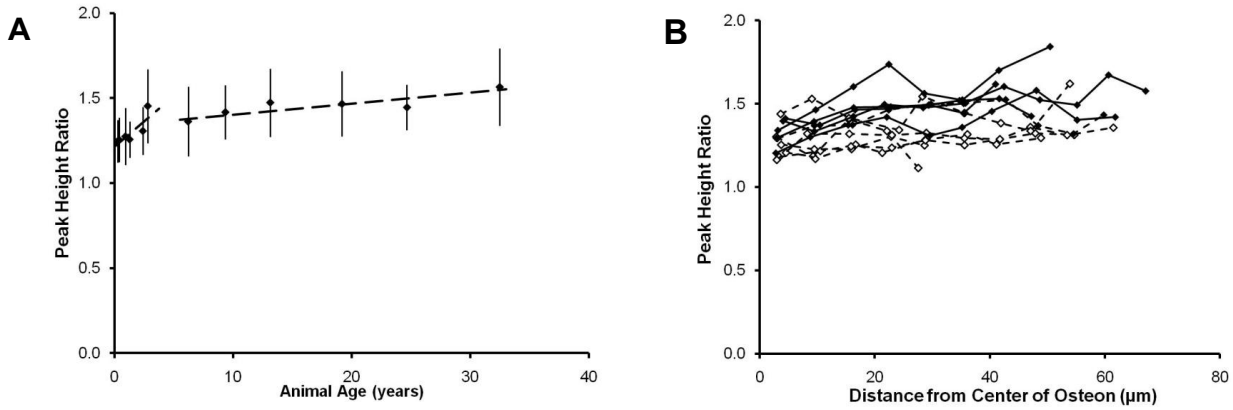

Figure 2.4 *SHG results with animal and tissue age. (A) Peak height ratio (lamellar/interlamellar aligned collagen) increased more with animal age in young than in mature animals. Each point represents the mean ± SD of all measurements for a single animal (means ± SD used only for visual representation). The dashed lines are from the ANOVA models for young and mature animals, which were performed on the raw, unaveraged data (45-135 measurements per animal) (B) Peak height ratio increased with tissue age. Increasing distance from the center of the osteon corresponds with increasing tissue age. Open symbols with dashed lines represent young animals and solid symbols with solid lines represent mature animals.*

When correlations between nanomechanical properties and composition were examined, indentation modulus and hardness were most influenced by mineral-to-matrix ratio (Figure 2.5). Mineral-to-matrix ratio alone explained 78% of the variation in indentation modulus ($p<0.0001$) and 70% of the variation in hardness ($p<0.0004$). The only other significant relationship was with lamellar aligned collagen, which explained 30% of the variation in indentation modulus

(p=0.0386), but did not significantly predict the variation in hardness (p=0.0939). Combining lamellar aligned collagen with mineral-to-matrix ratio did not improve the predictive power for indentation modulus.

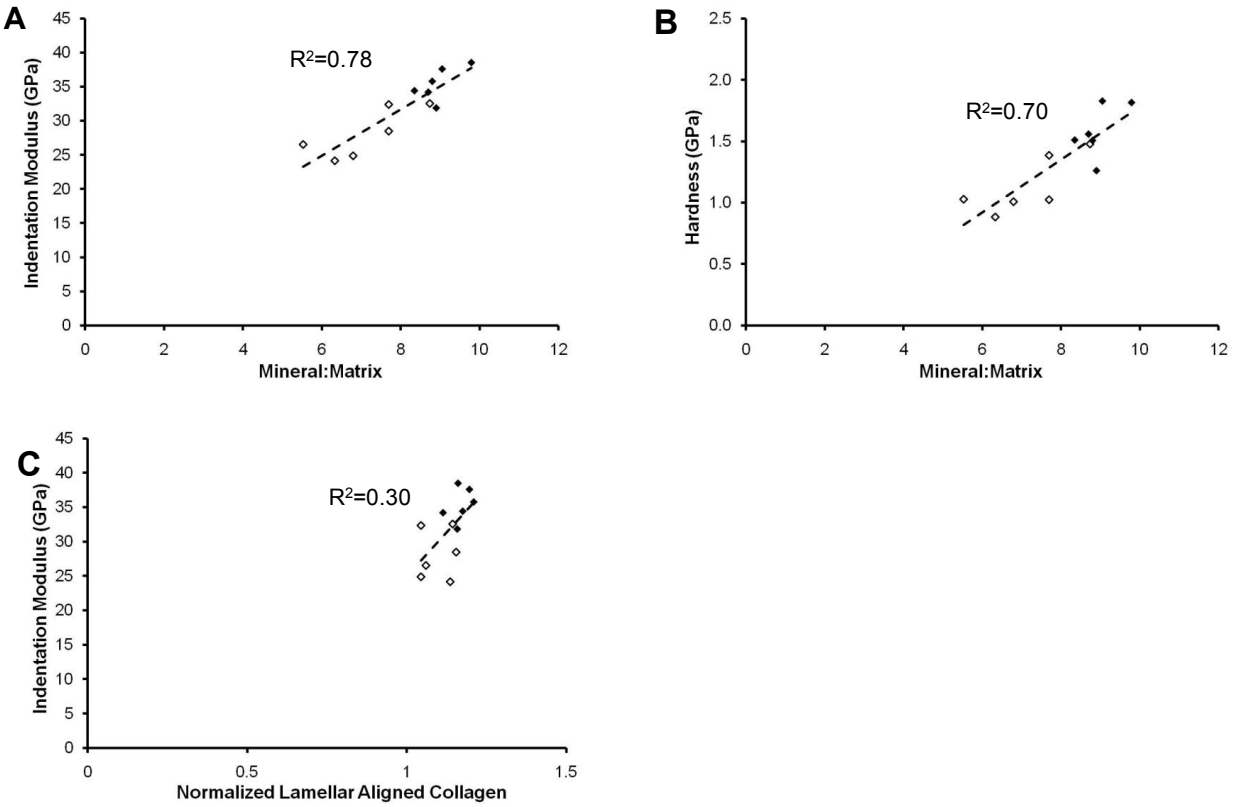

Figure 2.5 *Significant correlations between mean nanomechanical parameters and composition measures obtained from each animal. Open symbols represent young animals and solid symbols represent mature animals. Dashed lines and R^2 values are from the ANOVA models. (A) Indentation modulus versus mineral-to-matrix ratio. (B) Hardness versus mineral-to-matrix ratio. (C) Indentation modulus versus lamellar aligned collagen content.*

2.4 Discussion

We hypothesized that tissue mechanical properties would vary with changes in mineral and aligned collagen content as a function of both tissue and animal age. Indeed, variations in the tissue mechanical properties correlated with mineral-to-matrix ratio and aligned collagen content. Variations in mineral-to-matrix ratio were the most important predictor of variations in indentation modulus and hardness. The addition of other parameters to mineral-to-matrix ratio

did not add significant predictive value to the ANOVA models. Mineral-to-matrix ratio effectively captured the variations explained by carbonate substitution and crystallinity (measures of the mineral), and lamellar aligned collagen (measure of the matrix).

When the behavior of individual mechanical and compositional parameters was examined, indentation modulus, hardness, mineral-to-matrix ratio, carbonate substitution, and aligned collagen peak height ratio, followed biphasic relationships with animal age, increasing sharply in the first years of life, and then remaining constant with age after sexual maturity. Based on the linear fits, mineral-to-matrix ratio increased nearly twice as fast as indentation modulus and hardness in young, growing animals. Of course, other microstructural factors such as mineral crystal size and orientation, collagen alignment, and noncollagenous matrix proteins may also contribute to the tissue mechanical properties [20,21,45]. Indeed, similar to stiffness, peak height ratio, a measure of aligned collagen content, followed a bi-phasic relationship with animal age. Furthermore, after sexual maturity, stiffness increased at a gradual rate almost identical to that of the lamellar aligned collagen. Although crystallinity showed a significant increase with animal age in mature animals, the percent changes were extremely small and may not be physiologically significant.

Carbonate substitution, crystallinity, and aligned collagen peak height ratio increased with tissue age, whereas mineral-to-matrix ratio and the mechanical parameters did not. Carbonate substitution increased at a gradual, constant rate throughout the lifespan of the baboon, suggesting that carbonate ions are substituted into the crystal lattice at a constant rate. Crystallization increased nearly an order of magnitude more rapidly in young than in mature animals, although again the percent changes were small.

In rodent models, increased mineralization, carbonate substitution, and crystallinity corresponded with increased stiffness and hardness, and similar to the current study, stiffness and hardness increased more gradually than did tissue mineralization [21,22,45,46]. Based on our data, these relationships hold true in a primate model that more closely parallels human bone

than other preclinical models. Furthermore, variations in composition and nanomechanical properties were functions of tissue and animal age, a novel finding because prior studies have focused only on mature animals and showed variable relationships with ageing [14–17]. The mechanical properties also related to collagen content and organization, as previously reported in a small sample of human vertebrae [31,34]. This relationship held over the entire lifespan of the baboon, and reflected that both stiffness and aligned collagen content increased as functions of animal age. Mineral-to-matrix ratio, carbonate substitution, indentation modulus, and hardness increased rapidly in the rat cortex to reach levels of mature tissue within the first four days after formation, but thereafter increased only slightly [20,21,45,46]. As baboon osteons selected for this study were not visibly remodeling, the tissue material properties would have already reached levels of the mature tissue and no steep increases in tissue material properties would be expected. Carbonate substitution and crystallinity did increase with tissue age across osteon radii, in agreement with data obtained through FTIR, a complementary spectroscopic technique [12].

As in any experiment, certain limitations may affect the interpretation of our results. One consideration is that the exact age of the osteons could not be distinguished because fluorochrome labels were not administered to the animals. However, by sampling three non-remodeling osteons within the same anatomical region of the cortex, we hoped to reduce variability due to anatomical location. The lack of steep gradients in tissue mineralization and stiffness near the Haversian canals confirmed that the selected osteons were not remodeling at the time of animal death. Furthermore, although our composition data obtained by Raman spectroscopy is consistent with key points from that obtained by FTIR, one discrepancy is evident. Namely, carbonate-to-phosphate ratio measured by FTIR decreased with animal age, whereas our Raman data showed increasing carbonate substitution during growth, followed by no change following sexual maturity [12,18]. This discrepancy may arise from fundamental differences between these two techniques; for example, Raman carbonate substitution is calculated from the peak height ratio rather than the peak area ratio used for FTIR. Finally,

although dehydration increases tissue modulus and hardness [47–49], all samples were treated similarly, and therefore our ability to detect variations in these properties with tissue and animal age was presumably not compromised.

In summary, composition and mechanical function were closely related in baboon osteonal bone and depended on tissue and animal age. When the entire lifespan of the animal was examined, tissue from the young, growing animals had lower stiffness and hardness, associated with lower mineralization, carbonate substitution, crystallinity, and aligned collagen content than tissue from sexually mature animals. In future studies, fluorochrome labeling could help identify newly formed osteons to determine the full effect of tissue age within osteonal bone, while studies of male animals would allow identification of sex-based differences that are not age-dependent. Based on the current results, we would expect the lamellae of newly formed osteons to have tissue properties similar to young, sexually immature animals. These results provide a baseline for variations that occur in healthy bone tissue with the natural ageing process and may have clinical implications in osteoporosis, where increased bone loss is not coupled with new bone formation. However, the relationship between fracture resistance and these age-related changes in tissue composition and nanomechanical properties must be examined further.

BIBLIOGRAPHY

[1] Burge R, Dawson-hughes B, Solomon DH, Wong JB, King A, Tosteson A. Incidence and Economic Burden of Osteoporosis-Related Fractures in the United States, 2005–2025. Journal of Bone and Mineral Research 2007;22.

[2] Schneider DL. Management of osteoporosis in geriatric populations. Current Osteoporosis Reports 2008;6:100-7.

[3] Cummings SR, Melton LJ. Epidemiology and outcomes of osteoporotic fractures. Lancet 2002;359:1761-7.

[4] Delmas PD, Seeman E. Changes in bone mineral density explain little of the reduction in vertebral or nonvertebral fracture risk with anti-resorptive therapy. Bone 2004;34:599-604.

[5] Garnero P. Biomarkers for osteoporosis management: utility in diagnosis, fracture risk prediction and therapy monitoring. Molecular Diagnosis Therapy 2008;12:157-170.

[6] Tai K, Dao M, Suresh S, Palazoglu A, Ortiz C. Nanoscale heterogeneity promotes energy dissipation in bone. Nature Materials 2007;6:454-462.

[7] Fratzl P, Gupta H. Nanoscale mechanisms of bone deformation and fracture. Handbook of Biomineralization. Verlag, Weinheim: Weiley-VCH, 2007. pp. 307-313.

[8] Boskey AL, Mendelsohn R. Infrared analysis of bone in health and disease. Journal of Biomedical Optics 2005;10:031102.

[9] Gadeleta SJ, Boskey AL, Paschalis E, Carlson C, Menschik F, Baldini T, et al. A physical, chemical, and mechanical study of lumbar vertebrae from normal, ovariectomized, and nandrolone decanoate-treated cynomolgus monkeys (Macaca fascicularis). Bone 2000;27:541-50.

[10] Roschger P, Paschalis EP, Fratzl P, Klaushofer K. Bone mineralization density distribution in health and disease. Bone 2008;42:456-466.

[11] Lin J, Lane J. Osteoporosis: A Review. Clinical Orthopaedics and Related Research 2004;425:126-134.

[12] Gourion-arsiquaud S, Burket JC, Havill LM, Dicarlo E, Doty SB, Mendelsohn R, et al. Spatial Variation in Osteonal Bone Properties Relative to Tissue and Animal Age. Journal of Bone and Mineral Research 2009;24:1271-1281.

[13] Parfitt A M. Osteonal and hemi-osteonal remodeling: the spatial and temporal framework for signal traffic in adult human bone. Journal of Cellular Biochemistry 1994;55:273-86.

[14] Akkus O, Polyakova-Akkus A, Adar F, Schaffler MB. Aging of microstructural compartments in human compact bone. Journal of Bone and Mineral Research 2003;18:1012-1019.

[15] Gupta HS, Stachewicz U, Wagermaier W. Mechanical modulation at the lamellar level in osteonal bone. Scanning Electron Microscopy 2006;12:1913-1921.

[16] Rho JY, Roy ME, Tsui TY, Pharr GM. Elastic properties of microstructural components of human bone tissue as measured by nanoindentation. Journal of Biomedical Materials Research 1999;45:48-54.

[17] Rho JY, Zioupos P, Currey JD, Pharr GM. Microstructural elasticity and regional heterogeneity in human femoral bone of various ages examined by nano-indentation. Journal of Biomechanics 2002;35:189-198.

[18] Paschalis EP, DiCarlo E, Betts F, Sherman P, Mendelsohn R, Boskey a L. FTIR microspectroscopic analysis of human osteonal bone. Calcified Tissue International 1996;59:480-7.

[19] Paschalis EP, Betts F, DiCarlo E, Mendelsohn R, Boskey AL. FTIR microspectroscopic analysis of normal human cortical and trabecular bone. Calcified Tissue International 1997;61:480-486.

[20] Busa B, Miller LM, Rubin CT, Qin Y-X, Judex S. Rapid establishment of chemical and mechanical properties during lamellar bone formation. Calcified Tissue International 2005;77:386-94.

[21] Donnelly E, Boskey AL, Baker SP, van der Meulen MCH. Effects of tissue age on bone tissue material composition and nanomechanical properties in the rat cortex. Journal of Biomedical Materials Research A 2010;92:1048-56.

[22] Miller LM, Little W, Schirmer A, Sheik F, Busa B, Judex S. Accretion of Bone Quantity and Quality in the Developing Mouse Skeleton. Journal of Bone and Mineral Research 2007;22.

[23] Carden A, Morris MD. Application of vibrational spectroscopy to the study of mineralized tissues (review). Journal of Biomedical Optics 2000;5:259-268.

[24] Havill LM, Mahaney MC, Czerwinski SA, Carey KD, Rice K, Rogers J. Bone mineral density reference standards in adult baboons (Papio hamadryas) by sex and age. Bone 2003;33:877-888.

[25] Havill LM, Levine SM, Newman DE, Mahaney MC. Osteopenia and osteoporosis in adult baboons (Papio hamadryas). Journal of Medical Primatology 2008;37:146-153.

[26] Pfeilschifter J, Köditz R, Pfohl M, Schatz H. Changes in proinflammatory cytokine activity after menopause. Endocrine Reviews 2002;23:90-119.

[27] Bronikowski A, Alberts S, Altmann J, Packer C, Carey K, Tartar M. The aging baboon: comparative demography in a non-human primate. Proceedings of the National Academy of Sciences 2002;99:9591-9595.

[28] Martin L., Carey K., Comuzzie A. Variation in menstrual cycle length and cessation of menstruation in captive raised baboons. Mechanisms of Ageing and Development 2003;124:865-871.

[29] Bellino F, Wise P. Nonhuman primate models of menopause workshop. Biology of Reproduction 2003;68:10-18.

[30] Erben RG. Embedding of bone samples in methylmethacrylate: an improved method suitable for bone histomorphometry, histochemistry, and immunohistochemistry. The Journal of Histochemistry and Cytochemistry 1997;45:307-313.

[31] Donnelly E, Baker SP, Boskey AL, van der Meulen MCH. Effects of surface roughness and maximum load on the mechanical properties of cancellous bone measured by nanoindentation. Journal of Biomedical Materials Research 2006;77:426-435.

[32] Burstein A, Reilly D, Martens M. Aging of bone tissue: mechanical properties. The Journal of Bone and Joint Surgery 1976;58:82-86.

[33] McCalden RW, McGeough JA, Barker MB, Court-Brown CM. Age-related changes in the tensile properties of cortical bone. The relative importance of changes in porosity, mineralization, and microstructure. The Journal of Bone and Joint Surgery 1993;75:1193-1205.

[34] Donnelly E, Baker SP, Boskey AL, van der Meulen MCH. Quasistatic and dynamic nanomechanical properties of cancellous bone tissue relate to collagen content and organization. Journal of Biomedical Materials Research A 2006;21.

[35] Oliver WC, Pharr GM. An improved technique for determining hardness and elastic modulus using load and displacement sensing indentation experiments. Journal of Materials Research 1992;7:1564-1583.

[36] Freeman JJ, Wopenka B, Silva MJ, Pasteris JD. Raman spectroscopic detection of changes in bioapatite in mouse femora as a function of age and in vitro fluoride treatment. Calcified Tissue International 2001;68:156-162.

[37] Penel G, Leroy G, Rey C, Bres E. MicroRaman spectral study of the PO4 and CO3 vibrational modes in synthetic and biological apatites. Calcified Tissue International 1998;63:475-481.

[38] Tarnowski CP, Ignelzi MA, Wang W, Taboas JM, Goldstein SA, Morris MD. Earliest mineral and matrix changes in force-induced musculoskeletal disease as revealed by Raman microspectroscopic imaging. Journal of Bone and Mineral Research 2004;19:64-71.

[39] Boyd R. Nonlinear Optics. 2nd ed. Amsterdam, The Netherlands: Academic Press. 2003.

[40] Campagnola PJ, Loew LM. Second-harmonic imaging microscopy for visualizing biomolecular arrays in cells, tissues and organisms. Nature Biotechnology 2003;21:1356-1360.

[41] Moreaux L, Sandre O, Mertz J. Membrane imaging by second-harmonic generation microscopy. Journal Of The Optical Society Of America B Optical Physics 2000;17:1685-1694.

[42] Williams RM, Zipfel WR, Webb WW. Interpreting second-harmonic generation images of collagen I fibrils. Biophysical Journal 2005;88:1377-86.

[43] Zipfel WR, Williams RM, Christie R, Nikitin AY, Hyman BT, Webb WW. Live tissue intrinsic emission microscopy using multiphoton-excited native fluorescence and second harmonic generation. Proceedings of the National Academy of Sciences of the United States of America 2003;100:7075-80.

[44] Martin L, Mahaney M, Bronikowski A, Dee Carey K, Dyke B, Comuzzie A. Lifespan in captive baboons is heritable. Mechanics of Ageing and Development 2002;123:1461-1467.

[45] Donnelly E, Chen DX, Boskey AL, Baker SP, van der Meulen MCH. Contribution of mineral to bone structural behavior and tissue mechanical properties. Calcified Tissue International 2010;87:450-460.

[46] Tarnowski CP, Ignelzi M a, Morris MD. Mineralization of developing mouse calvaria as revealed by Raman microspectroscopy. Journal of Bone and Mineral Research 2002;17:1118-26.

[47] Bushby A, Ferguson V, Boyde A. Nanoindentation of bone: comparison of specimens tested in liquid and embedded in polymethylmethacrylate. Journal of Materials Research 2004;19:249-259.

[48] Hengsberger S, Kulik A, Zysset P. Nanoindentation discriminates the elastic properties of individual human bone lamellae under dry and physiological conditions. Bone 2002;30.

[49] Rho J, Pharr G. Effects of drying on the mechanical properties of bovine femur measured by nanoindentation. Journal of Materials Science1 1999;10:485-488.

CHAPTER 3

VARIATIONS IN NANOMECHANICAL PROPERTIES AND TISSUE COMPOSITION WITHIN TRABECULAE FROM AN OVINE MODEL OF OSTEOPOROSIS AND TREATMENT*

3.1 Introduction

One in three women and one in five men over the age of fifty will experience an osteoporotic fracture in their lifetime [1–3]. The risk for additional fractures increases markedly after experiencing the first fracture [4]. Antiresorptive agents and selective estrogen receptor modulators (SERMs) reduce fracture risk from 30-50%, but increase BMD only slightly by 0-8% [5–10], suggesting that BMD alone is unable to fully capture skeletal alterations with treatment. BMD reflects the total amount of bone mineral (and the overall level of mineralization) but cannot capture effects at smaller length scales where failure initiates. At these smaller length scales, skeletal fracture risk depends on tissue micro-architecture and properties of mineral and matrix constituents that can vary spatially within individual bone microstructures due to the remodeling process [11–18]. These spatial distributions are particularly important because small tissue property changes in critical locations for resisting trabecular failure can profoundly affect skeletal fracture resistance. Imbalances or alterations in the remodeling process with osteoporosis and treatment may alter levels and spatial distributions of mineral and matrix properties within bone microstructures and could play a crucial role in our understanding of fracture risk and our ability to develop and evaluate successful therapies.

The mineralization gradient within trabeculae of healthy human bone is positive from surface to center and produces a positive gradient in tissue stiffness [15,19–22]. The manner in which individual trabeculae bear load is influenced by these tissue-level properties and their

* Burket JC, Brooks DJ, MacLeay JM, Baker SP, Boskey AL, van der Meulen MCH. Variations in nanomechanical properties and tissue composition within trabeculae from an ovine model of osteoporosis and treatment. Submitted to Bone May 2012.

arrangement within trabeculae. Osteoporosis reduces the overall heterogeneity of both tissue mineralization and mineral crystallinity [22–24], and bisphosphonate treatment further reduces heterogeneity in these properties [25–29]. However, the effects of osteoporosis and treatments on specific spatial distributions of compositional properties within trabeculae are not well-documented and may depend on treatment type. Mineral and matrix composition ultimately determine tissue mechanical function. Thus, any heterogeneity in tissue compositional properties results in nanomechanical heterogeneity that alters profiles of stress and strain within trabeculae and possibly affects the bone composite's ability to dissipate energy [14,17,18]. In healthy tissue, nanomechanical properties follow changes in mineralization and aligned collagen content [19,20,30]. Relationships between spatial compositional changes and the consequential nanomechanical alterations with osteoporosis and treatment have not yet been determined.

The goal of the present study was to compare spatial compositional and nanomechanical alterations in trabeculae with a large-animal model of osteoporosis and treatment. Two drugs were compared in this study. The first was a selective estrogen receptor modulator (SERM) that reduces turnover by acting through natural estrogen receptor pathways in bone and mimicking the effects of estrogen. The second treatment was from the widely-used bisphosphonate class of drugs that bind to bone matrix and directly inhibit osteoclastic activity upon resorption. SERMs and bisphosphonates reduce bone turnover to varying degrees yet produce similar reductions in fracture risk [31,32]. In a previous study, bisphosphonates altered collagen cross-linking in healthy female beagle vertebrae whereas SERMs did not [33]. SERMs improved vertebral mechanical performance independently of BMD in these same animals, suggesting that other changes in tissue composition might play an important role in fracture resistance [34].

Our hypotheses were that tissue stiffness and hardness would decrease in an ovine model of osteoporosis relative to healthy ewes due to alterations in tissue composition. Conversely treatment with either raloxifene (SERM) or zoledronate (bisphosphonate) would restore tissue nanomechanical properties through further alterations in tissue composition. Greatest effects

were expected near surfaces of trabeculae in regions of active remodeling and bone formation. Additionally, nanoscale rather than bulk tissue measures were predicted to better capture these changes with treatment because of their better spatial resolution. Tissue property effects with zoledronate were expected to be more pronounced than effects with raloxifene because bisphosphonates reduce turnover to a greater degree than SERMs [32,34]. However, raloxifene treatment was expected to better restore cancellous tissue properties to those present in healthy, ovary intact female sheep, since SERMs act through natural estrogen receptor pathways [35].

3.2 Materials and Methods

The present study utilized a dietary-induced ovine model of osteoporosis and treatment to examine alterations in bone tissue compositional and nanomechanical properties, and changes in the spatial arrangements of these properties within trabeculae. The microstructure of sheep bone is similar to that of humans [36–40]. In a previous study, dietary-induced metabolic acidosis (MA) in sheep increased bone turnover and reduced bone mineral and whole bone strength similar to postmenopausal osteoporosis in humans [36,39,41]. In contrast, the ovine ovariectomy (OVX) model decreased bone turnover and caused osteomalacia [41], making MA the appropriate model choice for post-menopausal, high-turnover osteoporosis. Two different antiresorptive treatments were examined in this study: the SERM, raloxifene (RAL), and the bisphosphonate, zoledronate (ZOL).

3.2.1 Samples and Specimen Preparation

Femora were obtained from 25 mature adult ewes from 2 experiments (approved by the Colorado State University Institutional Animal Care and Use Committee). The first experiment had two experimental groups. Both groups were fed a diet to induce metabolic acidosis for six months followed by another six months of MA with either vehicle (MA1, n = 5) or raloxifene (RAL, 0.80 mg/kg daily, n = 4) administered daily through abomasal cannulae [39,41]. Both treatment

groups started with n = 6 sheep; however, two RAL sheep were euthanized early due to cannula pull-out and one MA sheep was euthanized due to injuries unrelated to the experiment. A group of healthy animals fed a normal diet (CONT, n = 5) were housed in the same facility and euthanized in the same season as Experiment 1. The second experiment had two treatment groups. Both groups received eight months of MA rather than 6 months due to a delay in receiving the medication for the study. Subsequently, the groups were maintained on the MA diet for an additional 6 months with an intravenous administration of either vehicle (MA2, n = 6) or zoledronate (ZOL, 5 mg/sheep, n = 6) at the beginning of the treatment period. Originally, the bisphosphonate and SERM treatments were planned as a single experiment; however, due to difficulty administering alendronate in the first study, the bisphosphonate study was repeated separately using zoledronate with the MA2 group for comparison. After euthanasia, femora were stored at -20º C prior to specimen preparation.

3.2.2 Bulk Cancellous Tissue Characterization

Cylindrical cores were taken from the medial-caudal quadrants of the distal femur for characterization by micro-computed tomography (microCT) and compression tests. Cores were excised with a diamond core drill (5 mm ID, Starlight Industries, Rosemont, PA) under constant irrigation with physiological saline, wrapped in saline-soaked gauze, and stored at -20˚C prior to scanning.

3.2.2.1 Micro-Computed Tomography (MicroCT)

Tissue architecture within the cancellous cores was quantified by microCT (55 kVp, 145 mA, 600 ms integration time, µCT 35, Scanco Medical, Bruttisellen, Switzerland). The axial central third of each core was scanned at 15 µm isotropic resolution. A calibrated HA standard was used to convert the linear attenuation for each voxel to g HA/cm^3. A 0.5 mm aluminum filter reduced the effects of beam hardening. A global threshold was chosen for all specimens. Outcomes

included bone volume fraction (BV/TV), tissue mineral density (tBMD, mg/cm^3), and trabecular thickness and separation (Tb.Th and Tb.Sp, mm).

3.2.2.2 Compression Testing and Ashing

Bulk cancellous mechanical properties were assessed by compression testing of the bone cores. Prior to testing, press-fit brass end-caps were bonded to the ends of each core to minimize end artifacts [42]. The average gage length and diameter of the exposed core between endcaps was measured and used for subsequent stress and strain calculations. The load function consisted of 5 preconditioning cycles of 0 to 0.1% compressive strain before monotonically loading to 3% compressive strain at a rate of 0.5% strain/sec using a servohydraulic test system (Mini-Bionix 858, MTS Systems Corporation, Eden Prairie, MN). Displacement was measured with an extensometer attached across the endcaps (Model 634.11F-24, MTS Systems Corporation). The apparent compressive modulus, yield strength, and ultimate compressive strength were determined for each core. The apparent compressive modulus was defined as the slope of the least-squares fit of the stress-strain data over 0.02-0.2% strain. The yield strength was determined using the 0.2% offset method, and the ultimate compressive strength was the maximum stress achieved [43]. Following compressive testing the bone cores were dried and heated to 600 ºC for 18 hours, and ash fraction was calculated as ash weight/dry weight [44].

3.2.3 Nanoscale Cancellous Tissue Characterization

Transverse cancellous sections were taken above the growth plate of the medial-cranial quadrants of the distal femora for nanoscale characterization of compositional and nanomechanical properties. Sections were fixed, dehydrated, and embedded in polymethlymethacrylate [45]. A thin section (3 μm) was taken from the surface of each embedded bone block and mounted on a barium fluoride infrared spectroscopy window (Spectral Systems, Hopewell Jct., NY). The adjacent surface of the remaining block was polished

anhydrously to a RMS surface roughness of less than 15 μm on a 5 μm^2 AFM Scan (Dimension 3100, Veeco, Plainview, NY) [30,46,47].

Three trabeculae in each block and adjacent thin section were selected for characterization. In the three trabeculae from the blocks, tissue nanomechanical properties and composition were probed at identical locations with nanoindentation, Raman spectroscopy, and second harmonic generation microscopy (SHG). In the three trabeculae from the thin sections, tissue compositional parameters were assessed with Fourier transform infrared spectroscopy (FTIR). All nanoscale tissue property measurements were recorded in transverse lines across the trabeculae avoiding locations of remodeling at the time of euthanasia, which were visibly evident as regions of eroded trabeculae with scalloped surfaces.

The criterion for selecting trabeculae in this study was critical for examining regional results within these structures. The mean width of selected trabeculae was no less than 70% of the mean Tb.Th computed individually from the micro-CT measurements. This criterion ensured that trabeculae selected for analysis were sectioned close to their midsection (bisected in the longitudinal plane of the trabeculae). Hence, properties could be examined in superficial regions near the edges of trabeculae and in deeper tissue near the center of the trabeculae. Additionally, the SHG instrument for this study could image up to 60 μm below the surface of the sample in confocal mode to confirm that the exposed plane for measurement was not superficial and contained sufficient tissue for nanomechanical analysis.

3.2.3.1 Nanoindentation

Tissue nanomechanical properties were assessed via nanoindentation at centers of lamellae in a transverse line across three trabeculae with a Berkovich diamond indenter (Hysitron, Inc., Minneapolis, MN) [48,49]. For accurate placement, surface topography scans (20 μm^2) were made with the scanning nanoindenter (TriboIndenter, Hysitron, Inc.) prior to each indentation [30,46–49]. The load function included a 10 second hold at 700 μN peak load with

loading/unloading rates of 50 μN/s [48]. The resulting indentation depth was approximately 150 nm.

Each trabecula contained a mean of 13 (± 3) lamellae, resulting in roughly 40 measurements per animal. Indentation modulus (E_i), a measure of tissue stiffness (i.e. elastic properties), and hardness, a measure of inelastic properties, were calculated from the unloading portion of the load-displacement curve and the mean pressure at maximum load, respectively [50].

3.2.3.2 Raman Spectroscopy

Tissue composition was characterized with Raman spectroscopy, as described previously [48], at the same lamellar locations characterized with nanoindentation (InVia microRaman, Renishaw, Gloucestershire, United Kingdom). The spot size was 2 μm^2. For each measurement, Raman peak heights were identified from smoothed spectra after cubic polynomial background subtraction (Matlab, The Math Works, Inc., Natik, MA). Three bone parameters were calculated: mineral-to-matrix ratio (Raman mineral:matrix), B-type carbonate substitution, and crystallinity (Raman crystallinity) [48,51–56]. Mineral-to-matrix ratio, a measure of the degree of mineralization of the tissue, was calculated as the peak height ratio of the phosphate υ1 (~965 cm^{-1}) to the CH_2 wag (~1450 cm^{-1}) peaks [48,52]. B-type carbonate substitution, a measure of the level of carbonate substitution for phosphate in the hydroxyapatite (HA) crystal lattice, was calculated as the peak height ratio of the carbonate υ1 (~1070 cm^{-1}) to the phosphate υ1 peak [48,55]. Raman crystallinity, a measure of crystal size and perfection, was estimated as the reciprocal of the full width at half maximum (FWHM) of the phosphate υ1 peak [48,54,56]. For this measure, a sharper phosphate υ1 peak decreases FWHM and indicates greater mineral crystal size and perfection.

3.2.3.3 Second Harmonic Generation Microscopy (SHG)

Aligned collagen content within a longitudinal plane of the trabeculae was assessed via SHG microscopy as described previously [48] in the same trabecular regions studied with nanoindentation and Raman spectroscopy (Mai Tai Deep See, Spectra Physics, Santa Clara, CA; BX61W1, Olympus, Center Valley, PA). The pixel size was 0.318 μm^2. Fiducial markers such as osteocyte lacunae were compared with light microscopy images to co-locate SHG measurements with nanoindentation and Raman measurements.

The concentration of aligned collagen molecules (aligned collagen content) is equal to the square root of SHG intensity [57–61]. The aligned collagen content was calculated for a transverse line across each trabecula resulting in a profile of aligned collagen content with distance (Matlab, The Math Works, Inc.). The line was 6 pixels wide, corresponding to the Raman spot size of 2 μm. From this profile, maxima corresponding to lamellar aligned collagen and minima corresponding to interlamellar aligned collagen were recorded [30].

3.2.3.4 Fourier Transform Infrared Spectroscopy (FTIR)

Tissue composition was characterized in three trabeculae with FTIR spectroscopy, a complementary vibrational spectroscopy to Raman (Spectrum Spotlight 3000, Perkin Elmer Instruments, Waltham, MA) [49,62,63]. Due to the thin-section requirements for FTIR, these trabeculae were not the same as those characterized with the other techniques; however, FTIR sections were taken adjacent to the polished bone surfaces so anatomically similar areas were characterized. The pixel size was 6.25 μm^2. Four outcome measures were calculated (ISYS 4.0, Spectral Dimensions, Olney, MD) [62,64]: Mineral-to-matrix ratio (FTIR mineral:matrix), a measure of tissue mineralization, was calculated as the integrated area of the phosphate peak from 916 – 1180 cm^{-1} over the area of the amide I mode from 1592 – 1712 cm^{-1}[65,66]; total carbonate substitution, a measure of all carbonate substituted in to the HA crystal lattice (substitution for phosphate and hydroxyl, and labile substitution) was calculated as the integrated

area of the carbonate v2 peak from 840 – 892 cm^{-1} to the area of the phosphate peak [67]; FTIR crystallinity, a measure of stoichiometric to non-stoichiometric mineral content that correlates with c-axis line broadening as assessed by x-ray diffraction, was calculated as the ratio of the peak height sub-band at 1030 over the sub-band at 1020 cm^{-1} within the phosphate contour [68,69]; and finally, collagen cross-linking network maturity (XLR), a measure of the ratio of mature pyridinoline cross-links (PYR) to immature, reducible collagen cross-links (deH-DHLNL, deH-HLNL, and deH-HHMD) was calculated as the ratio of the peak height sub-band at 1660 to the sub-band at 1690 cm^{-1} [70]. From the FTIR images, the mean value of each parameter versus distance from the edge of the trabecula was calculated (Matlab).

3.2.4 Statistical Analysis

Statistical analyses were performed separately for Experiment 1 and 2, i.e. RAL was compared only with MA1 and CONT, while ZOL was compared only with MA2 (JMP Pro 9.0, Cary, NC). CONT animals were included with Experiment 1 for statistical analyses because they were housed in the same facility and euthanized shortly after the first experiment in the same season (summer). Experiment 1 and 2 analyses were performed separately due to the experiments being conducted separately and because animals were euthanized in the summer for Experiment 1 and winter for Experiment 2. In the sheep, BMD is constant during summer months; however seasonal variations can be present between summer and winter [71].

The effects of treatment on bulk tissue outcome measures (from microCT, compression testing, and ashing) were assessed with single-factor ANOVAs with Tukey post-hoc tests. The significance level was $p \leq 0.05$. Results stated are significant unless noted otherwise. Figures display mean values with error bars representing 95% confidence intervals.

3.2.4.1 Nanoscale Effects of Treatment and Region

To determine effects of treatment and distance from the edge of the trabeculae on nanoscale mechanical and compositional properties from nanoindentation, Raman, SHG, and FTIR, measurements were classified by region within the trabeculae: Superficial (Sup, < 20 μm from the trabecular edge), Intermediate (Int, 20 – 40 μm from the trabecular edge), and Central (Ctr, > 40 μm from the trabecular edge) [19,20,72,73]. Multi-factor, nested ANOVAs with Tukey post-hoc tests determined effects of treatment (CONT, MA, and RAL; MA2 and ZOL), region (Superficial, Intermediate, and Central), treatment*region, sheep (nested), and trabeculae (nested).

3.2.4.2 Correlations Between Compositional and Nanomechanical Parameters

The contribution of compositional properties (Raman and SHG) to alterations in tissue nanomechanical properties was determined by regression analysis. The mean Superficial, Intermediate, and Central values for the compositional and mechanical parameters were calculated for each trabecula. Correlating these averaged values rather than each individual measurement location reduced variability from inherent heterogeneity of the bone tissue or slight misalignment between measurement locations.

Correlations were performed separately for Experiment 1 and Experiment 2. First, linear ANOVA models were performed for E_i and H vs. Raman mineral-to-matrix ratio, B-type carbonate substitution, Raman crystallinity, and lamellar aligned collagen. Subsequently, non-significant terms were removed from the model stepwise in order of decreasing p-value until only significant effects remained. Next, treatment and full interactions between compositional parameters and treatment were added to the ANOVA models. Non-significant terms were again removed in a stepwise fashion until only significant effects remained. For significant improvement in explanatory power, a minimum 5% increase in the R^2 value was considered practically meaningful.

3.3 Results

3.3.1 MA and Treatment

MA and treatment effects were more apparent at the nanoscale than at the bulk tissue level. MA did not differ significantly from controls for any of the bulk compression outcome measures (Figure 3.1), due at least in part to substantial variability between animals and small sample sizes. Bulk microCT demonstrated reduced tBMD with MA, with MA1 ewes having 3% lower tBMD than control animals (Figure 3.2). At the nanoscale, MA ewes had lower indentation modulus (-15%) and hardness (-13%) throughout trabeculae relative to control animals (Figure 3.3). Compositional measures at indentation locations showed reduced B-type carbonate substitution in Superficial (-11%) and Intermediate regions (-11%) in MA relative to control ewes (Figure 3.4). Complementary FTIR compositional measurements showed less total carbonate substitution throughout the trabeculae in MA sheep relative to controls, with the magnitude of the difference depending on region (Superficial -14%, Intermediate -8.3%, Central -12% vs. CONT; Figure 3.5). In addition, Superficial regions of MA trabeculae had lower FTIR mineral-to-matrix ratio (-8.1%), lower collagen cross-linking network maturity (-9.2%), and greater FTIR crystallinity (+3.4%) than that of controls (Figure 3.5).

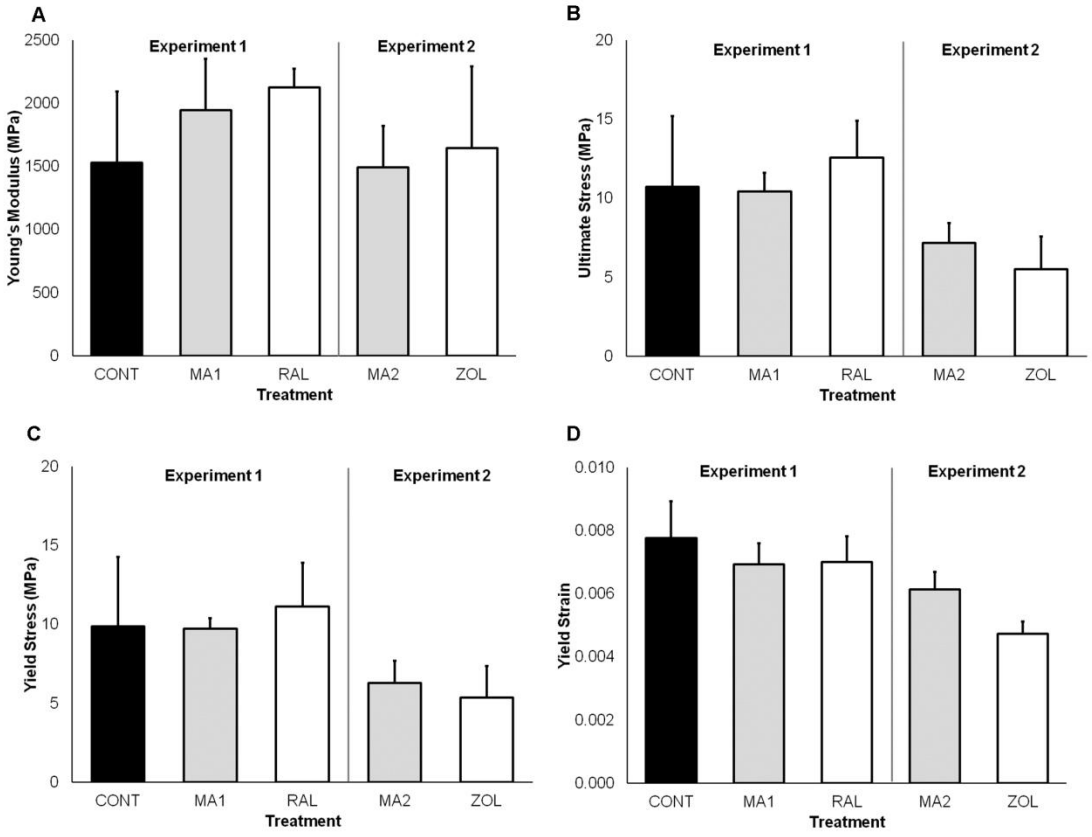

Figure 3.1 *Bulk tissue results from compression testing of cancellous cores. (A) Young's modulus, (B) ultimate stress, (C), yield stress, and (D) yield strain. Cores were ashed after compression testing but did not show any differences between treatment groups.* $* p < 0.05$ *All figures show mean ± 95% confidence interval.*

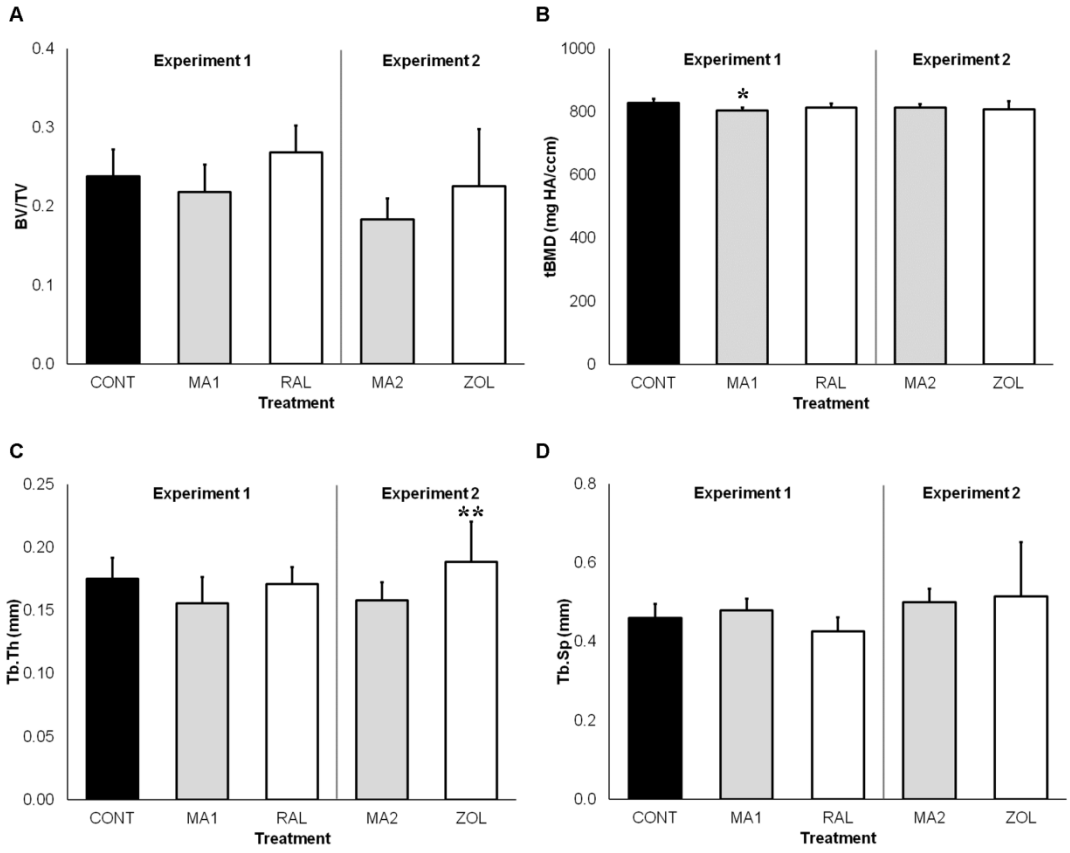

Figure 3.2 *Bulk tissue results from microCT of cancellous cores. (A) BV/TV, (B) tBMD, (C) Tb.Th., and (D) Tb.Sp. * $p < 0.05$ ** $p < 0.10$*

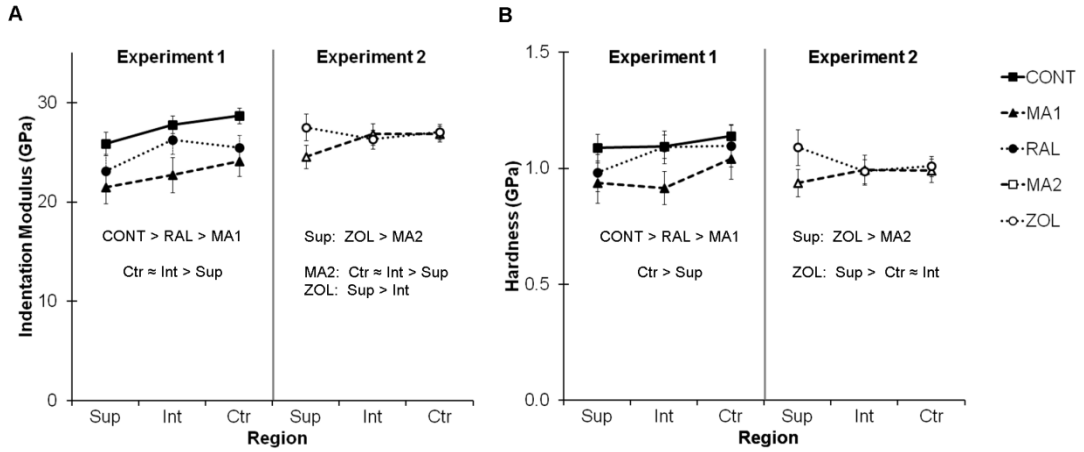

Figure 3.3 *Nanomechanical results. (A) Indentation modulus and (B) hardness by trabecular region. Effects of DIMA and RAL are evident throughout trabeculae, whereas ZOL alters only Superficial regions. Significant differences are indicated by < and > ; equivalence indicated by ≈.*

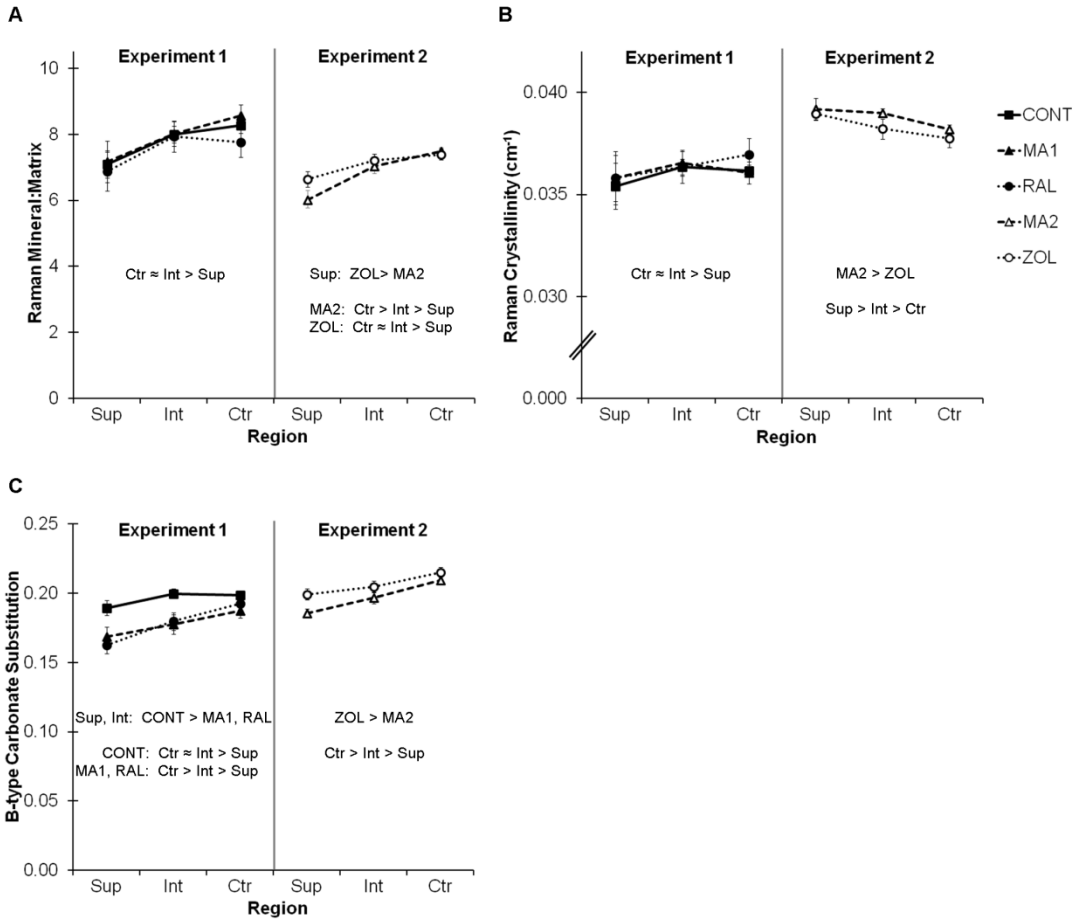

Figure 3.4 *Raman compositional results. (A) Raman mineral-to-matrix ratio, (B) Raman crystallinity, and (C) B-type carbonate substitution by trabecular region. Raman measurements were made at nanoindentation locations. Significant differences are indicated by < and > ; equivalence indicated by ≈.*

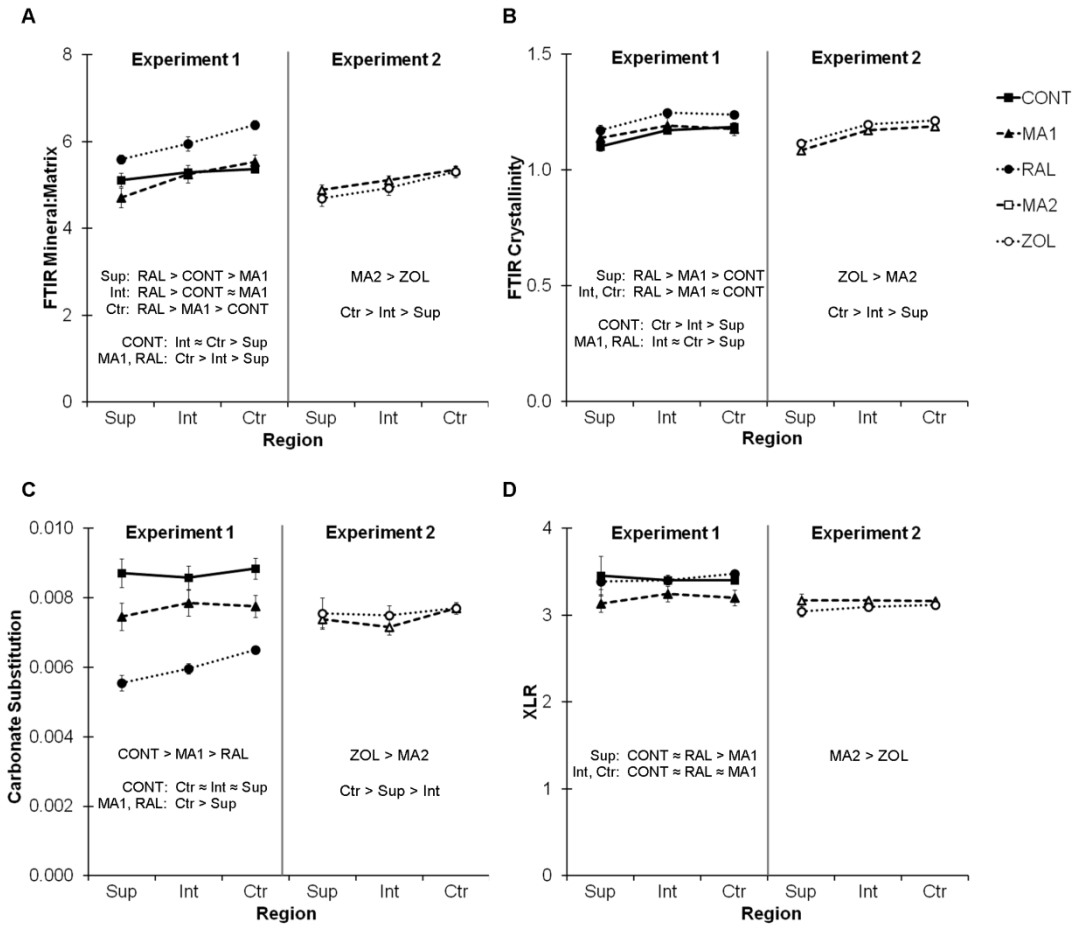

Figure 3.5 *FTIR compositional results. (A) FTIR mineral-to-matrix ratio, (B) FTIR crystallinity, (C) total carbonate substitution, and (D) collagen cross-linking network maturity by trabecular region. FTIR measurements were made in thin sections taken adjacent to trabeculae characterized with nanoindentation, Raman, and SHG. Significant differences are indicated by < and > ; equivalence indicated by ≈.*

Like MA, RAL treatment effects were greater at the nanoscale than at the bulk tissue level. The decreased bulk tBMD with MA was restored with RAL, with RAL-treated animals achieving tBMD levels equivalent to controls (Figure 3.2). At the nanoscale, indentation modulus (+9.6%) and hardness (+9.9%) increased with RAL compared to MA animals throughout trabeculae, but these properties were not fully restored to control levels (E_i -6.5%, H -4.6% vs. CONT; Figure 3.3). Measurements of tissue composition at indentation locations showed that RAL did not alter the reduction in B-type carbonate substitution that occurred with MA (Figure 3.4); furthermore, total carbonate substitution was reduced even further with RAL over MA, with the magnitude of the decrease greater at Superficial regions than in deeper tissue (Superficial -36%, Intermediate -30%, Central -27% vs. CONT, Figure 3.5). RAL restored collagen cross-linking network maturity (XLR) to levels in controls, and increased FTIR mineral-to-matrix ratio (Superficial +9.2%, Intermediate +12%, Central +19% vs. CONT) and FTIR crystallinity (Superficial +6.6%, Intermediate +6.5%, Central +4.6% vs. CONT) throughout trabeculae, with the magnitudes of the increases varying by region. FTIR mineral-to-matrix ratio and crystallinity reached levels greater than those in control animals (Figure 3.5).

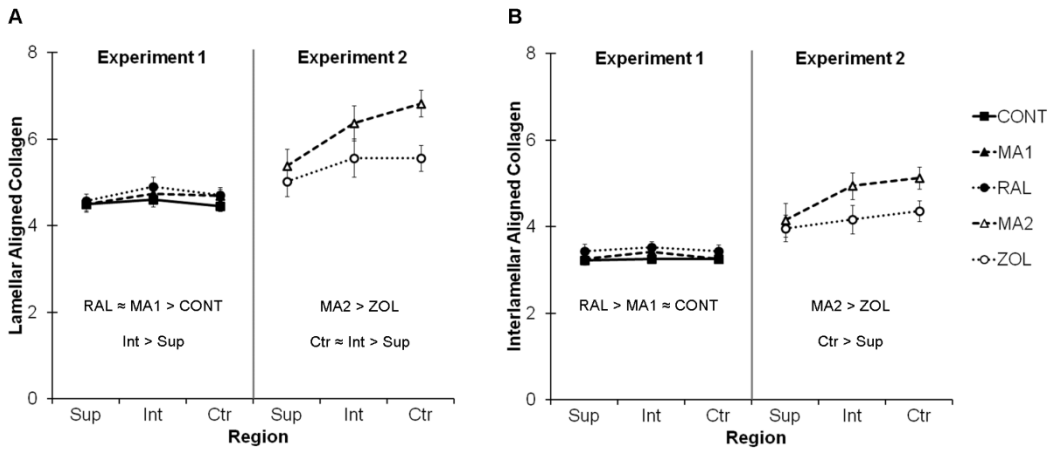

Figure 3.6 *SHG results. (A) Lamellar aligned collagen and (B) interlamellar aligned collagen by trabecular region. SHG measurements were taken at locations characterized with nanoindentation and Raman. Significant differences are indicated by < and > ; equivalence indicated by ≈.*

Treatment effects with ZOL differed from those with RAL at both the bulk tissue level and the nanoscale. In bulk tissue ZOL decreased yield strain (-23%) and trended towards increased trabecular thickness (+ 30 μm or 19%, $p < 0.06$) relative to MA animals (Figures 3.1 and 3.2). Consequently, Superficial regions of ZOL trabeculae consisted primarily of newly formed tissue. Unlike RAL, ZOL did not affect tBMD. Nanomechanical properties were altered exclusively in Superficial regions with ZOL, with these regions having greater indentation modulus (+12%) and hardness (+16%) than in MA animals (Figure 3.3). Nanoscale compositional measurements at indentation locations showed that Raman mineral-to-matrix ratio was also greater in Superficial regions with ZOL (+10%) than with MA, whereas B-type carbonate substitution increased (+4.7%) and aligned collagen content (lamellar -13%, interlamellar -12%) decreased throughout trabeculae with ZOL (Figures 3.4 and 3.6). From the adjacent thin sections, FTIR mineral-to-matrix ratio, FTIR crystallinity, total carbonate substitution, and collagen cross-linking network maturity were altered with ZOL relative to MA (Figure 3.5), but percent changes were less than 3% and likely not physiologically meaningful although statistically significant.

3.3.2 Correlations between Compositional and Nanomechanical Parameters

For Experiment 1 (CONT, MA1, and RAL), indentation modulus and hardness correlated with B-type carbonate substitution, Raman crystallinity, and lamellar aligned collagen (Table 3.1, Figure 3.7). These three compositional measures explained 28% and 25% of the variation in indentation modulus and hardness, respectively. The predictive power for indentation modulus and hardness increased to ~35% when treatment and its effects on compositional relationships were included. When the contributions of each compositional parameter were examined individually, B-type carbonate substitution and Raman crystallinity were the strongest predictors of nanomechanical function and correlated positively with both indentation modulus and hardness. B-type carbonate substitution and Raman crystallinity, respectively, explained 20%

and 10% of the variation in indentation modulus independent of treatment. In contrast, relationships between hardness and these two parameters varied between treatment groups. B-type carbonate substitution was only a significant predictor of hardness in MA and RAL ewes, both of which had lower levels of carbonate substitution than control animals. Raman crystallinity significantly predicted hardness only with RAL and accounted for 46% of the variation in hardness in these animals, the greatest explanatory effect measured.

Table 3.1 *Coefficients of variation (R^2) for nanomechanical properties modeled as linear functions of Raman and SHG compositional parameters for each experiment. "Composition Only" indicates the explanatory power of the linear models with four compositional parameters: Raman mineral:matrix, B-type carbonate substitution, Raman crystallinity, and lamellar aligned collagen. "Composition + treatment" indicates the explanatory power of the models with the four compositional parameters, treatment, and the effects of treatment on the nanomechanical relationships with composition.* $^{+}$ *Indicates compositional parameters whose effects varied with treatment. An increase in $R^2 > 0.05$ is considered a meaningful improvement.*

Nanomechanical Parameter	Composition Only	Composition + Treatment	
Experiment 1	R^2	R^2	**Significant Compositional Parameters**
Indentation Modulus	0.28	0.34	B-type carbonate substitution Raman crystallinity Lamellar aligned collagen
Hardness	0.25	0.35	B-type carbonate substitution^{+} Raman crystallinity^{+} Lamellar aligned collagen
Experiment 2			
Indentation Modulus	0.15	0.15	Raman mineral:matrix Raman crystallinity
Hardness	0.07	0.12	Raman mineral:matrix Raman crystallinity Lamellar aligned collagen^{+}

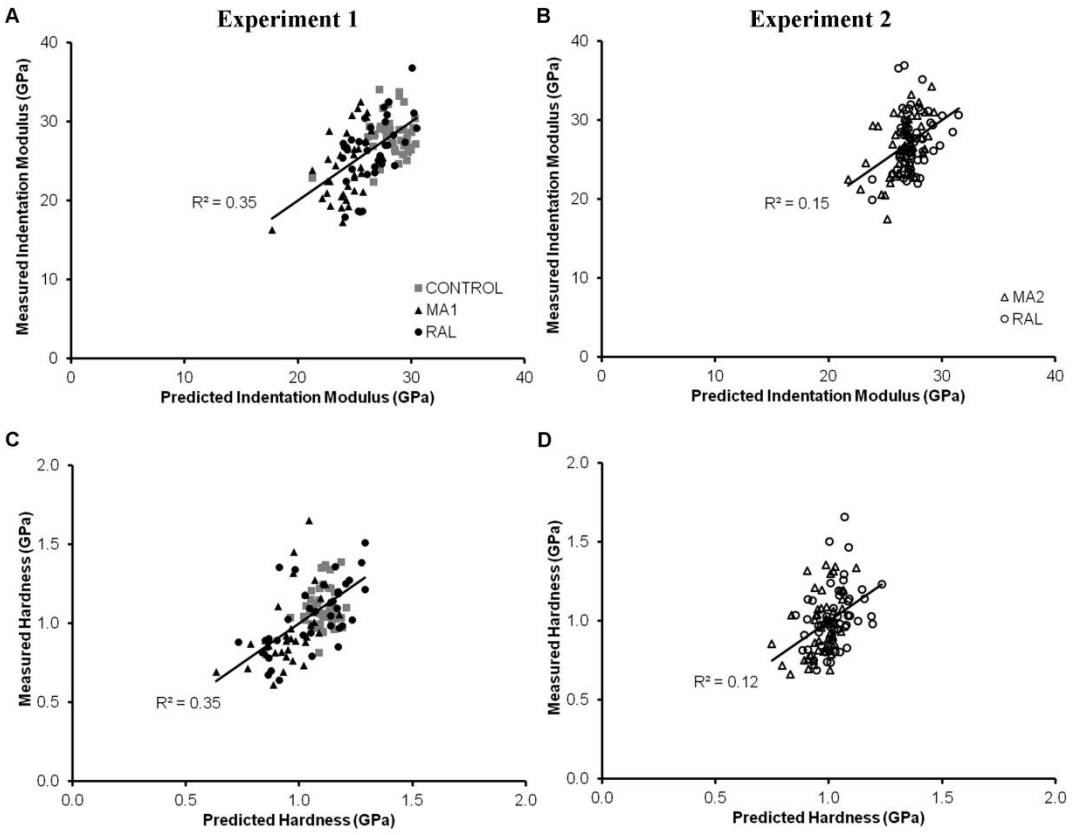

Figure 3.7 *Measured values of indentation modulus and hardness from Experiment 1 (A and C) and Experiment 2 (B and D) plotted versus the predicted values from the ANOVA models including treatment and significant compositional parameters (Table 1). Relationships between nanomechanical and compositional parameters were allowed to vary between treatment groups.*

The ANOVA models for Experiment 2 explained less of the variability in nanomechanical parameters than those for Experiment 1. Indentation modulus and hardness correlated positively with Raman mineral-to-matrix ratio and crystallinity. Hardness also correlated with lamellar aligned collagen. Composition accounted for 15% of the variability in indentation modulus and was not affected by treatment. Compositional parameters alone explained only 7% of the variability in hardness. Allowing the relationship between hardness and lamellar aligned collagen to vary with treatment increased the explanatory power to 12%. When the contributions of each compositional parameter to the ANOVA models were examined individually, Raman mineral-to-matrix ratio provided the most explanatory power and predicted 11% of the variation in indentation modulus independent of treatment. Hardness also correlated

with Raman mineral-to-matrix ratio, which explained only 2.4% of the variation and provided limited predictive utility.

3.4 Discussion

As hypothesized, raloxifene and zoledronate reversed changes in cancellous bone tissue properties in a large-animal model of human osteoporosis, and these improvements correlated with changes in composition. Bulk tissue properties such as tBMD were not sensitive enough to capture treatment effects, which became more apparent at the nanoscale and varied spatially within cancellous microstructures. Not surprisingly, nanoscale effects differed between the two treatments. Raloxifene reversed MA-induced losses in stiffness and hardness throughout the trabeculae but did not fully restore levels to those present in healthy ewes. Alterations in tissue mineralization, lamellar aligned collagen content, and Raman crystallinity accounted for one quarter to one third of the variation in nanomechanical parameters with MA and raloxifene. In comparison, zoledronate improved tissue stiffness and hardness over MA exclusively at the surfaces of trabeculae. Nanomechanical improvements with MA and zoledronate correlated with tissue mineralization, crystal size and perfection, and B-type carbonate substitution. In both experiments, the relationships between indentation modulus and compositional parameters were independent of treatment while relationships between hardness and compositional parameters differed between treatment groups.

The most pronounced treatment effects were expected at surfaces of trabeculae, regions where active remodeling and bone formation take place. Surface tissue is younger and less mineralized due to the remodeling process in cancellous bone and consequently has the greatest potential for gains in mineralization [21,74–76]. Tissue nanomechanical properties positively correlate with mineralization [48,74–77]. Additionally, bisphosphonates such as zoledronate target to bone matrix on trabecular surfaces where they directly inhibit osteoclast activity when resorbed by these cells [78–83]. Indeed, our results confirm zoledronate treatment effects were

primarily on surfaces of trabeculae and locally increased mineral-to-matrix ratio followed by gains in tissue stiffness and hardness. These results confirm findings from 12 months of zoledronate treatment in an ovine OVX model [20]. We further show that these surface regions consist primarily of newly formed tissue, as indicated by the trend towards increased trabecular thickness with zoledronate.

In contrast, treatment effects with the SERM, raloxifene, were distributed throughout the thickness of the trabeculae and not limited to surfaces. Raloxifene acts as an agonist in bone and reduces turnover by binding to estrogen receptors and acting through estrogen response elements and coregulator proteins (IL-6, IL-7, TGF-β, etc.) [35,84]. Turnover is reduced less with raloxifene than with zoledronate and other bisphosphonates both in women with osteoporosis and animals with replete estrogen levels [10,32]. Bulk tissue measures in the current study showed no increase in trabecular thickness with RAL. Thus, gains in tissue stiffness and hardness throughout trabeculae were achieved by increased mineralization of existing trabecular tissue, as evidenced by the increase in FTIR mineral-to-matrix ratio throughout trabeculae.

Our results provide interesting insights into the mechanisms by which anti-resorptive treatments achieve remarkable reductions in fracture risk despite only modest increases in BMD. If a single trabecula for each treatment were modeled as a perfect cylinder with average trabecular width and regional tissue stiffness as measured in these experiments, raloxifene and zoledronate would increase trabecular bending stiffness over their corresponding MA groups by 60% and 110%, respectively. With raloxifene, the trabecular bending stiffness would still be 15% less than that of healthy trabeculae, but with zoledronate, trabecular bending stiffness would be 28% greater than that from a healthy sheep from Experiment 1. The greater increase in trabecular bending stiffness with zoledronate is attributable to both the trend towards greater trabecular thickness and the localized increase in tissue stiffness near surfaces of trabeculae. Bending and buckling are two dominant failure modes for individual trabeculae within cancellous bone, and both are most influenced by the quantity and properties of tissue located

farthest away from the center (or neutral axis) of the trabeculae. By increasing tissue stiffness near the surface, zoledronate targets the exact region most critical for resisting bending and buckling failure. Though these effects within trabeculae did not translate to changes in the bulk tissue mechanical properties measured in this experiment, localized improvements with zoledronate treatment could account for some of the discrepancy between the small change in BMD and the much greater decrease in fracture risk observed clinically with bisphosphonate treatment. Continued treatment duration beyond the six months studied here could produce more pronounced effects and eventually translate to changes measurable in bulk tissue.

The nature of mineral-to-matrix alterations differed between raloxifene and zoledronate, as evidenced by differences in Raman and FTIR compositional parameters. Zoledronate affected primarily the peak vibrations of phosphate υ1 and CH_2 wag [48,52]. In contrast, raloxifene altered the entire phosphate υ1 and Amide I vibrational modes [65,66] but had little effect on peak phosphate υ1 and CH_2 wag vibrations. Zoledronate effects were most evident from Raman measurements made at peaks of lamellae, while raloxifene effects were most evident from SHG measurements that reflect both lamellar and interlamellar material due to the lower spatial resolution.

Previously, decreased carbonate substitution was associated with increased atomic order in synthetic apatites [85]. All types of carbonate substitution decreased with MA and raloxifene and indeed this corresponded with increased stoichoimetric/non-stoichiometric crystallinity ratio measured by FTIR. Unlike raloxifene, zoledronate increased B-type carbonate substitution over MA but decreased the combination of A-type and labile carbonate substitution. As a result, the difference in total carbonate substitution with zoledronate was small and likely not physiologically significant.

The treatment-dependent relationships between hardness and compositional parameters suggest that the nature of mineral and matrix alterations differ between treatments and depend on additional factors not captured by the four compositional parameters correlated in this study.

Furthermore, compositional correlations provided limited explanatory power for the nanomechanical parameters, particularly in Experiment 2, and also point towards contributions from aspects of mineral and matrix composition not measured here. Factors such as other non-enzymatic collagen cross-links, mineral crystal orientation, and non-collagenous proteins could also play a role in mechanical function. In addition, the nanoscale data from Experiment 2 fell in a narrow range, such that treatment and regional differences were on a scale not much larger than the biological variability.

The present study had several methodological limitations that could affect the interpretation of the results. First, the sample size of the large animal model was underpowered for the bulk tissue measures. In addition, large variations in bulk tissue measures between animals made differences with treatment difficult to detect. A power analysis based on our results showed that a three-fold increase in sample size was needed to detect significant changes in BV/TV and a two-fold increase for Tb.Th. Nanomechanical measurements benefitted from repeated measures to increase statistical power. Nonconcurrent performance of the two experiments prevented direct statistical comparison between all treatment groups. Ideally, controls would have been included as part of the experimental design; however, little effect was expected due to different treatment and euthanasia dates because control animals were housed in the same facility and euthanized in the same season. Additionally, performing statistical models without control animals did not significantly alter the results or predictive capability. The delay in administering zoledronate in Experiment 2 prolonged the DIMA period by two months and caused animals in Experiment 2 to be euthanized in a different season than in Experiment 1. Both factors could produce slight differences between the two MA groups and the severity of bone loss at the start of treatment. The MA model presents another limitation because ewes were estrogen-replete, unlike post-menopausal osteoporotic patients. Notably, the presence of estrogen in the MA animals may have blunted the effects of raloxifene, since SERMs and estrogen act through the same estrogen receptor pathways [35,84]. Finally, FTIR measurements

were not colocalized with other nanoscale measurements due to the thin-section requirement, limiting comparisons to trends rather than direct correlations among parameters.

In conclusion, both raloxifene and zoledronate improved cancellous tissue nanomechanical properties in the distal femur of a large-animal model for human high-turnover osteoporosis, and these improvements were attributable to changes in tissue composition. A companion study compares the FTIR changes in the distal femur to changes in other bones from the same animals [86]. In the present study, alterations were less evident at the bulk tissue level than at the nanoscale—the length scale at which failure initiates. Zoledronate improvements were localized to new tissue at surfaces of trabeculae, where the drug binds to bone matrix and directly reduces osteoclastic activity. In contrast, raloxifene acts through estrogen receptor pathways and improved tissue properties throughout the trabeculae. The nanoscale spatial alterations in composition and consequently nanomechanical properties resulted in improvements in estimated trabecular bending stiffness. As the fracture of cancellous bone ultimately arises due to the failure of individual trabecular elements, these findings may provide some explanation for the reductions in fracture risk with SERM and bisphosphonate treatment despite only modest gains in BMD.

BIBLIOGRAPHY

[1] Melton LJ, Atkinson EJ, O'Connor MK, O'Fallon M, Riggs L. Bone Density and Fracture Risk in Men. Journal of Bone and Mineral Research 1998;13:1915-1923.

[2] Melton LJ, Chrischilles E, Cooper C. Perspective. How many women have osteoporosis? Journal of Bone and Mineral Research 1992;7:1005.

[3] Kanis JA, Johnell O, Oden A, Sernbo I, Dawson A, de Laet C. International Long-Term Risk of Osteoporotic Fracture in Malmo. Bone 2000;11:669-674.

[4] Klotzbuecher CM, Ross PD, Landsman PB, Abbott TA, Berger M. Patients with prior fractures have an increased risk of future fractures: a summary of the literature and statistical synthesis. Journal of Bone and Mineral Research 2000;15:721-39.

[5] Ettinger B, Black DM, Mitlak BH, Knickerbocker RK, Nickelsen T, Genant HK, et al. Reduction of vertebral fracture risk in postmenopausal women with osteoporosis treated with raloxifene: results from a 3-year randomized clinical trial. The Journal of the American Medical Association 1999;282:637-45.

[6] Cummings SR, Karpf DB, Harris F, Genant HK, Ensrud K, LaCroix AZ, et al. Improvement in spine bone density and reduction in risk of vertebral fractures during treatment with antiresorptive drugs. The American Journal of Medicine 2002;112:281-289.

[7] Delmas PD, Bjarnason NH, Mitlak BH, Ravoux AC, Shah AS, Huster WJ, et al. Effects of raloxifene on bone mineral density, serum cholesterol concentrations, and uterine endometrium in postmenopausal women. The New England Journal of Medicine 1997;337:1641-1647.

[8] Lufkin EG, Whitaker MD, Nickelsen T, Argueta R, Caplan RH, Knickerbocker RK, et al. Treatment of established postmenopausal osteoporosis with raloxifene: a randomized trial. Journal of Bone and Mineral Research 1998;13:1747-54.

[9] Johnston CC, Bjarnason NH, Cohen FJ, Shah A, Lindsay R, Mitlak BH, et al. Long-term effects of Raloxifene on bone mineral density, bone turnover, and serum lipid levels in early postmenopausal women : Three-year data from 2 double-blind, randomized, placebo-controlled trials. Archives of Internal Medicine 2000;160:3444-3450.

[10] Allen MR, Iwata K, Sato M, Burr DB. Raloxifene enhances vertebral mechanical properties independent of bone density. Bone 2006;39:1130-5.

[11] Sornay-Rendu E, Boutroy S, Munoz F, Delmas PD. Alterations of Cortical and Trabecular Architecture Are Associated With Fractures in Postmenopausal Women, Partially

Independent of Decreased BMD Measured by DXA: The OFELY Study. Journal of Bone and Mineral Research 2007;22:425-433.

[12] van der Meulen MC, Jepsen KJ, Mikić B. Understanding bone strength: size isn't everything. Bone 2001;29:101-4.

[13] Viguet-Carrin S, Garnero P, Delmas PD. The role of collagen in bone strength. Osteoporosis International 2006;17:319-336.

[14] Renders GAP, Mulder L, van Ruijven LJ, Langenbach GEJ, van Eijden TMGJ. Mineral heterogeneity affects predictions of intratrabecular stress and strain. Journal of Biomechanics 2011;44:402-7.

[15] Renders GAP, Mulder L, Langenbach GEJ, Van Ruijven LJ, Van Eijden TMGJ. Biomechanical effect of mineral heterogeneity in trabecular bone. Journal of Biomechanics 2008;41:2793-2798.

[16] Cioffi I, Van Ruijven LJ, Renders GAP, Farella M, Michelotti A, Van Eijden TMGJ. Regional variations in mineralization and strain distributions in the cortex of the human mandibular condyle. Bone 2007;41:1051-1058.

[17] Tai K, Dao M, Suresh S, Palazoglu A, Ortiz C. Nanoscale heterogeneity promotes energy dissipation in bone. Nature Materials 2007;6:454-462.

[18] Yao H, Dao M, Carnelli D, Tai K, Ortiz C. Size-dependent heterogeneity benefits the mechanical performance of bone. Journal of the Mechanics and Physics of Solids 2011;59:64-74.

[19] Brennan O, Kennedy OD, Lee TC, Rackard SM, O'Brien FJ. Biomechanical properties across trabeculae from the proximal femur of normal and ovariectomised sheep. Journal of Biomechanics 2009;42:498-503.

[20] Brennan O, Kennedy OD, Lee TC, Rackard SM, O'Brien FJ, McNamara LM. The effects of estrogen deficiency and bisphosphonate treatment on tissue mineralisation and stiffness in an ovine model of osteoporosis. Journal of Biomechanics 2011;44:386-90.

[21] Willems NMBK, Mulder L, Langenbach GEJ, Grünheid T, Zentner A, Van Eijden TMGJ. Age-related changes in microarchitecture and mineralization of cancellous bone in the porcine mandibular condyle. Journal of Structural Biology 2007;158:421-427.

[22] Gadeleta SJ, Boskey AL, Paschalis E, Carlson C, Menschik F, Baldini T, et al. A physical, chemical, and mechanical study of lumbar vertebrae from normal, ovariectomized, and nandrolone decanoate-treated cynomolgus monkeys (Macaca fascicularis). Bone 2000;27:541-50.

[23] McCreadie BR, Morris MD, Chen T-C, Sudhaker Rao D, Finney WF, Widjaja E, et al. Bone tissue compositional differences in women with and without osteoporotic fracture. Bone 2006;39:1190-1195.

[24] Roschger P, Paschalis EP, Fratzl P, Klaushofer K. Bone mineralization density distribution in health and disease. Bone 2008;42:456-466.

[25] Gourion-Arsiquaud S, Allen MR, Burr DB, Vashishth D, Tang SY, Boskey AL. Bisphosphonate treatment modifies canine bone mineral and matrix properties and their heterogeneity. Bone 2010;46:666-672.

[26] Roschger P, Fratzl P, Klaushofer K, Rodan G. Mineralization of cancellous bone after alendronate and sodium fluoride treatment: a quantitative backscattered electron imaging study on minipig ribs. Bone 1997;20:393-397.

[27] Roschger P, Rinnerthaler S, Yates J, Rodan GA, Fratzl P, Klaushofer K. Alendronate increases degree and uniformity of mineralization in cancellous bone and decreases the porosity in cortical bone of osteoporotic women. Bone 2001;29:185-191.

[28] Boivin G, Meunier PJ. Effects of bisphosphonates on matrix mineralization. Journal of Musculoskeletal Neuronal Interactions 2002;2:538-543.

[29] Boskey AL, Spevak L, Weinstein RS. Spectroscopic markers of bone quality in alendronate-treated postmenopausal women. Osteoporosis International 2009;20:793-800.

[30] Donnelly E, Baker SP, Boskey AL, van der Meulen MCH. Quasistatic and dynamic nanomechanical properties of cancellous bone tissue relate to collagen content and organization. Journal of Biomedical Materials Research A 2006;21.

[31] Allen MR, Burr DB. Bisphosphonate effects on bone turnover, microdamage, and mechanical properties: What we think we know and what we know that we don't know. Bone 2011;49:56-65.

[32] Sambrook PN, Geusens P, Ribot C, Solimano JA, Ferrer-Barriendos J, Gaines K, et al. Alendronate produces greater effects than raloxifene on bone density and bone turnover in postmenopausal women with low bone density: results of EFFECT (Efficacy of FOSAMAX versus EVISTA Comparison Trial) International. Journal of Internal Medicine 2004;255:503-511.

[33] Allen MR, Gineyts E, Leeming DJ, Burr DB, Delmas PD. Bisphosphonates alter trabecular bone collagen cross-linking and isomerization in beagle dog vertebra. Osteoporosis International 2008;19:329-337.

[34] Allen MR, Iwata K, Phipps R, Burr DB. Alterations in canine vertebral bone turnover, microdamage accumulation, and biomechanical properties following 1-year treatment with clinical treatment doses of risedronate or alendronate. Bone 2006;39:872-9.

[35] Bryant HU, D P. Mechanism of Action and Preclinical Profle of Raloxifene , a Selective Estrogen Receptor Modulator. Reviews in Endocrine & Metabolic Disorders 2001;2:129-138.

[36] MacLeay JM, Olson JD, Enns RM, Les CM, Toth CA, Wheeler DL, et al. Dietary-induced metabolic acidosis decreases bone mineral density in mature ovariectomized ewes. Calcified Tissue International 2004;75:431-437.

[37] Newman E, Turner AS, Wark JD. The potential of sheep for the study of osteopenia: current status and comparison with other animal models. Bone 1995;16:277S-284S.

[38] Turner AS. The sheep as a model for osteoporosis in humans. Veterinary Journal 2002;163:232-239.

[39] Macleay JM, Sullivan E, Jackinsky S, Les C, Turner A. Ovine modeling of dietary induced metabolic acidosis and bone loss. International Congress Series 2007;1297:282-285.

[40] Zarrinkalam MR, Beard H, Schultz CG, Moore RJ. Validation of the sheep as a large animal model for the study of vertebral osteoporosis. European Spine Journal 2009;18:244-253.

[41] Macleay JM, Olson JD, Turner AS. Effect of dietary-induced metabolic acidosis and ovariectomy on bone mineral density and markers of bone turnover. Journal of Bone and Mineral Metabolism 2004;22:561-568.

[42] Keaveny TM, Guo XE, Wachtel EF, McMahon TA, Hayes WC. Trabecular bone exhibits fully linear elastic behavior and yields at low strains. Journal of Biomechanics 1994;27:1127-36.

[43] Bartel DL, Davy DT, Keaveny TM. Orthopaedic Biomechanics. 1st Editio. Prentice Hall. 2006.

[44] Carter DR, Caler WE, Spengler DM, Frankel VH. Fatigue behavior of adult cortical bone: the influence of mean strain and strain range. Acta Orthopaedica Scandinavica 1981;52:481-90.

[45] Erben RG. Embedding of bone samples in methylmethacrylate: an improved method suitable for bone histomorphometry, histochemistry, and immunohistochemistry. The Journal of Histochemistry and Cytochemistry 1997;45:307-313.

[46] Donnelly E, Baker SP, Boskey AL, van der Meulen MCH. Effects of surface roughness and maximum load on the mechanical properties of cancellous bone measured by nanoindentation. Journal of Biomedical Materials Research 2006;77:426-435.

[47] Donnelly E, Chen DX, Boskey AL, Baker SP, van der Meulen MCH. Contribution of mineral to bone structural behavior and tissue mechanical properties. Calcified Tissue International 2010;87:450-460.

[48] Burket JC, Gourion-Arsiquaud S, Havill LM, Baker SP, Boskey AL, van der Meulen MCH. Microstructure and nanomechanical properties in osteons relate to tissue and animal age. Journal of Biomechanics 2011;44:277-84.

[49] Gourion-arsiquaud S, Burket JC, Havill LM, Dicarlo E, Doty SB, Mendelsohn R, et al. Spatial Variation in Osteonal Bone Properties Relative to Tissue and Animal Age. Journal of Bone and Mineral Research 2009;24:1271-1281.

[50] Oliver WC, Pharr GM. An improved technique for determining hardness and elastic modulus using load and displacement sensing indentation experiments. Journal of Materials Research 1992;7:1564-1583.

[51] Akkus O, Polyakova-Akkus A, Adar F, Schaffler MB. Aging of microstructural compartments in human compact bone. Journal of Bone and Mineral Research 2003;18:1012-1019.

[52] Carden A, Morris MD. Application of vibrational spectroscopy to the study of mineralized tissues (review). Journal of Biomedical Optics 2000;5:259-268.

[53] Tarnowski CP, Ignelzi MA, Wang W, Taboas JM, Goldstein SA, Morris MD. Earliest mineral and matrix changes in force-induced musculoskeletal disease as revealed by Raman microspectroscopic imaging. Journal of Bone and Mineral Research 2004;19:64-71.

[54] Freeman JJ, Wopenka B, Silva MJ, Pasteris JD. Raman spectroscopic detection of changes in bioapatite in mouse femora as a function of age and in vitro fluoride treatment. Calcified Tissue International 2001;68:156-162.

[55] Penel G, Leroy G, Rey C, Bres E. MicroRaman spectral study of the PO4 and CO3 vibrational modes in synthetic and biological apatites. Calcified Tissue International 1998;63:475-481.

[56] Turunen MJ, Saarakkala S, Rieppo L, Helminen HJ, Jurvelin JS, Isaksson H. Comparison between infrared and Raman spectroscopic analysis of maturing rabbit cortical bone. Applied spectroscopy 2011;65:595-603.

[57] Williams RM, Zipfel WR, Webb WW. Interpreting second-harmonic generation images of collagen I fibrils. Biophysical journal 2005;88:1377-86.

[58] Zipfel WR, Williams RM, Webb WW. Nonlinear magic: multiphoton microscopy in the biosciences. Nature Biotechnology 2003;21:1369-77.

[59] Moreaux L, Sandre O, Mertz J. Membrane imaging by second-harmonic generation microscopy. Journal Of The Optical Society Of America B Optical Physics 2000;17:1685-1694.

[60] Campagnola PJ, Loew LM. Second-harmonic imaging microscopy for visualizing biomolecular arrays in cells, tissues and organisms. Nature Biotechnology 2003;21:1356-1360.

[61] Boyd R. Nonlinear Optics. 2nd ed. Amsterdam, The Netherlands: Academic Press. 2003.

[62] Gourion-Arsiquaud S, Boskey AL. Fourier transform infrared and Raman microspectroscopy and microscopic imaging of bone. Current Opinion in Orthopaedics 2007;18:499-504.

[63] Gourion-Arsiquaud S, West PA, Boskey AL. Fourier transform-infrared microspectroscopy and microscopic imaging. Methods In Molecular Biology 2008;455:293-303.

[64] Boskey AL, Mendelsohn R. Infrared spectroscopic characterization of mineralized tissues. Vibrational Spectroscopy 2005;38:107-114.

[65] Croucher PI, Garrahan NJ, Mellish RWE, Compston JE. Age-Related Changes in Resorption Cavity Characteristics in Human. Osteoporosis International 1991;1:257-261.

[66] Pienkowski D, Doers TM, Monier-Faugere MC, Geng Z, Camacho NP, Boskey AL, et al. Calcitonin alters bone quality in beagle dogs. Journal of Bone and Mineral Research 1997;12:1936-1943.

[67] Rey C, Renugopalakrishnan V, Collins B, Glimcher MJ. Fourier transform infrared spectroscopic study of the carbonate ions in bone mineral during aging. Calcified Tissue International 1991;49:251-258.

[68] Pleshko N, Boskey A, Mendelsohn R. Novel infrared spectroscopic method for the determination of crystallinity of hydroxyapatite minerals. Biophysical Journal 1991;60:786-793.

[69] Boskey AL, Pleshko Camacho N. FT-IR imaging of native and tissue-engineered bone and cartilage. Biomaterials 2007;28:2465-2478.

[70] Paschalis EP, Verdelis K, Doty SB, Boskey AL, Mendelsohn R, Yamauchi M. Spectroscopic characterization of collagen cross-links in bone. Journal of Bone and Mineral Research 2001;16:1821-1828.

[71] Arens D, Sigrist I, Alini M, Schawalder P, Schneider E, Egermann M. Seasonal changes in bone metabolism in sheep. Veterinary journal 2007;174:585-91.

[72] Kennedy OD, Brennan O, Rackard SM, Staines A, O'Brien FJ, Taylor D, et al. Effects of ovariectomy on bone turnover, porosity, and biomechanical properties in ovine compact bone 12 months postsurgery. Journal of Orthopaedic Research 2009;27:303-309.

[73] O'Brien FJ, Brennan O, Kennedy OD, Lee TC. Microcracks in cortical bone: how do they affect bone biology? Current Osteoporosis Reports 2005;3:39-45.

[74] Smith LJ, Schirer JP, Fazzalari NL. The role of mineral content in determining the micromechanical properties of discrete trabecular bone remodeling packets. Journal of Biomechanics 2010;43:3144-9.

[75] Miller LM, Little W, Schirmer A, Sheik F, Busa B, Judex S. Accretion of Bone Quantity and Quality in the Developing Mouse Skeleton. Journal of Bone and Mineral Research 2007;22.

[76] Donnelly E, Boskey AL, Baker SP, van der Meulen MCH. Effects of tissue age on bone tissue material composition and nanomechanical properties in the rat cortex. Journal of Biomedical Materials Research A 2010;92:1048-56.

[77] Busa B, Miller LM, Rubin CT, Qin Y-X, Judex S. Rapid establishment of chemical and mechanical properties during lamellar bone formation. Calcified Tissue International 2005;77:386-94.

[78] Drake MT, Clarke BL, Khosla S. Bisphosphonates: mechanism of action and role in clinical practice. Mayo Clinic Proceedings 2008;83:1032-45.

[79] Roelofs AJ, Thompson K, Gordon S, Rogers MJ. Molecular mechanisms of action of bisphosphonates: current status. Clinical Cancer Research 2006;12:6222s-6230s.

[80] Roelofs AJ, Thompson K, Ebetino FH, Rogers MJ, Coxon FP. Bisphosphonates : Molecular Mechanisms of Action and Effects on Bone Cells , Mono- cytes and Macrophages. Current Pharmaceutical Design 2010;16:2950-2960.

[81] Rogers MJ, Crockett JC, Coxon FP, Mönkkönen J. Biochemical and molecular mechanisms of action of bisphosphonates. Bone 2010;49:34-41.

[82] Reszka AA, Rodan GA. Mechanism of action of bisphosphonates. Current Osteoporosis Reports 2003;1:45-52.

[83] Reszka AA, Rodan GA. Nitrogen-containing bisphosphonate mechanism of action. Mini Reviews in Medicinal Chemistry 2004;4:711-9.

[84] Riggs BL, Hartmann LC. Selective estrogen-receptor modulators -- mechanisms of action and application to clinical practice. Journal of Medicine Cincinnati 2003;348.

[85] Antonakos A, Liarokapis E, Leventouri T. Micro-Raman and FTIR studies of synthetic and natural apatites. Biomaterials 2007;28:3043-54.

[86] Garcia IJ, Burket JC, MacLeay J, Calton E, van der Meulen, M C H Boskey AL. Effect of Zoledronic Acid on Trabecular Bone of an Ovine Model of Osteopenia at Multiple Skeletal Sites. Proceedings of the Orthopedic Research Society Annual Meeting. Moscone West Convention Center, San Francisco, CA, 2012.

CHAPTER 4

COMPOSITIONAL AND MECHANICAL EFFECTS OF BISPHOSPHONATE AND SERM TREATMENTS IN CORTICAL TISSUE FROM AN OVINE MODEL FOR HUMAN OSTEOPOROSIS

4.1 Introduction

The increased propensity for fracture with osteoporosis results from deterioration of both cancellous and cortical bone [1–10]. Fragility fractures occur at primarily cancellous sites such as the hip, wrist, and vertebrae [11,12], and consequently most studies focus on treatment effects in cancellous tissue while neglecting effects in cortical bone. The cortical shell becomes increasingly important for load bearing and fracture resistance with the preferential loss of cancellous bone with osteoporosis [2–5,13]. Additionally, The effects of treatments are often markedly different in cortical and cancellous tissue [14–17]. Therefore, cortical tissue is critical to evaluate the effectiveness and success of potential osteoporosis therapies.

Failure of cortical bone initiates with damage and microcracking at the tissue-level and is influenced by spatial distributions of properties within osteons and interstitial tissue [18–24]. Tissue composition and nanomechanical properties vary spatially within cortical bone due to the remodeling process and random biological variability, with tissue stiffness and hardness generally following trends in mineralization and aligned collagen content [25–30]. Thus, the newer, less-mineralized osteons in healthy human cortical bone have lower stiffness and hardness than older, more mineralized interstitial tissue [28,31–33]. Micro-CT based models of human cortical bone suggest nanoscale mechanical heterogeneity within cortical bone may promote energy dissipation [18,19]. Experimentally, nanomechanical differences between osteons and interstitial tissue influence fracture toughness [20–24].

Few studies have examined the effects of osteoporosis and antiresorptive treatments on nanoscale distributions of tissue composition and nanomechanical properties within cortical bone

[15,34]. Furthermore, the effects of nanoscale compositional and nanomechanical alterations on cortical tissue's resistance to cracking have not been investigated directly. Therefore, the present study utilized an ovine model for human high-turnover osteoporosis to examine effects of antiresorptive treatment on cortical tissue composition, nanomechanical properties, and microcrack resistance. Antiresorptive treatments reduce fracture risk by up to 60%, despite only modest increases (from 0 – 8%) in bone mineral density (BMD) [35–37]. This discrepancy suggests that tissue-level properties not measureable through macro-scale BMD measures play an important role in the reduction in fracture risk with antiresorptive treatments.

For the current study, treatment effects with a drug from the most widely-prescribed class of osteoporosis treatments—bisphosphonates—were compared with effects from another antiresorptive agent that acts through endogenous estrogen pathways in bone—a selective estrogen receptor modulator (SERM). Bisphosphonates reduce turnover by incorporating into bone matrix in regions of active remodeling and directly inhibiting osteoclastic activity upon resorption by these cells [38–41]. Vertebrae from canines treated with clinical doses of bisphosphonates have similar strength but reduced energy absorption relative to control animals with similar areal BMD, pointing to alterations in nanoscale tissue properties [42]. Indeed, cortical tissue from these animals showed increased levels of mineralization and reduced mineral heterogeneity after one year of treatment [42,43]. Excessive mineralization coupled with the reduced ability to repair microdamage with bisphosphonate treatment may promote the development and accumulation of microcracks [14,42].

In comparison, SERMs reduce bone turnover by binding to estrogen receptors and acting through estrogen response elements and coregulator proteins [44,45]. Bisphosphonates and SERMs produce similar reductions in vertebral fracture risk [46], despite reducing bone turnover by varying degrees and having distinctly different mechanisms of action. In canine studies, raloxifene enhanced vertebral strength independent of a change in BMD [47], and in vertebral cortical bone from rats, raloxifene increased indentation modulus and hardness relative to

ovariectomized controls [48].

The goals of this study were four-fold: 1) examine osteoporosis and treatment-induced alterations in nanoscale mechanical properties and tissue composition within osteons and interstitial cortical tissue, 2) determine the manner in which changes in tissue composition alter nanomechanical function, 3) investigate whether osteoporosis and antiresorptive treatments affect the ability of bone tissue to resist microcracking, and, 4) study the contributions of nanoscale tissue properties and crack resistance to mechanical function at higher length scales. We hypothesized that both bisphosphonate and SERM treatments would increase cortical tissue stiffness and hardness relative to osteoporotic tissue through increased mineralization and altered mineral and matrix properties. In a previous study of cancellous tissue from these ewes, increased tissue stiffness and hardness with treatment correlated with increased tissue mineralization, carbonate substitution in the mineral lattice, and lamellar aligned collagen content [49]. Effects in cortical tissue were predicted to be less than those in cancellous tissue because cortical tissue is less metabolically active and bisphosphonate uptake is greater in cancellous than cortical tissue [50,51].

4.2 Materials and Methods

The present study utilized cortical tissue from the femora of ewes (Swiss-Ramboulet, aged 6-7 years at the start of the experiments) subjected to a dietary metabolic acidosis model (MA) for human osteoporosis and treated with a SERM, raloxifene (RAL), or a bisphosphonate, zoledronate (ZOL). Effects in cortical bone were examined at the whole bone scale and at the bulk and nanoscale tissue levels.

4.2.1 Samples and Specimen Preparation

Femora were obtained from 25 mature adult ewes (6-7 years old at the start of the experiment) from 2 experiments described previously (approved by the Colorado State University

Institutional Animal Care and Use Committee) [49]. Originally, the bisphosphonate and SERM treatments were planned as a single experiment; however, due to difficulty administering alendronate in the first study, the bisphosphonate study was repeated with zoledronate and the MA group for comparison. The first experiment (Experiment 1) had two groups. Both were fed a diet to induce metabolic acidosis for six months followed by another six months of MA with either vehicle (MA1, n = 5) or a clinically equivalent dose of raloxifene (RAL, 0.80 mg/kg daily, n = 4) administered daily through abomasal cannulae [52,53]. Both treatment groups started with n = 6 sheep, based on a power analysis for nanoscale measurements in a pilot study plus one additional sheep per treatment group in accordance with standard procedure for ovine experiments at Colorado State University. Two RAL sheep were euthanized early due to cannula pull-out and one MA sheep was euthanized due to injuries unrelated to the experiment. A group of healthy animals fed a normal diet (CONT, n = 5) were housed in the same facility and euthanized in the same season (summer) as Experiment 1. The second experiment (Experiment 2) also had two treatment groups. Both groups received eight months of MA rather than six months due to a delay in receiving the medication for the study. Subsequently, the groups were maintained on the MA diet for an additional 6 months before euthanasia (winter) with intravenous administration of either vehicle (MA2, n = 6) or a clinically equivalent dose of zoledronate (ZOL, 5 mg/sheep, n = 6) at the beginning of the treatment period. The second experiment included a MA group to compare the effects of zoledronate treatment with the ovine osteoporosis model, but did not include a normal diet control group. After euthanasia, femora were stored at -20º C prior to specimen preparation.

Whole bone mechanical testing was performed on the right femora. Left limbs were used for bulk mechanical tests of cortical beams (supplementary content, Figure 4.1s), nanoscale compositional and mechanical analysis, and indentation fracture tests. Three millimeter-thick transverse sections from the mid-diaphysis were used for nanoscale tissue characterization and indentation fracture tests. Cranial-caudal diameter, medial-lateral diameter, and cortical

thickness (average of 4 measurements) were also measured from these transverse sections (Image J, NIH, Bethesda, MD).

4.2.2 Whole Bone Mechanical Analysis

Whole bone mechanical properties were assessed via four-point bending. The ends of the femora were potted with methylmethacrylate (COE tray plastic, GC America, Inc., Alsip, IL) in square aluminum tubing to ensure reliable positioning between tests. The span between pots was 110 mm for all femora. For testing, the femora were placed in a four-point bending fixture (inner span 130 mm, outer span 210 mm) attached to a servohydraulic material testing machine (858 Mini Bionix with Flextest 40 controller, MTS Systems Corporation, Eden Prarie, MN). The fixture contacted the pots rather than the bone directly to reduce stress concentrations and ensure that the diaphysis was subjected to a constant bending moment. Each femur was first loaded non-destructively in the medial-lateral, lateral-medial, cranial-caudal, and caudal-cranial directions. These non-destructive tests consisted of ten preconditioning cycles of 10 to 1000 N of compression applied at a rate of 7200 N/min. Finally, the femora were loaded to failure in the caudal-cranial direction (caudal aspect subjected to compression and cranial aspect subjected to tension) at a rate of 5 mm/min. Bending stiffness, the slope of the linear portion of the moment-displacement graph, was determined via linear regression. For non-destructive tests, the regression was performed on the tenth loading cycle. The failure moment was defined as the maximum moment achieved in the destructive test.

4.2.3 Nanoscale Tissue Characterization

The transverse mid-diaphyseal sections were prepared for nanoscale mechanical testing as reported previously [29,49,54]. Sections were fixed, dehydrated, embedded in polymethlymethacrylate, and polished anhydrously to a RMS surface roughness of less than 15 nm on a 5 x 5 μm^2 AFM Scan (Dimension 3100, Veeco Metrology Group, Plainview, NY)

[27,54–56]. Three osteons and three nearby interstitial regions from each sample were selected for characterization. The osteons chosen were quiescent and showed no evidence of remodeling activity such as ruffled or enlarged Haversian canals.

Tissue was characterized at the center of each lamella in a radial line from the center to the periphery of the osteons and at five locations in each of the nearby interstitial regions (at centers of lamellae if present). Nanomechanical properties were probed first with nanoindentation and then the residual indentations and fiducial markers were used to co-locate Raman spectroscopy and second harmonic generation microscopy (SHG) compositional measurements.

4.2.3.1 Nanoindentation

A scanning nanoindenter with a Berkovich diamond tip (Triboindenter, Hysitron, Inc., Minneapolis, MN) was used to probe tissue nanomechanical properties within osteons and interstitial tissue. To accurately place indentations at centers of lamellae, surface topography scans (20 μm^2) were made prior to each indentation [27,29,30,54,56]. The load function included a 10 second hold at 700 μN peak load with loading/unloading rates of 50 μN/s [29]. The resulting indentation depth was approximately 150 nm. Each osteon contained a mean of 13 (± 3) lamellae, resulting in roughly 40 osteonal and 15 interstitial measurements (5 per adjacent interstitial region) per animal. Indentation modulus (E_i), a measure of the tissue's elastic properties, and hardness, a measure of inelastic properties, were calculated from the unloading portion of the load-displacement curve [57].

4.2.3.2 Raman Spectroscopy

Tissue composition was characterized with Raman spectroscopy (InVia microRaman, Renishaw, Gloucestershire, United Kingdom) at the same locations characterized by nanoindentation [29,49]. The spot size was 2 μm^2. For each measurement, Raman peak heights were identified

from smoothed spectra after cubic polynomial background subtraction (Matlab, The Math Works, Inc., Natik, MA). Three bone parameters were calculated: mineral-to-matrix ratio (Raman mineral:matrix), B-type carbonate substitution, and crystallinity (Raman crystallinity) [29,58–63]. Mineral-to-matrix ratio, a measure of the degree of mineralization of the tissue, was calculated as the peak height ratio of the phosphate υ1 (~965 cm^{-1}) to the CH_2 wag (~1450 cm^{-1}) peaks [29,59]. B-type carbonate substitution, a measure of the level of carbonate substitution for phosphate in the hydroxyapatite (HA) crystal lattice, was calculated as the peak height ratio of the carbonate υ1 (~1070 cm^{-1}) to the phosphate υ1 peak [29,62]. Raman crystallinity, a measure of crystal size and perfection, was estimated as the reciprocal of the full width at half maximum (FWHM) of the phosphate υ1 peak [29,61,63]. For this measure, a sharper phosphate υ1 peak (decreased FWHM) indicates greater mineral crystal size and perfection.

4.2.3.3 Second Harmonic Generation Microscopy (SHG)

Aligned collagen content was assessed via SHG as described previously (Mai Tai Deep See, Spectra Physics; BX61W1, Olympus, Santa Clara, CA) [29,49]. The pixel size was 0.318 μm^2. A SHG image was taken of each osteon and interstitial region previously characterized with nanoindentation and Raman spectroscopy. The square root of SHG intensity in these images equals the concentration of aligned collagen molecules (aligned collagen content) within the transverse plane of the sample [64–68]. For each osteon, the aligned collagen content was calculated for the radial line across the osteon from center to periphery, resulting in a profile of aligned collagen content with distance from the center of the osteon (Matlab, The Math Works, Inc.). The line was 6 pixels wide, corresponding to the Raman spot size of 2 μm. From this profile, maxima corresponding to lamellar aligned collagen and minima corresponding to interlamellar aligned collagen were recorded [27]. For each interstitial region, a 20 μm^2 region surrounding the 5 interstitial indents was analyzed. For this region, the mean and FWHM of aligned collagen content were recorded rather than maxima and minima corresponding to

lamellar and interlamellar regions because interstitial tissue often did not contain well-defined lamellae.

4.2.4 Indentation Fracture Tests

The relative ability of the cortical tissue to resist cracking was assessed via indentation fracture. After analysis with nanoindentation, Raman spectroscopy, and SHG, the transverse sections were sputter coated under vacuum with a 10 nm-thick layer of Au-Pd. Images of 5 osteonal and 5 interstitial regions were taken at 1000 X magnification with a scanning electron microscope (SEM) at an accelerating voltage of 15 keV (Leica Stereoscan 440, Buffalo Grove, IL). These images were used to identify pre-existing cracks. A microindenter with a custom cube-corner tip (Highwood Digital Micro Hardness Tester HWMMT, TTS Unlimited, Inc., Osaka, Japan; Micro Star Technologies, Huntsville, Texas) was used to induce cracking [69] in the pre-imaged osteonal and interstitial regions by indenting to a peak load of 490 mN with a 10 second hold period at peak load. In preliminary tests, this peak load was reliably produced cracking. Indentation depth was over three orders of magnitude greater than the thickness of the Au-Pd surface coating for SEM imaging, and cracking behavior was not different between samples indented with and without the Au-Pd coating. After indenting, the regions were re-imaged with SEM. Pre-and post-images were compared to identify new cracks visible on the surface. Surface cracks were measured manually via Image J software (NIH, Bethesda, MD). Four outcome measures were recorded for each indentation: the total amount of cracking, number of cracks, mean crack length, and maximum crack length. The total amount of cracking was the sum of all new crack lengths (new cracks plus extensions of pre-existing cracks) created by each individual indentation fracture. The number of cracks was the total number of new cracks and crack extensions formed by each indentation fracture. The mean crack length was the average of the crack lengths formed by each indentation fracture. The maximum crack length was the longest crack measured for each indentation fracture.

4.2.5 Statistical Analysis

Statistical analyses were performed separately for Experiment 1 and 2, i.e. RAL was compared only with MA1 and CONT, while ZOL was compared only with MA2. All statistical models were linear. Effects of treatment on whole bone mechanical testing parameters were assessed with single-factor ANOVAs with Tukey post-hoc tests. The significance level was $p \leq 0.05$. Results stated are significant unless noted otherwise. Figures display mean values with error bars representing 95% confidence intervals.

Osteonal measurements were analyzed first to determine whether nanomechanical and compositional parameters varied across the osteon radii with treatment. Multi-factor, nested ANOVAs with Tukey post-hoc tests determined effects of treatment (CONT, MA, and RAL; MA2 and ZOL), distance from the center of the osteon, treatment*distance, sheep (nested), and trabeculae (nested). Next, osteonal and interstitial measurements were analyzed together to determine differential effects of treatment between these tissue regions. Multi-factor ANOVAs determined effects of treatment, tissue type (osteonal or interstitial), treatment*tissue type, sheep (nested) and trabeculae (nested).

The contribution of compositional properties (SHG and Raman) to alterations in tissue nanomechanical properties was determined by multiple linear regression analysis. The mean values for the compositional and nanomechanical parameters were calculated for each osteon. Correlating these averaged values rather than each individual measurement location reduced variability from inherent heterogeneity of the bone tissue or slight misalignment between measurement locations. Correlations were performed separately for Experiment 1 and Experiment 2. First, ANOVA models were performed for E_i and H vs. mineral-to-matrix ratio, B-type carbonate substitution, crystallinity, lamellar aligned collagen, and treatment, allowing the relationships between compositional and nanomechanical parameters to vary with treatment. Subsequently, non-significant terms were removed from the model stepwise in order of decreasing p-value until only significant effects remained. Finally, all compositional parameters

were removed leaving only treatment. Thus, the added explanatory power of the significant compositional measures over a model with treatment alone could be determined. For significant improvement in explanatory power, a minimum 5% increase in the R^2 value was considered statistically significant.

The effects of treatment on micro-cracking were also assessed with multi-factor ANOVAs with Tukey post-hoc testing. Model parameters included treatment (CONT, MA, and RAL; or MA2 and ZOL), tissue type (osteonal or interstitial), treatment*tissue type, and sheep (nested).

4.3 Results

4.3.1 Whole Bone Mechanical Analysis

Zoledronate but not raloxifene improved whole bone mechanical performance relative to the MA model (Figures 4.1). MA did not alter whole bone mechanical performance relative to control animals. Zoledronate increased whole bone bending stiffness by 30% and failure moment by 49% in the cranial-caudal direction over MA in whole bone non-destructive and failure tests of the diaphysis (Figure 4.1). Mid-diaphyseal cortical diameter, thickness, and area were not different between treatment groups (Appendix 1).

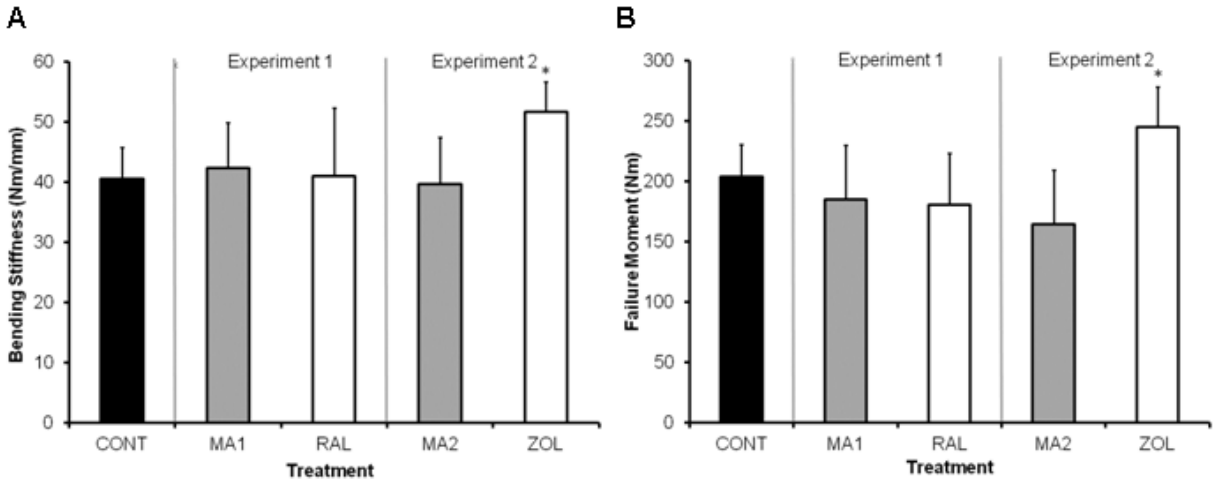

Figure 4.1 *Whole bone mechanical testing results from four-point bending tests to failure in the cranial-caudal direction. Zoledronate increased both bending stiffness and failure moment relative to the MA model. * $p < 0.05$*

4.3.2 Nanoscale Tissue Characterization

Indentation modulus, hardness, and aligned collagen content decreased in the cortical tissue of MA ewes relative to controls (Figure 4.2). The decrease in indentation modulus depended on the tissue type and was 8.5% in osteons and 12% in interstitial tissue. Hardness decreased by 10% independently of tissue type. Within osteons, lamellar aligned collagen decreased by 18% and interlamellar aligned collagen decreased by 11% with MA relative to controls (Figure 4.3). Interstitial aligned collagen and crystallinity did not vary with MA.

Raloxifene restored indentation modulus, hardness, and lamellar aligned collagen to control levels in osteonal tissue (Figures 4.2 and 4.3). In interstitial tissue, only hardness was fully restored to control levels. Indentation modulus increased by 9.2%in osteons with raloxifene relative to MA and was equal to that of controls, while interstitial indentation modulus increased by 7.3% relative to MA but was still 5.0% below control levels. Hardness increased 9.5% with raloxifene and reached control levels regardless of tissue type. Within osteons, lamellar aligned collagen increased by 22% relative to MA to reach control levels (Figure 4.3).

Interlamellar aligned collagen also increased relative to MA (+10%) and was restored to control levels.

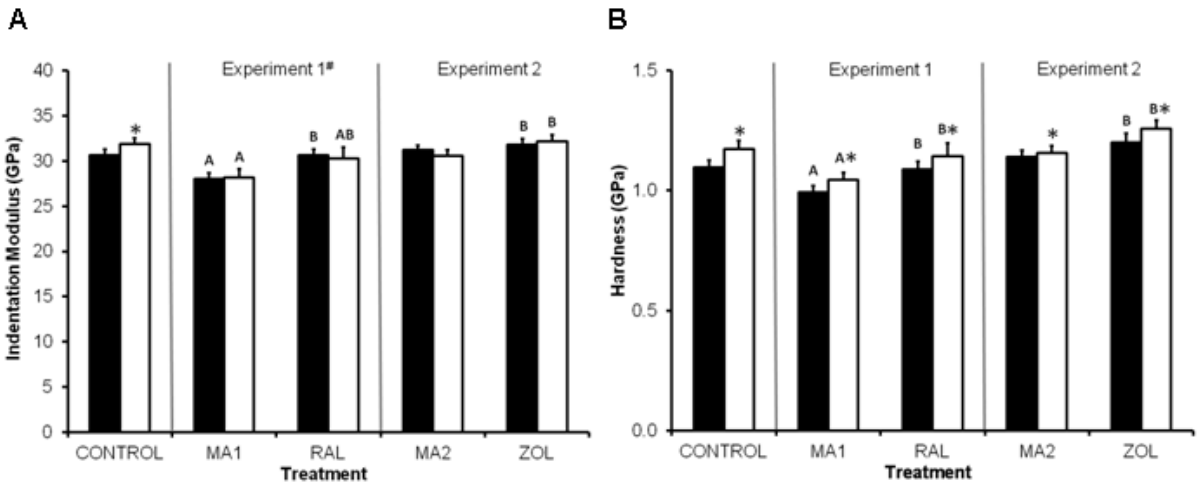

Figure 4.2 *Nanomechanical testing results by treatment for osteonal and interstitial tissue. Both raloxifene and zoledronate increased indentation modulus and hardness relative to the MA model. Solid bars = lamellar osteonal tissue. Osteonal properties were fully restored to CONTROL levels. Open bars = interstitial tissue. A = different from CONTROL. B = different from MA. * = different from osteonal tissue. # = effects of treatment varied by tissue type.*

Zoledronate increased indentation modulus and hardness in osteons and interstitial regions relative to MA (Figure 4.2). Indentation modulus increased by 3.6% and hardness increased by 6.9%, regardless of tissue type. Aligned collagen content did not vary with zoledronate (Figure 4.3). Alterations in Raman compositional parameters with MA, raloxifene, and zoledronate were minimal (supplementary content, Figure 4.2s).

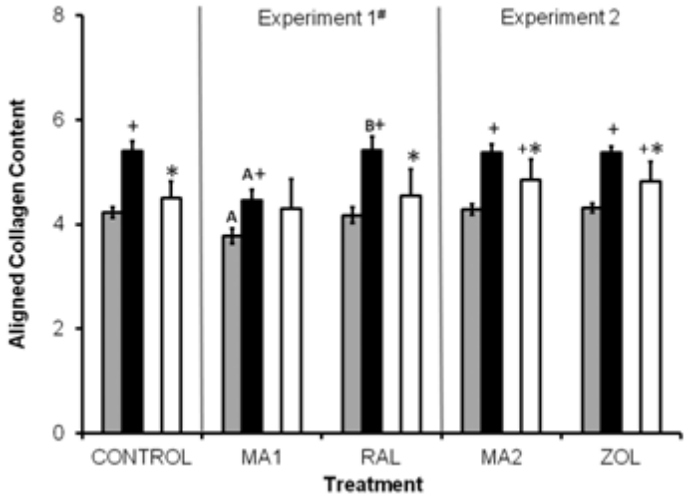

Figure 4.3 *Aligned collagen content by treatment for interlamellar and lamellar osteonal tissue and interstitial tissue. Gray bars = interlamellar osteonal tissue. Black bars = lamellar osteonal tissue. Open bars = interstitial tissue (average over 20 μm² area surrounding indentations). A = different from CONTROL. B = different from MA. + = different from interlamellar osteonal tissue. * = different from lamellar osteonal tissue. # = effects of treatment varied by tissue type.*

4.3.3 Correlations between Nanoscale Composition and Nanomechanical Parameters

For Experiment 1 (CONT, MA1, and RAL), indentation modulus and hardness correlated with B-type carbonate substitution, lamellar aligned collagen, and crystallinity, and indentation modulus additionally correlated with mineral-to-matrix ratio (Table 4.2, Figure 4.6). Compositional parameters alone explained only 21% of the variation in indentation modulus and did not significantly predict variations in hardness. Allowing compositional relationships to vary with treatment improved the predictive values of the models to 48% for indentation modulus and 19% for hardness. The positive relationship between indentation modulus and mineral-to-matrix ratio was independent of treatment (5% explanatory power). Though small in magnitude (supplementary content, Figure 4.2s), alterations in B-type carbonate substitution explained 36% of the variation in indentation modulus with MA and 10% of the variation in hardness in controls. In other treatment groups, B-type carbonate substitution did not significantly predict nanomechanical variations. The positive correlation with crystallinity predicted 14% of the variation in indentation modulus and 12% of the variation in hardness in control and MA animals

but did not predict nanomechanical parameters within RAL-treated animals. Lamellar aligned collagen explained 26% and 19% of the variation in hardness in controls and MA animals, respectively, but was not a predictor for hardness within RAL-treated animals.

Nanomechanical Parameter	Composition Only	Treatment + Composition	
Experiment 1	**R^2**	**R^2**	**Significant Parameters**
Indentation Modulus	0.21	0.48	Mineral:matrix B-type carbonate substitution$^+$ Crystallinity$^+$ Lamellar aligned collagen
Hardness	N.S.	0.19	B-type carbonate substitution$^+$ Crystallinity$^+$ Lamellar aligned collagen$^+$
Experiment 2			
Indentation Modulus	N.S.	0.11	B-type carbonate substitution$^+$ Crystallinity
Hardness	N.S.	0.09	B-type carbonate substitution$^+$

Table 4.1 *Coefficients of variation (R^2) for osteonal nanomechanical properties modeled as linear functions of compositional parameters. "Composition Only" indicates the explanatory power of the linear models with significant compositional parameters only ($p < 0.05$). "Composition + treatment" indicates the explanatory power of the models with significant compositional parameters, treatment, and the effects of treatment on the nanomechanical relationships with composition.* $^+$ *Indicates compositional parameters whose effects varied with treatment. An increase in $R^2 > 0.05$ is considered a meaningful improvement.*

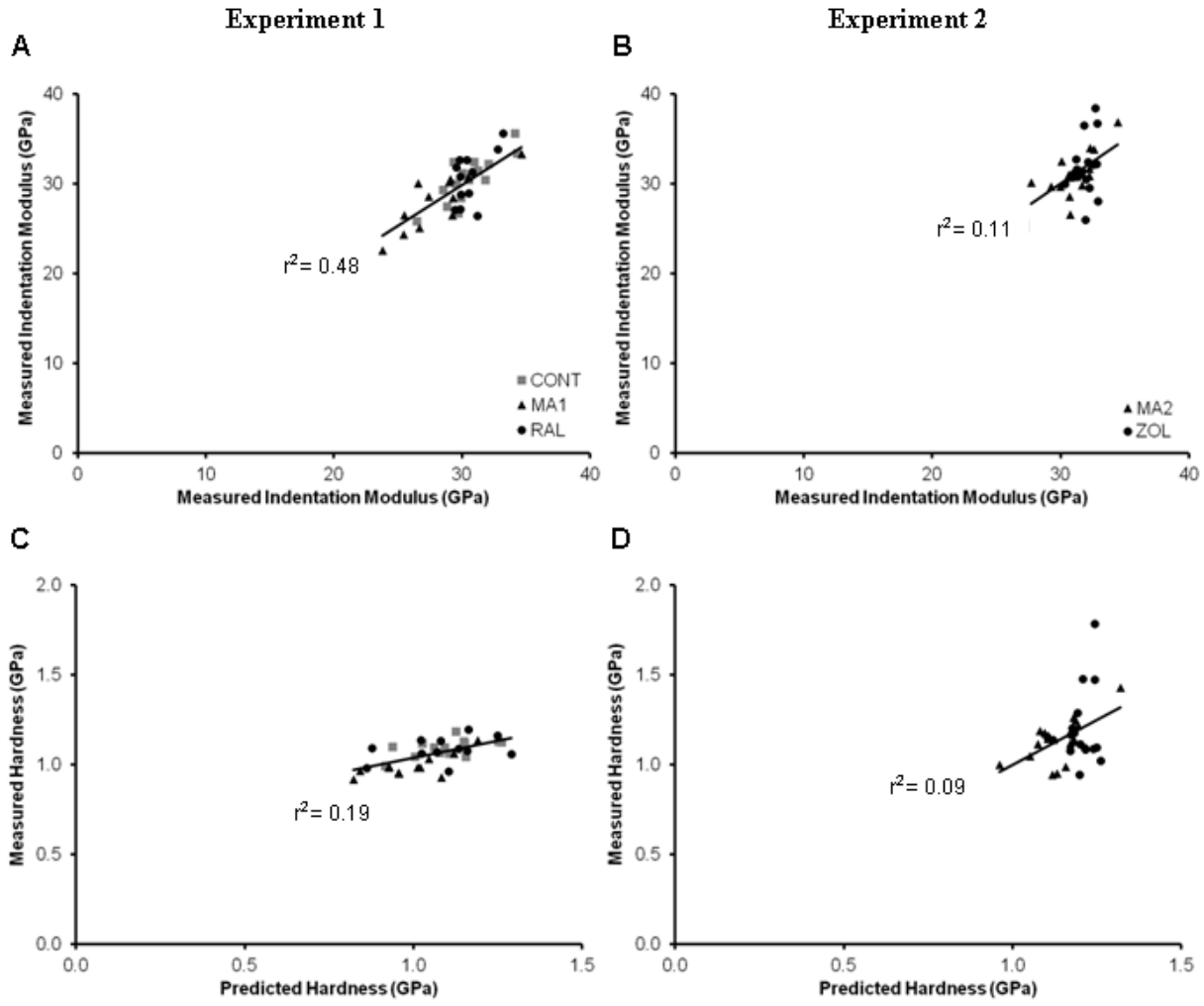

Figure 4.4 *Measured nanomechanical parameters vs. predicted values from the compositional ANOVA models for each experiment (Table 2). Relationships between nanomechanical and compositional parameters were allowed to vary between treatment groups.*

For Experiment 2 (MA2 and ZOL), composition alone did not predict variations in nanomechanical parameters because compositional relationships depended on treatment. B-type carbonate substitution predicted 31% and 39% of the variation in indentation modulus and hardness with MA, respectively, but predicted less than 5% of the nanomechanical variations in zoledronate-treated animals. The explanatory power of the models for indentation modulus and hardness was much poorer for Experiment 2 than for Experiment 1.

4.3.4 Indentation Fracture Tests

Cracks formed during cube-corner indentation were classified into three main types: circumferential cracking and deformation immediately around the indentations, radial cracks extending outward from the indentations, and cracks extensions from nearby stress concentrators such as osteocytes or pre-existing cracks (Figures 4.7 and 4.8). The total amount of cracking around the indentations did not vary between treatment groups; however, the mean crack length was 45% longer in MA1 than in control sheep (Figure 4.9). Raloxifene reduced the mean crack length relative to MA (-20%), but the mean length was still greater than that present in controls (+17%). From visual inspection, the increased crack length in MA1 sheep was due to more radial cracking that extended farther from the indentations. In contrast to raloxifene, zoledronate did not have any effect on mean crack length relative to MA animals.

Interstitial tissue had a greater total amount of cracking in both experiments due to both increased numbers of cracks and extended crack lengths. The total amount of cracking was 18% and 29% greater in interstitial tissue than in osteons in Experiments 1 and 2, respectively. For Experiment 1, the maximum crack length was 12% longer for interstitial tissue than osteons and interstitial tissue trended towards having increased numbers of cracks (+10%, Appendix 1). In Experiment 2, interstitial cracks had a greater mean crack length (+8%) and trended towards increased maximum crack length (+10%) relative to osteons. Interstitial tissue also had greater numbers of cracks in Experiment 2 (+21% vs. MA2).

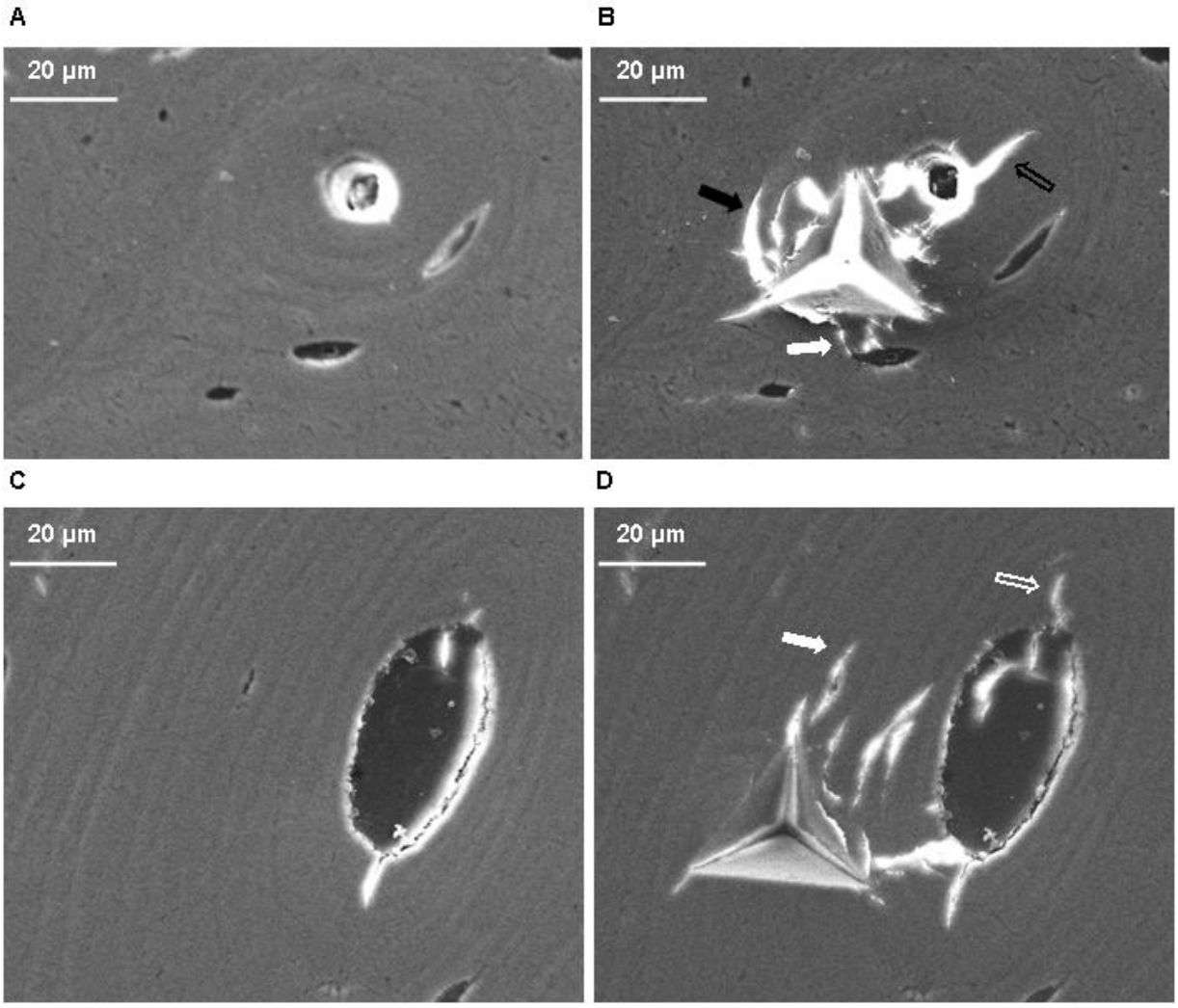

Figure 4.5 *SEM images of osteons taken before (A,C) and after (B,D) indentation fracture for a sheep from MA1 (A, B) and raloxifene (C, D) treatment groups. Dark areas are Haversian canals and osteocyte lacunae. Cracks and some edges around Haversian canals and osteocyte lacunae appear white due to edge brightening from the SEM. Several crack behaviors are evident: cracks deflected along lamellae and cement lines (solid black arrow), and extended from stress concentrators such as Haversian canals (outlined black arrow), osteocytes (solid white arrows), and pre-existing cracks (outlined white arrow).*

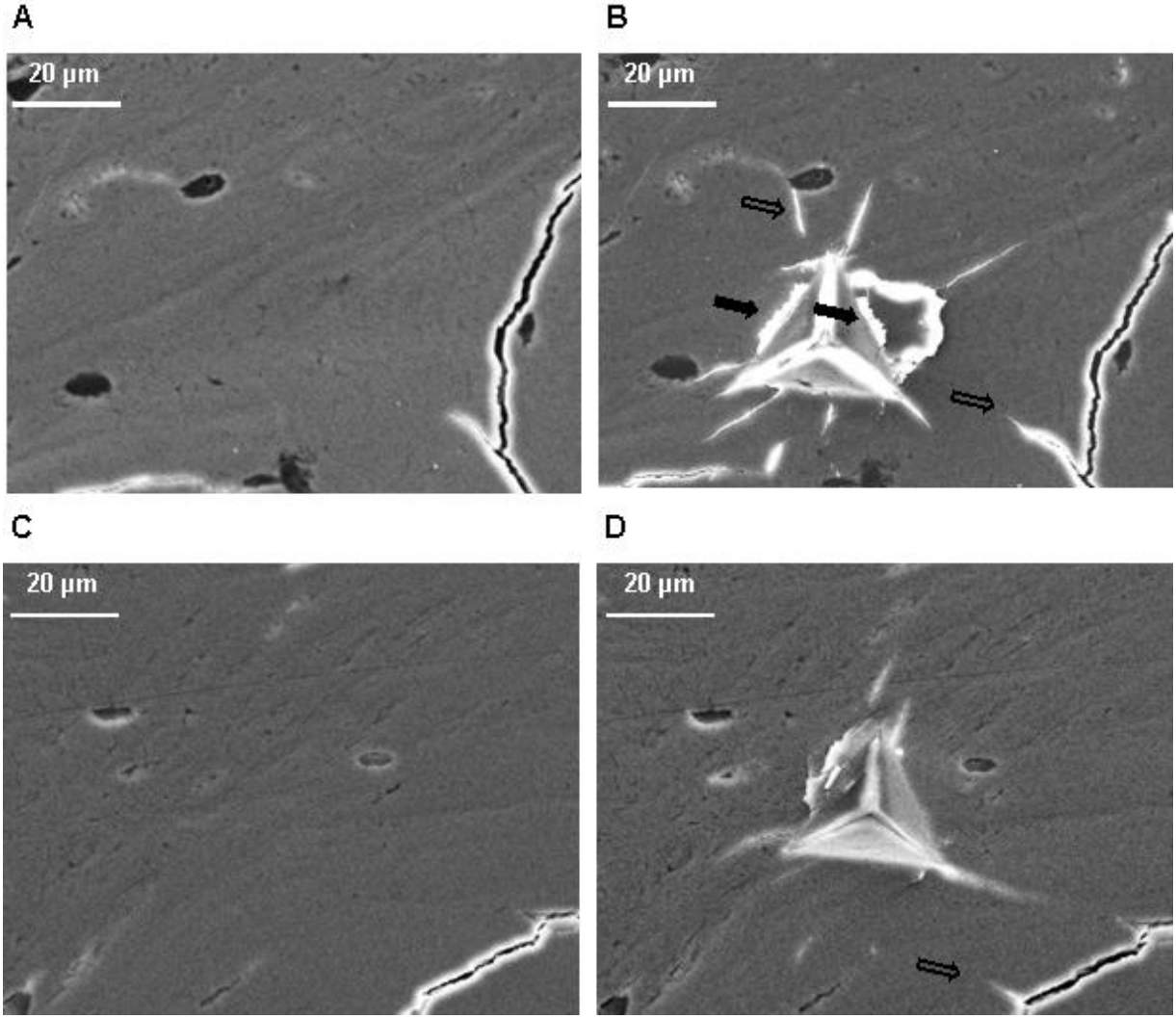

Figure 4.6 *SEM images of interstitial regions taken before and after indentation fracture for a sheep from (A,B) MA1, and (C,D) raloxifene treatment groups. Dark areas are osteocyte lacunae. Cracks and edges around some osteocyte lacunae appear white due to edge brightening from the SEM. Cracking/crushing around sides of indentations was evident (solid black arrows) as well as cracks extending radially away from the indentations and crack extensions from stress concentrators such as osteocytes or pre-existing cracks (hollow black arrows). Cracks initiated from osteocytes but were also arrested by osteocytes.*

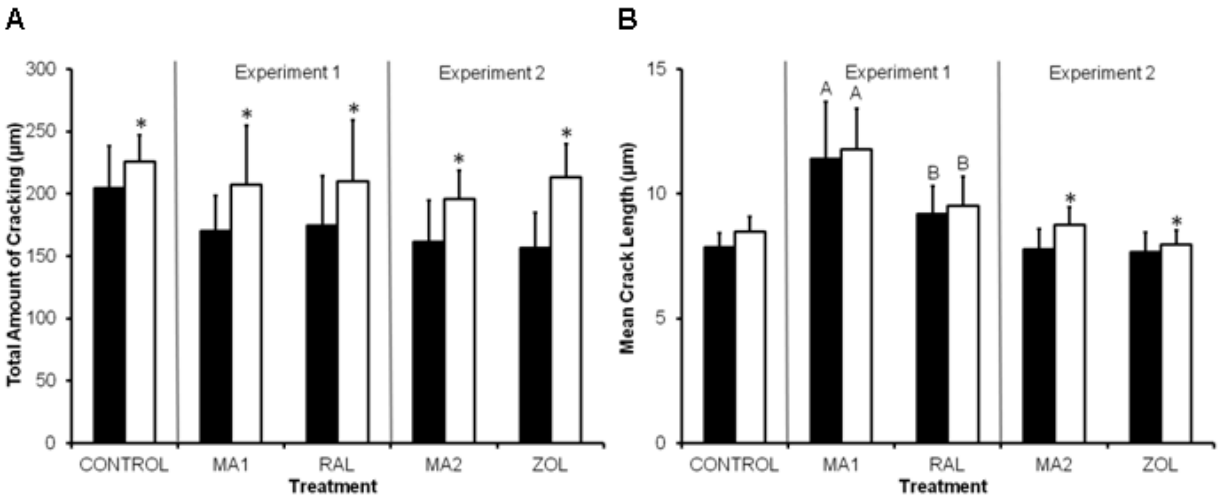

Figure 4.7 *Indentation fracture results by treatment for osteons and interstitial regions. The total amount of cracking (sum of all crack lengths) was greater in interstitial than osteonal tissue but did not vary between treatment groups. The mean crack length was greater with MA1 than CONTROL and was reduced relative to MA1 with raloxifene treatment to reach levels equivalent to control. Treatment affected osteonal and interstitial tissue similarly. Solid bars = osteonal regions. Open bars = interstitial regions. A = different from CONTROL. B = different from MA. * = different from osteonal tissue.*

4.4 Discussion

At the nanoscale, six months of treatment with either raloxifene or zoledronate reversed the degradation in cortical nanomechanical properties in an ovine model for human high-turnover osteoporosis. Raloxifene restored indentation modulus and hardness to control levels in osteons and also increased these properties in interstitial tissue. Alterations in all four compositional parameters—mineral-to-matrix ratio, B-type carbonate substitution, lamellar aligned collagen and crystallinity—explained nearly 50% of the variation in indentation modulus in control, MA, and raloxifene-treated ewes. Alterations in all but mineral-to-matrix ratio explained up to 20% of the variations in hardness. B-type carbonate substitution and lamellar aligned collagen provided the majority of the predictive power for both models. Nanomechanical properties with MA2 and zoledronate also correlated with alterations in B-type carbonate substitution, with the relationships depending on treatment; however, the predictive power of the models was limited.

Cortical nanomechanical improvements with raloxifene were similar to those seen previously in cancellous tissue from these animals; however, improvements with zoledronate were markedly less in cortical tissue (supplementary content, Table 4.1s) [49]. In both cancellous and cortical bone, raloxifene increased tissue stiffness and hardness by nearly 10% relative to MA. Raloxifene acts through the natural estrogen receptor pathways present in bone [44,45] and consequently seems to produce relatively uniform nanomechanical effects throughout cancellous and cortical bone tissue. In comparison, zoledronate increased stiffness and hardness, respectively, by 12 and 16% in cancellous tissue (near the surfaces of trabeculae), but only increased these properties by 3.5 and 6.9% in cortical tissue. Bisphosphonate uptake is greater in cancellous than cortical bone due to the greater surface area and number of active remodeling sites where the drugs preferentially incorporate [50,51]. Bisphosphonates provide less improvement in BMD in the peripheral skeleton, where the proportion of cortical to cancellous bone is greater than in the central skeleton [70].

Mineralization and tissue stiffness became more uniform throughout cortical tissue with the MA model. In Experiment 1, interstitial tissue was more mineralized and stiffer than osteonal tissue in healthy animals, but had equivalent mineralization and stiffness to osteons with MA (Figures 4.1 and supplementary content, Figure 4.2s). Additionally, the positive gradients in mineralization, stiffness, and mineral crystallinity from center to periphery of osteons present in healthy ewes were no longer present with MA (supplementary content, Table 4.2s). The increased homogeneity in osteoporotic tissue is well documented [71–74], and the present results show the manner in which this homogenization occurs spatially within the osteons and interstitial tissue of an ovine model of post-menopausal osteoporosis. Computational modeling suggests that nanoscale mechanical heterogeneity promotes energy dissipation [18,19]. The osteonal structure of cortical bone and the ratio of interstitial to osteonal mechanical properties influence crack behavior and fracture toughness [20–24].

The total amount of cracking associated with indentation fracture did not vary between treatment groups; however, treatment did affect cracking behavior. The mean crack length was greater with MA than in healthy sheep, indicating that the cortical tissue was less able to withstand crack growth once cracking was initiated. Interestingly, MA ewes had less aligned collagen content within osteons, and collagen fiber bridging is a known toughening mechanism in bone that acts to prevent the elongation of cracks [75]. With raloxifene, aligned collagen content was restored to control levels and crack length decreased. Other toughening mechanisms common to bone were also observed in this experiment, such as uncracked ligament bridging and crack deflection along cement lines and lamellae in osteons (Figures 4.7 and 4.8) [75]. In comparison with raloxifene, no improvements in crack length or number were observed relative to MA sheep with zoledronate treatment. Beagles treated for three years with a clinical dose of bisphosphonates showed no difference in crack density or numbers but had increased crack length relative to healthy animals [42]. In this study, six months of zoledronate did not increase crack length or the total amount of cracking in comparison with a model more representative of human osteoporosis.

Older, interstitial cortical tissue was more mineralized and harder than younger, osteonal tissue and showed an increased propensity for cracking. Interstitial tissue had both greater numbers of cracks—indicating decreased resistance to microcrack formation—and longer cracks—indicating decreased resistance to crack propagation once initiated. Similar increases in tissue age and mineralization with the long-term suppression of remodeling (as with long-term bisphosphonate treatment) may result in tissue less able to prevent crack initiation and propagation.

Although raloxifene produced greater effects than zoledronate at the nanoscale, only zoledronate increased bending stiffness and failure moment in whole bone tests relative to the osteoporosis model. Stiffness and strength also increased with four months of bisphosphonate treatment in the tibiae of ovariectomized rats [76]. No increase in stiffness or strength was

observed in the beagle ribs; however, the beagles were not osteopenic or osteoporotic and differences could exist between the femur and the rib, a non-load-bearing site [42]. In the current study, a trend towards increased bulk tissue stiffness was observed with zoledronate but not raloxifene relative to the MA model in apparent-level bending tests of cortical beams (supplementary content, Figure 4.1s). Similarly, one year of treatment with a clinical dose of raloxifene did not alter the strength or stiffness of cortical beams machined from beagle femora [77]. In both the present study and the beagle stud, animals were ovary-intact and had replete levels of estrogen that could blunt the effects of raloxifene. Raloxifene improved post-yield behavior in cortical tissue loaded in bending [77]; however, the ovine whole bone and apparent-level cortical tests in the present study had little post-yield behavior, which precluded comparison between studies.

Changes in Raman compositional parameters in cortical tissue were less pronounced than those observed previously in cancellous bone from these ewes (supplementary content, Table 4.1s) [49]. Cortical compositional alterations were expected to be less pronounced due to the lower metabolic activity in cortical bone and the aforementioned bisphosphonate targeting to cancellous tissue. Furthermore, the limited explanatory power of some of the nanomechanical versus compositional correlations and the fact that some compositional relationships varied between treatment groups indicates that additional compositional factors not measured in this study also play an important role in mechanical function. These factors could include non-enzymatic collagen cross-links, accumulation of advanced glycation end-products, mineral crystal orientation, and non-collagenous proteins [43,78,79].

Several limitations could affect the interpretation of our results. Previously in the MA model, adaptive changes were seen in cortical bone after six months of exposure to the acidifying diet [80]. BMD of the femur showed little change because the decrease in cancellous BMD was accompanied by an increase in BMD in the diaphysis. In the current study, mineral-to-matrix ratio in the cortical tissue of the mid-diaphysis of the femur increased slightly with MA relative

to healthy ewes (supplementary content, Figure 4.2s), consistent with these adaptive changes. Additionally, the range of the nanoscale data for Experiment 2 was quite small due to the smaller changes in cortical tissue properties with zoledronate. The small range of the data likely contributed to the limited explanatory power of the nanomechanical vs. compositional correlations for Experiment 2.

A few methodological limitations are also worth noting. First, the sample size of the large animal model was adequately powered for nanoscale measurements that benefit from repeated measures, but the sample size was underpowered for bulk tissue characterization. Additionally, large variations in bulk tissue measures between animals affected our ability to detect treatment effects; therefore, the lack of bulk-level effects reflects a combination of lower resolution and inadequate sample size. Secondly, nonconcurrent performance of the two experiments of this study prevented direct statistical comparison between all treatment groups. Ideally, controls would have been included as part of the Experiment 1 design; however, animals were housed in the same facility and euthanized in the same season. The delay in administering zoledronate in Experiment 2 prolonged the MA period by two months. Also, animals in Experiment 2 were euthanized in a different season than Experiment 1 (winter vs. summer, respectively). Both factors could produce differences between the two MA groups at the start of treatment, which might influence treatment effectiveness. Consequently, direct comparisons between Experiment 2 and both Experiment 1 and controls were avoided. A limitation of our characterization was that fluorochromes were not administered to the animals and hence newly formed osteons could not be identified. Previously, zoledronate increased mineralization and mineral crystallinity in newly formed tissue in cancellous bone [81]. Future study with fluorochrome labeling to indicate osteon age will allow full characterization of spatial nanoscale changes within newly formed osteons with treatment.

Finally, the SEM crack imaging of the indentation fracture experiment only allowed visualization of surface cracks and did not allow analysis of sub-surface damage or cracks that

deflected in the longitudinal direction of the bone. In addition, whether or not cracks visible on the surface were connected sub-surface could not be determined. Error could also arise from the subjective nature of measuring the cracks manually. However, the microcrack measurement was performed by a single individual with all samples measured consistently. Thus, artifacts due to measurement error were minimized and treatment effects could be compared because all samples were characterized in the same manner.

In conclusion, six months of raloxifene or zoledronate treatment improved tissue nanomechanical properties in osteons and interstitial cortical tissue in an ovine model for human high-turnover osteoporosis. Raloxifene acts through the natural estrogen receptor pathways in bone and produced similar changes in the cortical and cancellous tissue of the sheep femora. In contrast, tissue effects with zoledronate were more pronounced in cancellous bone where bisphosphonates preferentially incorporate. Zoledronate improved the stiffness of bulk cortical tissue and whole bone stiffness and strength, while raloxifene improved the ability of cortical tissue to resist microcrack elongation. Older, more highly mineralized interstitial tissue in the cortex showed an increased propensity for crack initiation and propagation relative to osteonal tissue. Thus, the long-term suppression of bone remodeling with bisphosphonate treatment may result in cortical tissue more prone to microcracking. The results of the present study suggest that combined or sequential treatment with bisphosphonates and SERMs could potentially combine the best aspects of each treatment—the ability to quickly improve strength and stiffness with zoledronate, followed by an improvement in crack resistance provided by raloxifene. Combined bisphosphonate/SERM treatment is known to provide greater improvements in BMD over either therapy, alone, and sequential treatment with SERMs after bisphosphonates preserves gains in BMD better than bisphosphonate withdrawal without additional treatment [82]. Thus, the effects of combined or sequential treatment improving tissue microcrack initiation and propagation warrants further investigation.

BIBLIOGRAPHY

[1] Seeman E. Pathogenesis of bone fragility in women and men. Lancet 2002;359:1841-50.

[2] Christiansen BA, Kopperdahl DL, Kiel DP, Keaveny TM, Bouxsein ML. Mechanical contributions of the cortical and trabecular compartments contribute to differences in age-related changes in vertebral body strength in men and women assessed by QCT-based finite element analysis. Journal of Bone and Mineral Research 2010;26:974-983.

[3] Rico H. The Therapy of Osteoporosis and the Importance of Cortical Bone. Calcified Tissue International 1997;61:431-432.

[4] Khosla S, Melton LJ, Riggs BL. The unitary model for estrogen deficiency and the pathogenesis of osteoporosis: is a revision needed. Journal of Bone and Mineral Research 2011;26:441-51.

[5] Riggs BL, Melton Iii LJ, Robb R a, Camp JJ, Atkinson EJ, Peterson JM, et al. Population-based study of age and sex differences in bone volumetric density, size, geometry, and structure at different skeletal sites. Journal of Bone and Mineral Research 2004;19:1945-54.

[6] Sornay-Rendu E, Boutroy S, Munoz F, Delmas PD. Alterations of Cortical and Trabecular Architecture Are Associated With Fractures in Postmenopausal Women, Partially Independent of Decreased BMD Measured by DXA: The OFELY Study. Journal of Bone and Mineral Research 2007;22:425-433.

[7] Sornay-Rendu E, Boutroy S, Munoz F, Bouxsein ML. Cortical and trabecular architecture are altered in postmenopausal women with fractures. Osteoporosis International 2009;20:1291-7.

[8] Oleksik A, Ott SM, Vedi S, Bravenboer N, Compston J, Lips P. Bone structure in patients with low bone mineral density with or without vertebral fractures. Journal of Bone and Mineral Research 2000;15:1368-75.

[9] Johannesdottir F, Poole KES, Reeve J, Siggeirsdottir K, Aspelund T, Mogensen B, et al. Distribution of cortical bone in the femoral neck and hip fracture: a prospective case-control analysis of 143 incident hip fractures; the AGES-REYKJAVIK Study. Bone 2011;48:1268-76.

[10] Hordon LD, Peacock M. The architecture of cancellous and cortical bone in femoral neck fracture. Bone and Mineral 1990;11:335-345.

[11] Cummings SR, Melton LJ. Epidemiology and outcomes of osteoporotic fractures. Lancet 2002;359:1761-7.

[12] WHO. Assessment of fracture risk and its application to screening for postmenopausal osteoporosis. WHO Technical Report Series 843. 1994.

[13] Eswaran S, Gupta A, Adams M, Keaveny T. Cortical and trabecular load sharing in the human vertebral body. Journal of Bone and Mineral Research 2006;21:307-314.

[14] Gallacher SJ, Dixon T. Impact of treatments for postmenopausal osteoporosis (bisphosphonates, parathyroid hormone, strontium ranelate, and denosumab) on bone quality: a systematic review. Calcified Tissue International 2010;87:469-84.

[15] Boskey AL, Spevak L, Weinstein RS. Spectroscopic markers of bone quality in alendronate-treated postmenopausal women. Osteoporosis International 2009;20:793-800.

[16] Chappard D, Petitjean M, Alexandre C, Vico L, Minaire P, Riffat G. Cortical osteoclasts are less sensitive to etidronate than trabecular osteoclasts. Journal of Bone and Mineral Research 1991;6:673-80.

[17] Reeve J, Davies UM, Hesp R, McNally E, Katz D. Treatment of osteoporosis with human parathyroid peptide and observations on effect of sodium fluoride. British Medical Journal (Clinical research ed.) 1990;301:314-8.

[18] Yao H, Dao M, Carnelli D, Tai K, Ortiz C. Size-dependent heterogeneity benefits the mechanical performance of bone. Journal of the Mechanics and Physics of Solids 2011;59:64-74.

[19] Tai K, Dao M, Suresh S, Palazoglu A, Ortiz C. Nanoscale heterogeneity promotes energy dissipation in bone. Nature Materials 2007;6:454-462.

[20] O'Brien FJO, Taylor D, Lee TC. The effect of bone microstructure on the initiation and growth of microcrack. Journal of Orthopaedic Research 2005;23.

[21] Saha S, Hayes WC. Relations between tensile impact properties and microstructure of compact bone. Calcified Tissue Research 1977;24:65-72.

[22] Hiller LP, Stover SM, Gibson VA, Gibeling JC, Prater CS, Hazelwood SJ, et al. Osteon pullout in the equine third metacarpal bone: effects of ex vivo fatigue. Journal of Orthopaedic Research 2003;21:481-8.

[23] Guo XE, Liang LC, Goldstein SA. Micromechanics of Osteonal Cortical Bone Fracture. Transactions of the ASME 1998;120:112-117.

[24] Phelps JB, Hubbard GB, Wang X, Agrawal CM. Microstructural heterogeneity and the fracture toughness of bone. Journal of Biomedical Materials Research 2000;51:735-741.

[25] Donnelly E, Boskey AL, Baker SP, van der Meulen MCH. Effects of tissue age on bone tissue material composition and nanomechanical properties in the rat cortex. Journal of Biomedical Materials Research A 2010;92:1048-56.

[26] Miller LM, Little W, Schirmer A, Sheik F, Busa B, Judex S. Accretion of Bone Quantity and Quality in the Developing Mouse Skeleton. Journal of Bone and Mineral Research 2007;22.

[27] Donnelly E, Baker SP, Boskey AL, van der Meulen MCH. Quasistatic and dynamic nanomechanical properties of cancellous bone tissue relate to collagen content and organization. Journal of Biomedical Materials Research A 2006;21.

[28] Gupta HS, Stachewicz U, Wagermaier W. Mechanical modulation at the lamellar level in osteonal bone. Scanning Electron Microscopy 2006;12:1913-1921.

[29] Burket JC, Gourion-Arsiquaud S, Havill LM, Baker SP, Boskey AL, van der Meulen MCH. Microstructure and nanomechanical properties in osteons relate to tissue and animal age. Journal of Biomechanics 2011;44:277-84.

[30] Gourion-Arsiquaud S, Burket JC, Havill LM, Dicarlo E, Doty SB, Mendelsohn R, et al. Spatial Variation in Osteonal Bone Properties Relative to Tissue and Animal Age. Journal of Bone and Mineral Research 2009;24:1271-1281.

[31] Rho JY, Tsui TY, Pharr GM. Elastic properties of human cortical and trabecular lamellar bone measured by nanoindentation. Biomaterials 1997;18:1325-1330.

[32] Zysset PK, Guo XE, Hoffler CE, Moore KE, Goldstein SA. Elastic modulus and hardness of cortical and trabecular bone lamellae measured by nanoindentation in the human femur. Journal of Biomechanics 1999;32:1005-1012.

[33] Rho JY, Zioupos P, Currey JD, Pharr GM. Microstructural elasticity and regional heterogeneity in human femoral bone of various ages examined by nano-indentation. Journal of Biomechanics 2002;35:189-198.

[34] Roschger P, Rinnerthaler S, Yates J, Rodan GA, Fratzl P, Klaushofer K. Alendronate increases degree and uniformity of mineralization in cancellous bone and decreases the porosity in cortical bone of osteoporotic women. Bone 2001;29:185-191.

[35] Cummings SR, Karpf DB, Harris F, Genant HK, Ensrud K, LaCroix AZ, et al. Improvement in spine bone density and reduction in risk of vertebral fractures during treatment with antiresorptive drugs. The American Journal of Medicine 2002;112:281-289.

[36] Liberman UA, Weiss SR, Bröll J, Minne HW, Quan H, Bell NH, et al. Effect of oral alendronate on bone mineral density and the incidence of fractures in postmenopausal

osteoporosis. The Alendronate Phase III Osteoporosis Treatment Study Group. The New England Journal of Medicine 1995;333:1437-43.

[37] Faulkner KG. Bone matters: are density increases necessary to reduce fracture risk? Journal of Bone and Mineral Research 2000;15:183-7.

[38] Rogers MJ, Crockett JC, Coxon FP, Mönkkönen J. Biochemical and molecular mechanisms of action of bisphosphonates. Bone 2010;49:34-41.

[39] Roelofs AJ, Thompson K, Ebetino FH, Rogers MJ, Coxon FP. Bisphosphonates : Molecular Mechanisms of Action and Effects on Bone Cells , Mono- cytes and Macrophages. Current Pharmaceutical Design 2010;16:2950-2960.

[40] Drake MT, Clarke BL, Khosla S. Bisphosphonates: mechanism of action and role in clinical practice. Mayo Clinic Proceedings 2008;83:1032-45.

[41] Reszka AA, Rodan GA. Nitrogen-containing bisphosphonate mechanism of action. Mini Reviews in Medicinal Chemistry 2004;4:711-9.

[42] Allen MR, Reinwald S, Burr DB. Alendronate reduces bone toughness of ribs without significantly increasing microdamage accumulation in dogs following 3 years of daily treatment. Calcified Tissue International 2008;82:354-60.

[43] Gourion-Arsiquaud S, Allen MR, Burr DB, Vashishth D, Tang SY, Boskey AL. Bisphosphonate treatment modifies canine bone mineral and matrix properties and their heterogeneity. Bone 2010;46:666-672.

[44] Riggs BL, Hartmann LC. Selective estrogen-receptor modulators -- mechanisms of action and application to clinical practice. Journal of Medicine Cincinnati 2003;348.

[45] Bryant HU, D P. Mechanism of Action and Preclinical Profle of Raloxifene , a Selective Estrogen Receptor Modulator. Reviews in Endocrine & Metabolic Disorders 2001;2:129-138.

[46] MacLean C, Newberry S, Maglione M, McMahon M, Ranganath V, Suttorp M, et al. Systematic Review : Comparative Effectiveness of Treatments to Prevent Fractures in Men and Women with Low Bone Density or Osteoporosis. Annals of Internal Medicine 2008;148:197-213.

[47] Allen MR, Iwata K, Sato M, Burr DB. Raloxifene enhances vertebral mechanical properties independent of bone density. Bone 2006;39:1130-5.

[48] Brennan TC, Rizzoli R, Ammann P. Selective Modification of Bone Quality by PTH, Pamidronate, or Raloxifene. Journal of Bone and Mineral Research. 2009;24:800-808.

[49] Burket JC, Brooks DJ, MacLeay JM, Baker SP, Boskey AL, van der Meulen MCH. Variations in nanomechanical properties and tissue composition within trabeculae from an ovine model of osteoporosis and treatment. in submission to Bone 2012.

[50] Cremers S, Papapoulos S. Pharmacology of bisphosphonates. Bone 2011;49:42-49.

[51] Weiss HM, Pfaar U, Schweitzer A, Wiegand H, Skerjanec A, Schran H. Biodistribution and Plasma Protein Binding of Zoledronic Acid. Drug Metabolism and Disposition 2008;36:2043-2049.

[52] Macleay JM, Sullivan E, Jackinsky S, Les C, Turner A. Ovine modeling of dietary induced metabolic acidosis and bone loss. International Congress Series 2007;1297:282-285.

[53] Macleay JM, Olson JD, Turner AS. Effect of dietary-induced metabolic acidosis and ovariectomy on bone mineral density and markers of bone turnover. Journal of Bone and Mineral Metabolism 2004;22:561-568.

[54] Donnelly E, Baker SP, Boskey AL, van der Meulen MCH. Effects of surface roughness and maximum load on the mechanical properties of cancellous bone measured by nanoindentation. Journal of Biomedical Materials Research 2006;77:426-435.

[55] Erben RG. Embedding of bone samples in methylmethacrylate: an improved method suitable for bone histomorphometry, histochemistry, and immunohistochemistry. The Journal of Histochemistry and Cytochemistry 1997;45:307-313.

[56] Donnelly E, Chen DX, Boskey AL, Baker SP, van der Meulen MCH. Contribution of mineral to bone structural behavior and tissue mechanical properties. Calcified Tissue International 2010;87:450-460.

[57] Oliver WC, Pharr GM. An improved technique for determining hardness and elastic modulus using load and displacement sensing indentation experiments. Journal of Materials Research 1992;7:1564-1583.

[58] Akkus O, Polyakova-Akkus A, Adar F, Schaffler MB. Aging of microstructural compartments in human compact bone. Journal of Bone and Mineral Research 2003;18:1012-1019.

[59] Carden A, Morris MD. Application of vibrational spectroscopy to the study of mineralized tissues (review). Journal of Biomedical Optics 2000;5:259-268.

[60] Tarnowski CP, Ignelzi MA, Wang W, Taboas JM, Goldstein SA, Morris MD. Earliest mineral and matrix changes in force-induced musculoskeletal disease as revealed by Raman microspectroscopic imaging. Journal of Bone and Mineral Research 2004;19:64-71.

[61] Freeman JJ, Wopenka B, Silva MJ, Pasteris JD. Raman spectroscopic detection of changes in bioapatite in mouse femora as a function of age and in vitro fluoride treatment. Calcified Tissue International 2001;68:156-162.

[62] Penel G, Leroy G, Rey C, Bres E. MicroRaman spectral study of the PO4 and CO3 vibrational modes in synthetic and biological apatites. Calcified Tissue International 1998;63:475-481.

[63] Turunen MJ, Saarakkala S, Rieppo L, Helminen HJ, Jurvelin JS, Isaksson H. Comparison between infrared and Raman spectroscopic analysis of maturing rabbit cortical bone. Applied spectroscopy 2011;65:595-603.

[64] Williams RM, Zipfel WR, Webb WW. Interpreting second-harmonic generation images of collagen I fibrils. Biophysical Journal 2005;88:1377-86.

[65] Zipfel WR, Williams RM, Webb WW. Nonlinear magic: multiphoton microscopy in the biosciences. Nature Biotechnology 2003;21:1369-77.

[66] Moreaux L, Sandre O, Mertz J. Membrane imaging by second-harmonic generation microscopy. Journal Of The Optical Society Of America B Optical Physics 2000;17:1685-1694.

[67] Campagnola PJ, Loew LM. Second-harmonic imaging microscopy for visualizing biomolecular arrays in cells, tissues and organisms. Nature Biotechnology 2003;21:1356-1360.

[68] Boyd R. Nonlinear Optics. 2nd ed. Amsterdam, The Netherlands: Academic Press. 2003.

[69] Mullins LP, Bruzzi MS, McHugh PE. Measurement of the microstructural fracture toughness of cortical bone using indentation fracture. Journal of Biomechanics 2007;40:3285-8.

[70] Eastell R, Walsh JS, Watts NB, Siris E. Bisphosphonates for postmenopausal osteoporosis. Bone 2011;49:82-8.

[71] Roschger P, Paschalis EP, Fratzl P, Klaushofer K. Bone mineralization density distribution in health and disease. Bone 2008;42:456-466.

[72] McCreadie BR, Morris MD, Chen T-C, Sudhaker Rao D, Finney WF, Widjaja E, et al. Bone tissue compositional differences in women with and without osteoporotic fracture. Bone 2006;39:1190-1195.

[73] Gadeleta SJ, Boskey AL, Paschalis E, Carlson C, Menschik F, Baldini T, et al. A physical, chemical, and mechanical study of lumbar vertebrae from normal, ovariectomized, and nandrolone decanoate-treated cynomolgus monkeys (Macaca fascicularis). Bone 2000;27:541-50.

[74] Boskey AL, DiCarlo E, Paschalis E, West P, Mendelsohn R. Comparison of mineral quality and quantity in iliac crest biopsies from high- and low-turnover osteoporosis: an FT-IR microspectroscopic investigation. Osteoporosis International 2005;16:2031-2038.

[75] Ritchie RO. The conflicts between strength and toughness. Nature materials 2011;10:817-22.

[76] Shahnazari M, Yao W, Dai W, Wang B, Ionova-Martin SS, Ritchie RO, et al. Higher doses of bisphosphonates further improve bone mass, architecture, and strength but not the tissue material properties in aged rats. Bone 2010;46:1267-74.

[77] Allen MR, Hogan HA, Hobbs WA, Koivuniemi AS, Koivuniemi MC, Burr DB. Raloxifene enhances material-level mechanical properties of femoral cortical and trabecular bone. Endocrinology 2007;148:3908-13.

[78] Tang SY, Allen MR, Phipps R, Burr DB, Vashishth D. Changes in non-enzymatic glycation and its association with altered mechanical properties following 1-year treatment with risedronate or alendronate. Osteoporosis International 2009;20:887-94.

[79] Allen MR, Gineyts E, Leeming DJ, Burr DB, Delmas PD. Bisphosphonates alter trabecular bone collagen cross-linking and isomerization in beagle dog vertebra. Osteoporosis International 2008;19:329-337.

[80] MacLeay JM, Olson JD, Enns RM, Les CM, Toth CA, Wheeler DL, et al. Dietary-induced metabolic acidosis decreases bone mineral density in mature ovariectomized ewes. Calcified Tissue International 2004;75:431-437.

[81] Gamsjaeger S, Buchinger B, Zwettler E, Recker R, Black D, Gasser JA, et al. Bone material properties in actively bone-forming trabeculae in postmenopausal women with osteoporosis after three years of treatment with once-yearly Zoledronic acid. Journal of bone and Mineral Research 2011;26:12-8.

[82] Pinkerton JV, Dalkin AC. Combination therapy for treatment of osteoporosis: A review. American Journal of Obstetrics and Gynecology 2007;197:559-65.

CHAPTER 4 SUPPLEMENTARY CONTENT

APPARENT LEVEL MECHANICAL TESTS OF CORTICAL BEAMS AND NANOSCALE RAMAN COMPOSITIONAL CHARACTERIZARION

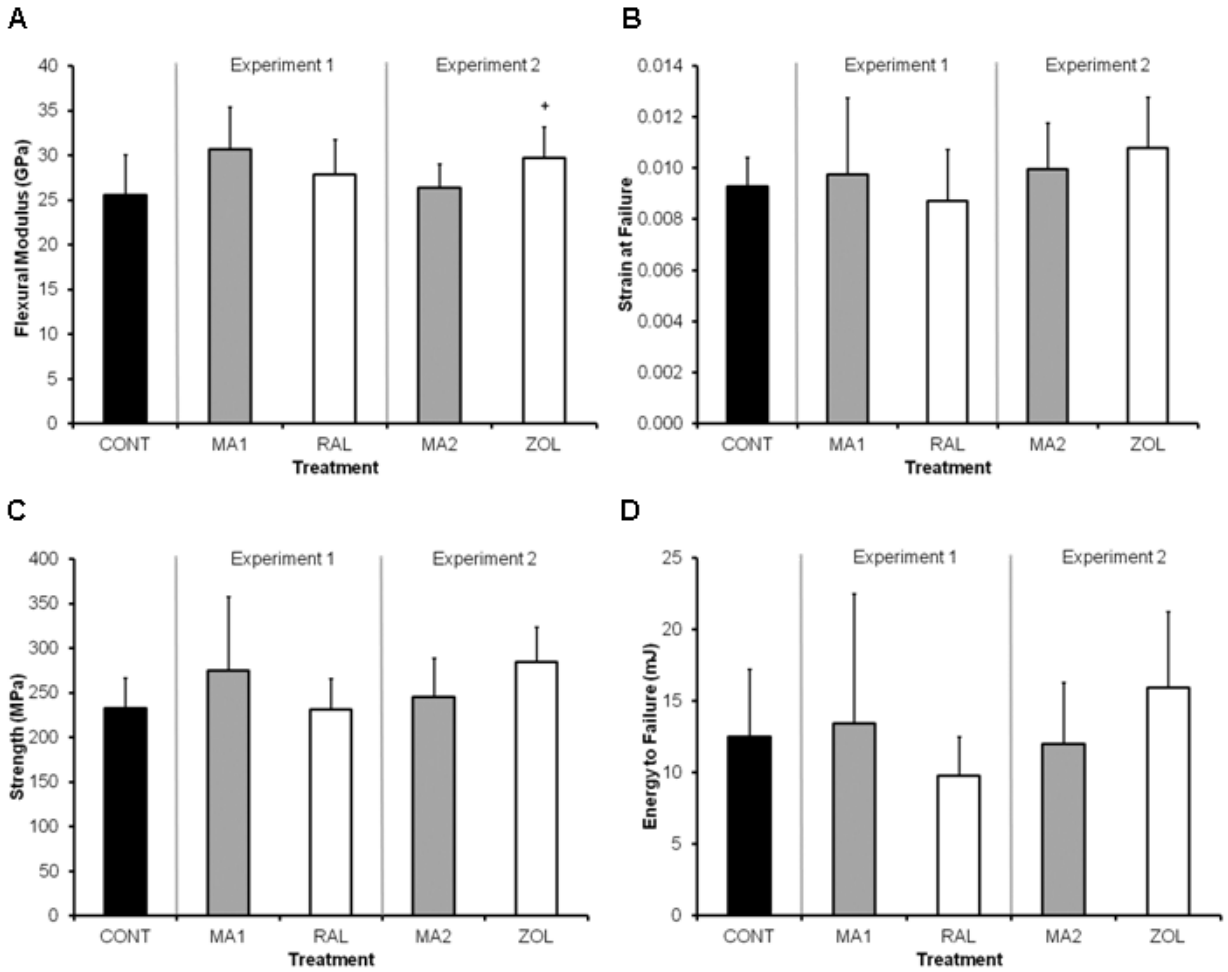

Figure 4.1s *Bulk tissue mechanical testing results from three-point bending tests of cortical beams. Flexural modulus trended towards an increase with zoledronate relative to the MA model (+ 12%, $p^{+} = 0.08$). MA and raloxifene did not alter whole bone or bulk tissue properties relative to controls $p < 0.10$*

Supplementary Methods for Figure 4.1s.

Bulk cortical tissue properties were assessed via three-point bending tests of rectangular cortical beams taken from the lateral aspect of the distal femur just below the mid-diaphysis. Three mm-wide longitudinal sections were excised from the lateral aspect of the distal femoral shaft using a

precision diamond saw (IsoMet 1000, Buehler, Lake Bluff, IL). Sections were polished to a 2 mm-square cross section with 30 μm and 15 μm lapping films (MetaServ 250, Buehler, Lake Bluff, IL) and the length was cut to 25 mm (IsoMet). Ethylene glycol was used as a lubricant for polishing to prevent mineral leaching [1]. The beams were wrapped in saline soaked gauze and stored at -20˚C prior to testing.

The cortical beams were tested with servohydraulic material testing machine (858 Mini Bionix) with a 445 N load cell (SSM-100, Transducer Techniques, Temecula, CA). The span between the two outer supports of the testing fixture was 20 mm. To reduce local deformation at the contact-points, 3 mm^3 metal blocks were adhered to the periosteal surface of the beams via a positioning fixture that ensured 20 mm spacing between blocks. Beams were positioned for testing with the lower supports in contact with the metal blocks, placing the periosteal side of the beams in tension during the tests. A linearly variable differential transformer (LVDT) (LBB375PA-100, Measurement Specialties, Hampton, VA) mounted in the base of the three-point bending fixture measured beam deflection mid-span during the tests. Beams were tested to failure at a deflection rate of 5 mm/min. The bending modulus (E_B), flexural strength (σ_f), strain at failure (ε), and energy to failure (E_F) of the cortical beams were determined from the load-displacement data. Effects of treatment on these outcome measures were assessed with single-factor ANOVAs with Tukey post-hoc tests.

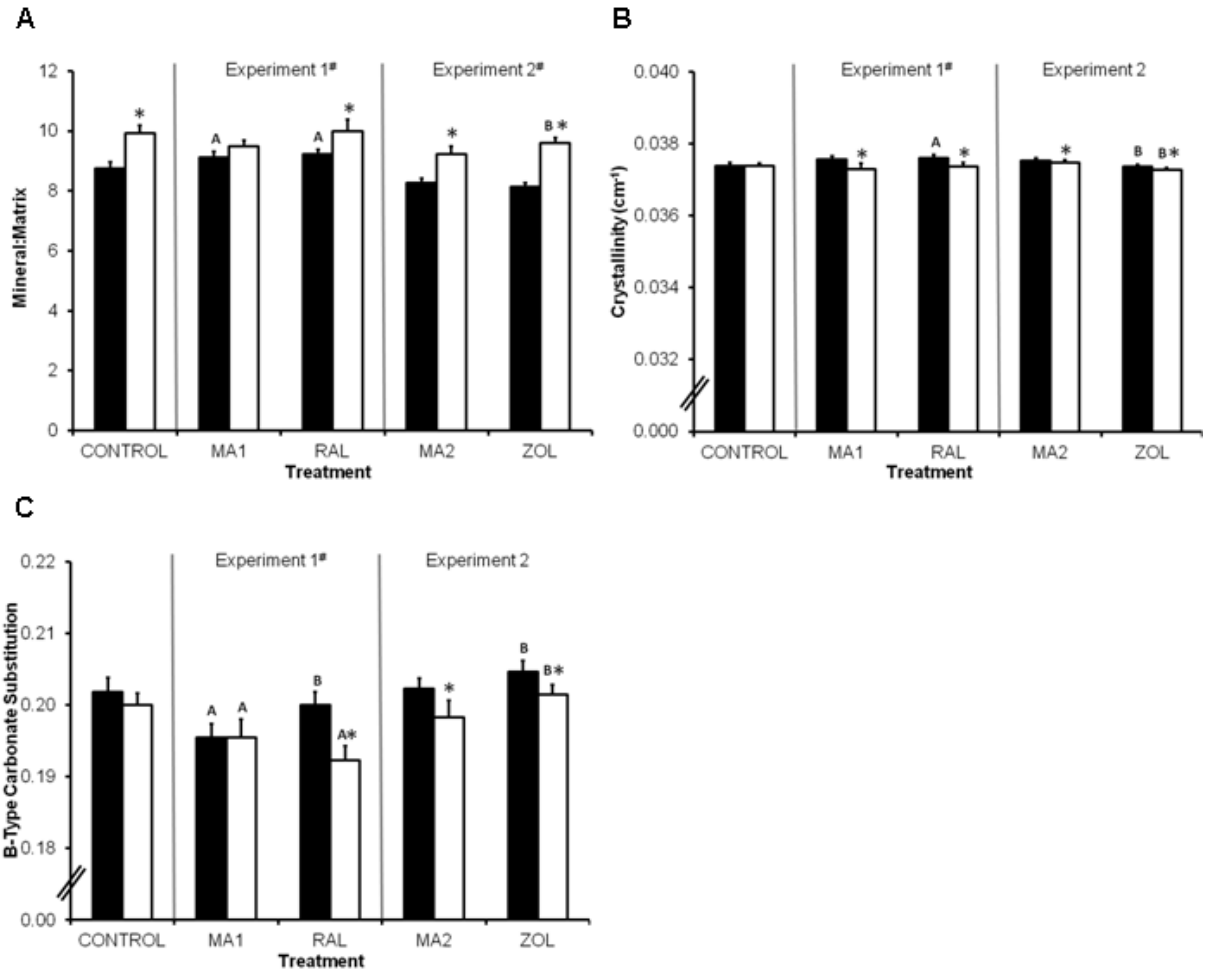

Figure 4.2s *Raman compositional parameters by treatment for osteonal and interstitial tissue. Changes in Raman compositional parameters in cortical tissue with MA and treatments were minimal. Solid bars = osteonal tissue. Open bars = interstitial tissue. A = different from CONTROL. B = different from MA. * = different from osteonal tissue. # = effects varied by tissue type.*

Table 4.1s *Percentage change in compositional and nanomechanical parameters with treatment in cancellous* [2] *and cortical bone. If changes with treatment varied by region (superficial, intermediate or central in cancellous bone; osteonal or interstitial in cortical bone), then percent changes are listed for each region separately. S = superficial region; I = intermediate region in cancellous/interstitial region in cortical; C = central region; O = osteonal region.*

		Cancellous Tissue		Cortical Tissue	
Parameter	**Treatment**	**vs. CONT**	**vs. MA**	**vs. CONT**	**vs. MA**
Indentation Modulus (GPa)	MA1	-15		O: -8.5 I: -12	
	RAL	-6.5	+9.6	O: N.S. I: -5.0	O: +9.2 I: +7.3
	ZOL		S: +12 I: N.S. C: N.S.		+3.5
Hardness (GPa)	MA1	-13		-10	
	RAL	-4.6	+9.9	N.S.	+9.5
	ZOL		S: +16 I: N.S. C: N.S.		+6.9
Mineral:Matrix	MA1	N.S.		O: +4.2 I: N.S.	
	RAL	N.S.	N.S.	O: +5.6 I: N.S.	O: N.S. I: N.S.
	ZOL		S: +10 I: N.S. C: N.S.		O: N.S. I: +4.1
B-Type Carbonate Substitution	MA1	S: -11 I: -11 C: N.S		O: -3.1 I: -2.3	
	RAL	S: -14 I: -10 C: N.S.	N.S.	O: N.S. I: -3.9	O: +2.3 I: N.S.
	ZOL		+4.7		+1.4
Crystallinity (cm^{-1})	MA1	N.S.		N.S.	
	RAL	N.S.	N.S.	N.S.	+0.56
	ZOL		N.S.		-0.45
Lamellar Aligned Collagen	MA1	+2.6		-18	
	RAL	+4.6	N.S.	N.S.	+22
	ZOL		-13		N.S.
Interlamellar Aligned Collagen	MA1	N.S.		-11	
	RAL	+6.6	+4.6	N.S.	+10
	ZOL		-12		N.S.

Table 4.2s *Percentage increase in nanomechanical and compositional parameters from the center to the periphery of the average osteon. Average osteon radius = 150 µm. The "ALL" column denotes gradients that were independent of treatment type. If gradients were dependent on treatment, then results are listed individually by treatment group. $p < 0.05$ unless indicated by $^{+}$. $^{+} = p < 0.1$*

	Experiment 1				Experiment 2		
Outcome Parameter:	CONT	ALL	MA1	RAL	ALL	MA2	ZOL
Indentation Modulus	15		3.0^{+}	7.2	5.5		
Hardness		5.8			N.S.		
Mineral:Matrix	11		N.S	7.4	5.0		
B-Type Carbonate Substitution		3.1			N.S.		
Crystallinity	11		N.S.	N.S.		5.2	N.S.
Lamellar Aligned Collagen		25			30		
Interlamellar Aligned Collagen		20			23		

BIBLIOGRAPHY

[1] Donnelly E, Baker SP, Boskey AL, van der Meulen MCH. Effects of surface roughness and maximum load on the mechanical properties of cancellous bone measured by nanoindentation. Journal of Biomedical Materials Research 2006;77:426-435.

[2] Burket JC, Brooks DJ, MacLeay JM, Baker SP, Boskey AL, van der Meulen MCH. Variations in nanomechanical properties and tissue composition within trabeculae from an ovine model of osteoporosis and treatment. in submission to Bone 2012.

CHAPTER 5

SUMMARY AND CONCLUSIONS

The objectives of this research were to determine variations in tissue composition and nanomechanical properties within the microstructures of cortical and cancellous bone with ageing, osteoporosis, and antiresorptive treatment, correlate tissue composition with nanomechanical function, and examine the effects of these tissue property changes on microcracking resistance and mechanical performance at higher length scales. Tissue stiffness and hardness followed changes in mineral and matrix properties with the natural ageing process and increased sharply in young, growing animals while remaining relatively constant after sexual maturity. Both the bisphosphonate, zoledronate, and the SERM, raloxifene, improved tissue nanomechanical function in a model of high-turnover osteoporosis, with zoledronate effects localized at surfaces of trabeculae while raloxifene effects were uniform throughout cortical and cancellous tissue. Tissue-level alterations with raloxifene improved cortical resistance to microcrack elongation while alterations with zoledronate led to improved stiffness and hardness at higher length scales. Understanding these relationships will improve our understanding of normal and pathological bone function and may enable us to improve upon current therapies for skeletal diseases.

5.1 Nanoscale Material Alterations in Bone with Ageing

The gradient in tissue age from center to periphery of osteons was utilized to examine tissue material property changes resulting from the natural ageing process in a baboon model for human ageing. Tissue compositional and nanomechanical alterations were studied with tissue age across osteons and animal age within baboons of different ages covering the entire lifespan. Indentation modulus and hardness followed biphasic relationships with animal age, following trends in mineral-to-matrix ratio, carbonate substitution, and the ratio of lamellar to interlamellar

aligned collagen, which increased sharply during rapid growth in young animals and then leveled off after sexual maturity. Across the osteon radii, carbonate substitution, crystallinity, and the ratio of lamellar to interlamellar aligned collagen increased with tissue age. These results were the first to demonstrate the relationships with tissue and animal age over an entire lifespan, as previous studies have produced mixed results due to their focus on small numbers of mature, aged subjects [1–4]. The positive relationships between nanomechanical properties and tissue mineralization, carbonate substitution, and collagen content and organization demonstrated previously in rodent models and small numbers of human vertebrae [5–8] held over the entire lifetime of a closely-related non-human primate. Additionally, mineral-to-matrix ratio effectively captured variations in nanomechanical parameters explained by both mineral (b-type carbonate substitution) and matrix (lamellar aligned collagen) components bone tissue. Mineral-to-matrix ratio explained 78% of the variation in indentation modulus and 70% of the variation in hardness with ageing.

A strength of this study was that the baboons were part of a primate colony without experimental intervention. Therefore, their bone tissue presents an accurate picture of the skeletal changes that naturally occur over a lifetime. As a closely related primate, baboons have similar bone microstructure and follow a similar progression with ageing as humans, including reproductive senescence and menopause accompanied by changes in hormone levels that are important in bone metabolism and loss [9–12]. However, a significant limitation of this approach was that animals were not injected with fluorochromes and therefore osteon age could not be readily determined. The osteons chosen for characterization were not visibly in the process of remodeling. In the future, fluorochrome labeling to identify new osteons will allow the full effects of tissue age within osteons to be determined. Newly formed osteons would be expected to have tissue properties similar to young, sexually immature animals from this study, with lower stiffness and hardness associated with lower levels of mineralization, carbonate substitution, crystallinity, and aligned collagen content. Additionally, studies of male animals

will allow identification of sex-based differences. Finally, relationships between the age-related changes in tissue material properties observed in this study and the resistance to damage and microcracking should be determined. Bulk and whole-bone fracture toughness is known to decrease with ageing [13,14], and ultimately the failure of bone starts with crack initiation and propagation at the tissue-level. Indentation fracture tests such as the methods developed for Aim 3 of this thesis could be used to identify relationships between age-related tissue property changes and the ability of the tissue to resist microcrack initiation and propagation.

5.2 Alterations with Osteoporosis and Antiresorptive Treatment

Once variations in nanoscale material properties with the natural ageing process were established, pathological alterations with osteoporosis and antiresorptive treatment were documented in a large ovine study utilizing a dietary model for human high-turnover osteoporosis. In cancellous tissue, six months with antiresorptive treatment—the bisphosphonate, zoledronate, or the SERM, raloxifene—improved tissue nanomechanical properties in the distal femur relative to the osteoporosis model. Zoledronate improved tissue stiffness and hardness at the surfaces of trabeculae, where bisphosphonates are known to incorporate into regions of active remodeling [15–20]. Nanomechanical improvements with raloxifene were of lesser magnitude (percentage increase) than those with zoledronate and were distributed throughout trabeculae rather than focused exclusively near surfaces.

Unlike nanoscale techniques, measurements of bulk cancellous properties detected few alterations with the osteoporotic model and treatment. Not only do bulk tissue measures lack the spatial resolution of nanoscale techniques, but they also do not have the ability for repeated measures to improve power. Based on a power analysis, the sample size for the bulk tissue measurements of the ovine study would need to increase three-fold for trends in BV/TV and Tb.Th and to become significant. The nanoscale improvements in tissue stiffness did produce substantial increases in the estimated bending stiffness of individual trabeculae. Future study

with a larger sample size appropriately powered for bulk tissue and whole bone measures would definitively determine whether the nanomechanical improvements observed here with antiresorptive treatment produce improvements at higher length scales. Bulk tissue and whole bone testing in beagles with zoledronate and raloxifene do suggest that there are contributions to whole bone strength from tissue-level alterations [21,22]. Other aspects of tissue-level mechanical function not measured with the nanoindentation experiments here could also play an important role in bulk and whole bone mechanical function and fracture resistance. For example, the interlamellar or interface regions between lamellae could be particularly important because shearing or cracking of these regions could compromise the composite structure. Indeed, microcracks in cancellous bone appear to form parallel to the lamellar structure within trabeculae, possibly along these interface regions. Additionally, the amount of these microcracks was increased with bisphosphonate treatment in the beagle studies [23–25].

In cortical tissue, raloxifene and zoledronate also improved nanomechanical properties in osteons and interstitial regions relative to the MA osteoporosis model. In contrast to cancellous tissue, improvements in cortical tissue stiffness and hardness were greater with raloxifene than with zoledronate. By acting through the natural estrogen receptor pathways in bone, raloxifene affected both cancellous and cortical tissue similarly, increasing stiffness and hardness in both tissues by roughly 10% over the osteoporotic model (Tables 5.1, 5.2). Increases in cortical nanomechanical properties with zoledronate were less than half of those that occurred at the surfaces of trabeculae in cancellous bone. Bisphosphonate uptake is greater in cancellous than in cortical tissue, and again these results indicate that zoledronate produces the greatest improvements in regions where bisphosphonates preferentially incorporate [26,27].

Table 5.1 *Percentage change in compositional and nanomechanical parameters with treatment in cancellous and cortical bone. If treatment changes varied by region (superficial, intermediate or central in cancellous bone; osteonal or interstitial in cortical bone), then percent changes are listed for each region separately. S = superficial region; I = intermediate region in cancellous/interstitial region in cortical; C = central region; O = osteonal region.*

		Cancellous Tissue		Cortical Tissue	
Parameter	**Treatment**	**vs. CONT**	**vs. MA**	**vs. CONT**	**vs. MA**
Indentation Modulus (GPa)	MA1	-15		O: -8.5 I: -12	
	RAL	-6.5	+9.6	O: N.S. I: -5.0	O: +9.2 I: +7.3
	ZOL		S: +12 I: N.S. C: N.S.		+3.5
Hardness (GPa)	MA1	-13		-10	
	RAL	-4.6	+9.9	N.S.	+9.5
	ZOL		S: +16 I: N.S. C: N.S.		+6.9
Mineral:Matrix	MA1	N.S.		O: +4.2 I: N.S.	
	RAL	N.S.	N.S.	O: +5.6 I: N.S.	O: N.S. I: N.S.
	ZOL		S: +10 I: N.S. C: N.S.		O: N.S. I: +4.1
B-Type Carbonate Substitution	MA1	S: -11 I: -11 C: N.S		O: -3.1 I: -2.3	
	RAL	S: -14 I: -10 C: N.S.	N.S.	O: N.S. I: -3.9	O: +2.3 I: N.S.
	ZOL		+4.7		+1.4
Crystallinity (cm^{-1})	MA1	N.S.		N.S.	
	RAL	N.S.	N.S.	N.S.	+0.56
	ZOL		N.S.		-0.45
Lamellar Aligned Collagen	MA1	+2.6		-18	
	RAL	+4.6	N.S.	N.S.	+22
	ZOL		-13		N.S.
Interlamellar Aligned Collagen	MA1	N.S.		-11	
	RAL	+6.6	+4.6	N.S.	+10
	ZOL		-12		N.S.

Table 5.2 *Absolute values for compositional and nanomechanical parameters by region in cancellous and cortical bone. *Different from CONT $^{+}$Different from MA ^{S}Different from Superficial, ^{I}Different from Intermediate, ^{O}Different from Osteonal*

		Cancellous Tissue			Cortical Tissue	
Parameter	**Treatment**	**Superficial**	**Intermediate**	**Central**	**Osteonal**	**Interstitial**
Indentation Modulus (GPa)	CONT	27.1 ± 1.2	28.7 ± 0.9^{S}	29.5 ± 0.8^{S}	30.6 ± 0.6	31.9 ± 0.6^{O}
	MA1	23.2 ± 1.7*	24.1 ± 1.4*^{S}	25.4 ± 1.3*^{S}	28.0 ± 0.7*	28.2 ± 0.9*
	RAL	24.8 ± 1.7*$^{+}$	27.5 ± 1.3*$^{+S}$	27.2 ± 1.8*$^{+S}$	30.6 ± 0.7*	30.3 ± 1.2*$^{+}$
	MA2	24.5 ± 1.1	26.8 ± 1.1^{S}	26.9 ± 0.8^{S}	31.2 ± 0.5	30.6 ± 0.6
	ZOL	27.5 ± 1.3^{+}	26.3 ± 1.0^{S}	27.0 ± 0.8	31.8 ± 0.6^{+}	32.2 ± 0.7^{+}
Hardness (GPa)	CONT	1.09 ± .06	1.09 ± 0.05	1.14 ± 0.05^{S}	1.10 ± 0.03	1.17 ± 0.04^{O}
	MA1	0.936 ± 0.087*	0.915 ± 0.071*	1.04 ± 0.09*^{S}	0.993 ± 0.026*	1.04 ± 0.03*^{O}
	RAL	0.981 ± 0.080*$^{+}$	1.09 ± 0.070*$^{+}$	1.10 ± 0.090*$^{+S}$	1.09 ± 0.03^{+}	1.14 ± 0.05^{+O}
	MA2	0.938 ± 0.059	0.993 ± 0.065	0.991 ± 0.051	1.14 ± 0.03	1.16 ± 0.03^{O}
	ZOL	1.09 ± 0.08^{+}	0.987 ± 0.052^{S}	1.01 ± 0.04^{S}	1.20 ± 0.04^{+}	1.26 ± 0.04^{+O}
Mineral:Matrix	CONT	7.09 ± 0.41	7.99 ± 0.25^{S}	8.27 ± 0.24^{S}	8.74 ± 0.21	9.92 ± 0.26^{O}
	MA1	7.17 ± 0.63	8.02 ± 0.37^{S}	8.57 ± 0.32^{S}	9.11 ± 0.20*	9.49 ± 0.21
	RAL	6.88 ± 0.59	7.94 ± 0.48^{S}	7.77 ± 0.46^{S}	9.23 ± 0.14*	9.99 ± 0.39^{O}
	MA2	6.01 ± 0.30	7.03 ± 0.24^{S}	7.48 ± 0.13^{SI}	8.27 ± 0.15	9.23 ± 0.26^{O}
	ZOL	6.64 ± 0.23^{+}	7.20 ± 0.21^{S}	7.39 ± 0.17^{S}	8.14 ± 0.12	9.60 ± 0.17*^{O}
B-Type Carbonate Substitution	CONT	0.189 ± 0.005	0.200 ± 0.003^{S}	0.199 ± 0.003^{S}	0.202 ± 0.002	0.200 ± 0.002
	MA1	0.168 ± 0.007	0.178 ± 0.007^{S}	0.187 ± 0.005^{SI}	0.195 ± 0.002*	0.195 ± 0.003*
	RAL	0.163 ± 0.006	0.180 ± 0.006^{S}	0.192 ± 0.006^{SI}	0.200 ± 0.002^{+}	0.192 ± 0.002*^{O}
	MA2	0.185 ± 0.003	0.197 ± 0.004^{S}	0.210 ± 0.003^{SI}	0.202 ± 0.002	0.198 ± 0.002^{O}
	ZOL	0.199 ± 0.004^{+}	0.205 ± 0.004^{+S}	0.215 ± 0.004^{+SI}	0.205 ± 0.002^{+}	0.201 ± 0.001^{+O}
Crystallinity (cm^{-1})	CONT	0.0354 ± 0.0011	0.0365 ± 0.0004^{S}	0.0362 ± 0.0003^{S}	0.0374 ± 0.0000	0.0374 ± 0.0001
	MA1	0.0358 ± 0.0013	0.0365 ± 0.0006^{S}	0.0361 ± 0.0005^{S}	0.0376 ± 0.0001	0.0373 ± 0.0002^{O}
	RAL	0.0358 ± 0.0011	0.0363 ± 0.0008^{S}	0.0369 ± 0.0008^{S}	0.0376 ± 0.0001*	0.0374 ± 0.0001^{O}
	MA2	0.0392 ± 0.0005	0.0390 ± 0.0002^{S}	0.382 ± 0.0002^{SI}	0.0375 ± 0.0001	0.0375 ± 0.0001^{O}
	ZOL	0.0390 ± 0.0003^{+}	0.0382 ± 0.0005^{+S}	0.0378 ± 0.0005^{+SI}	0.0374 ± 0.0001^{+}	0.0373 ± 0.0001^{+O}

Despite the more modest gains in cortical tissue material properties, six months of zoledronate but not raloxifene improved bending stiffness in bulk tissue tests of cortical beams and improved bending stiffness and failure moment in whole bone tests. The cortex of zoledronate treated sheep was larger in diameter (+28% cranial-caudal) and thicker (+14%) than that of the osteoporotic ewes, leading to an appreciably larger area moment of inertia. However, variations between animals were large and the sample size underpowered for the whole-bone and bulk measures and these trends did not reach statistical significance.

In both cancellous and cortical tissue, nanomechanical alterations with the osteoporotic model and treatment correlated with changes in tissue composition. Cortical tissue mineralization, carbonate substitution into the mineral lattice, mineral crystal size and perfection, and lamellar aligned collagen content combined to explain nearly 50% of the variation in indentation modulus with the osteoporosis model and raloxifene treatment. In cancellous tissue, carbonate substitution, crystal size and perfection, and aligned collagen explained 28% of the variations in indentation modulus with the ovine osteoporosis model and raloxifene treatment. B-type carbonate substitution was the strongest predictor of nanomechanical function in both the cortical and cancellous models. Compositional parameters also correlated with nanomechanical variations due to the ovine osteoporosis model and zoledronate treatment; however, the explanatory power of the models was much more limited, 15% or less.

The poor predictive power and the fact that many of the compositional relationships varied between treatment groups indicate that additional compositional factors not measured in these experiments also play a role in mechanical function with osteoporosis and treatment. These factors may include additional collagen cross-links not measured in these studies, mineral crystal orientation, and non-collagenous proteins, to name a few possibilities [28–30]. Advanced glycation end-product (AGE) accumulation has been observed with high doses of bisphosphonates in beagles [28]. AGEs form non-enzymatic collagen crosslinks (pentosidine, vesperlysine, and others) in bone and are associated with reduced post-yield work to fracture

[28]. Increases in these crosslinks, altered ratios of mature crosslinks (pyridinoline: deoxypridinoline), and altered ratios of native to isomerized collagen have also been noted with clinical doses of bisphosphonates in beagles [30]. Identifying relationships between these additional compositional factors and the nanomechanical behavior of bone tissue will provide a more complete picture of the manner by which composition ultimately determines mechanical function at the tissue level. However, many of the current techniques for measuring these factors (x-ray diffraction, HPLC, and protein assays) require tissue homogenization or digestion and do not allow spatially-resolved measurements.

5.3 Microcrack resistance

Finally, a method was developed to directly test the ability of cortical bone tissue to resist microcracking. Bisphosphonates have been linked with increased microcracking [23,31], and concern has arisen that excessive mineralization coupled with the reduced ability to repair microdamage with bisphosphonate treatment may promote the development and accumulation of microcracks [31,32]. Prior to the current work, a reliable method for directly testing the tissue-level microcracking resistance of bone with disease and treatment had not been developed. One previous study attempted to use indentation fracture to measure fracture toughness; however, samples were tested in a hydrated state and then dehydrated for imaging via SEM [33]. Observations during sample preparation and the development of the current testing protocol suggest that cracks observed in the previous study likely did not result from indentation, but were formed during the subsequent dehydration of the tissue due to residual strain energy left in the samples from indentation. Therefore, for the indentation fracture tests of this thesis, samples were dehydrated prior to testing and imaged pre and post-fracture so that measured cracks were guaranteed to be from the indentation fracture and not due to dehydration or cracks previously present in the sample. Dehydration is known to increase tissue stiffness and hardness [34–36] and possibly could influence crack resistance; however, all samples were treated similarly and

therefore our ability to detect relative variations in these properties with osteoporosis and treatments was presumably not compromised.

With the newly-developed methods, six months of treatment with raloxifene and zoledronate in a model for human high-turnover osteoporosis did not affect the total amount of cracking present with indentation fracture, but did appear to affect cracking behavior. The osteoporosis model had 45% longer crack length than healthy ewes, indicating that the cortical tissue was less able to withstand crack growth once microcracking was initiated. These ewes also had reduced aligned collagen content, and collagen fiber bridging is a known toughening mechanism in bone that acts to prevent crack elongation [37]. Raloxifene treatment restored aligned collagen content to controls levels and concomitantly reduced the mean crack length due to indentation fracture. In contrast to raloxifene, zoledronate did not alter cracking behavior relative to the osteoporosis model. Irrespective of treatment, interstitial cortical tissue that was more mineralized and harder than younger osteonal tissue had an increased propensity for cracking. Interstitial tissue had greater numbers of cracks and greater crack length indicating an inferior resistance to both microcrack initiation and elongation. This difference likely reflects the greater tissue age of interstitial relative to osteonal tissue. Similar increases in tissue age and mineralization with the long-term suppression of remodeling with bisphosphonate treatment could result in tissue less able to prevent crack initiation and propagation. The methods developed here can be used in future studies to investigate the effects of treatment duration (especially with longer-term treatment) on the ability of bone tissue to resist microcracking.

5.4 Conclusions and Further Study

Based on the results from this thesis and evidence from previous studies, raloxifene normalizes bone tissue material properties to levels similar to those found in healthy animals. Here, raloxifene reversed degradations of tissue nanomechanical properties in cancellous and cortical tissue with a model for high-turnover osteoporosis and reversed the change in cortical

tissue's resistance to microcrack elongation. Raman compositional parameters and aligned collagen content with raloxifene treatment were also similar to those present in healthy ewes, with the exception of B-type carbonate substitution. Differences in collagen crosslinking are present with bisphosphonates but not raloxifene relative to healthy animals [30]. Additionally, raloxifene normalized collagen crosslinks and restored toughness in cortical bone from a rabbit model with increased crosslinking from elevated homocystine levels [38]. These results suggest that raloxifene could potentially be used as a combination or sequential treatment with bisphosphonates to ameliorate bisphosphonate-induced alterations in tissue properties such as collagen crosslinking and microcrack accumulation. Combination treatment with Alendronate and raloxifene previously improved femoral neck BMD more than either treatment alone, and raloxifene subsequent to Alendronate treatment preserved gains in BMD in the spine and femoral neck [39]. Thus, combining bisphosphonate and SERM treatment either together or in succession could potentially combine the best aspects of both treatments—the ability to quickly improve strength and stiffness on active bone surfaces provided by zoledronate, followed by normalization of the material properties throughout the tissue provided by raloxifene. The methods presented in the current thesis can also be applied to these combined or sequential treatments to validate these hypotheses.

A considerable limitation of the ovine studies was that the sheep were estrogen replete, unlike women with post-menopausal osteoporosis. Circulating estrogen could blunt the effects of raloxifene treatment because both estrogen and SERMs act through estrogen receptor pathways. Another limitation was that cancellous and cortical strength was not reduced with six months of the metabolic acidosis model, as in a previous study of this model [40–42]. The researchers who developed the ovine MA model have also developed a combined OVX and metabolic acidosis to produce greater reductions in turnover and BMD [42,43]. Future use of this improved model would not only ensure that ewes are sufficiently osteopenic, but would also allow study of raloxifene with estrogen deficiency.

A limitation of the indentation fracture experiments developed in this thesis was that SEM imaging allows visualizes surface cracks and does not enable analysis of sub-surface damage or cracks deflected in the longitudinal direction of the bone. Future study of longitudinally oriented samples would allow crack propagation in the longitudinal direction to be examined. In addition, indentation fracture could be performed in hydrated bone, with pre-and post- staining (calcein, xylenol orange, or some other fluorochrome) to visualize damage and microcracking below the sample surface with confocal microscopy. The two-photon imaging system used for SHG in this thesis work can visualize microcracks stained with fluorescence up to 60-100 μm below the surface. Stacks of images (z-stacks) could then be used to build a three-dimensional image of cracking from indentation fracture tests and compare the complete amount of cracking and microcrack morphology in healthy, osteoporotic, and treated tissue. The two-photon system also has the ability to image different wavelengths in different channels simultaneously, allowing co-localized images of the collagen alignment and orientation to be collected with SHG to examine direct relationships between collagen structure and microcrack formation and propagation. Combination of these techniques with vibrational spectroscopy to measure tissue composition at indentation fractured locations could allow examination of the contribution of compositional parameters to crack initiation and crack elongation.

Finally, indentation of interstitial bone tissue near cement lines could be used to examine the interactions between cracks and these features known to be crucial for crack deflection and arrest in cortical bone [44–46]. These experiments could investigate the effects of osteoporosis and treatment induced alterations on crack behavior at cement lines (arrest, deflection or propagation) and determine whether this behavior is affected by the changes in relative osteonal to interstitial moduli observed in the current thesis work. Also, combining these tests with spectroscopic compositional measurements of the cement lines, themselves, could determine the effects of cement-line composition and collagen alignment on the manner in which cracks interact with these interfaces (and the effects of antiresorptive treatment).

The size of the indentations required for the fracture tests of this thesis preclude examination of cancellous bone because insufficient tissue exists subsurface in the trabeculae to support these large indentations. Previously, bending, tension, and buckling tests have been performed on single excised trabeculae [47–50]. A similar approach paired with the aforementioned confocal imaging techniques could determine differences in microcrack resistance and morphology in cancellous tissue with osteoporosis and treatments. Bending tests of single trabeculae could also determine if the improvements in estimated bending stiffness with raloxifene and zoledronate observed in this thesis hold true experimentally.

5.5 Extended Application– Increased Fracture Risk with Diabetes Mellitus

The techniques presented in this thesis along with the proposed future techniques for three dimensional imaging of microcracking behavior in bone tissue can be used to examine compositional alterations with other pathological skeletal conditions and determine the resulting effects on tissue nanomechanical properties and microcracking resistance. A particularly interesting and clinically important direction is the study of increased fracture risk due to diabetes mellitus.

Like osteoporosis, diabetes presents an increasing health and economic burden in the United States and throughout the world [51,52]. Interestingly, fracture risk increases in patients with both type-1 (diabetes mellitus 1, DM1) and type-2 diabetes (diabetes mellitus 2, DM2), although only DM1 is associated with a decrease in BMD [51,53–55]. At least 50% of patients with DM1 are estimated to have bone loss, and 20% of patients aged 20-56 have BMD t-scores less than the -2.5 defined as osteoporotic [52]. The decrease in BMD is associated with a 1-2 fold increase in fracture risk at the spine, 1.5-2.5 increase at the hip, and 2-fold increase at the radius [52]. A meta-analysis of 5 studies with fracture data show a much higher absolute risk for fracture at the hip than would be calculated based on BMD measurements, suggesting that alterations in micro- and nanoscale tissue properties may play a factor [52]. Even more

perplexing are the increases in fracture risk with DM2 that occur despite higher or normal BMD even after correcting for increased body size due to obesity [51,53,54].

The exact mechanisms for bone fragility in diabetes are not known and may differ between DM1 and DM2. Experimental and clinical evidence suggest that diabetes-associated bone abnormalities may differ from those in senile or post-menopausal osteoporosis [52]. Both DM1 and DM2 demonstrate remodeling imbalances. DM1 predominantly decreases formation due to a reduction in insulin production (insulin has anabolic effects in bone) [51,53,54], whereas DM2 both increases resorption and decreases formation [51,53,54]. These remodeling imbalances and effects of hyperglycemia in both DM1 and DM2 can alter tissue material properties and distributions of these properties within bone tissue that cannot be captured by BMD measurements and may explain the discrepancies between variations in BMD and fracture risk. Hyperglycemia can affect the skeleton through a variety of mechanisms and so far has been shown to increase the formation of advanced glycation end-products (through non-enzymatic glycation), resulting in increased detrimental collagen crosslinks in bone [52,56].

To date, few studies have examined tissue-level alterations with diabetes, and have focused on non-spatially specific changes in the levels AGEs and resulting collagen crosslinks [52,53,56]. A single study has examined alterations in tissue nanomechanical properties with DM1, yet no study has directly examined effects of changes in tissue mineral and matrix composition with diabetes on the tissue-level nanomechanical function or crack resistance of bone tissue [57]. In the osteoporosis literature, AGE accumulation with bisphosphonate treatment was associated with decreased post-yield work to fracture and increased microdamage in beagles [28]. Like bisphosphonates, low turnover sites with DM2 are particularly prone to AGE and microdamage accumulation [52]. Indeed, diabetic patients with fracture exhibit increased levels of pentosidine crosslinks.

The techniques presented in this thesis along with the proposed future techniques for three dimensional imaging of microcrack behavior in cortical and cancellous bone can be used to

document spatially-specific compositional alterations with DM1 and DM2 and the resulting effects on tissue nanomechanical properties and microcracking resistance. Combining these studies with examination of diabetic bone at higher length scales (bulk and whole bone architecture and mechanical performance) can determine the mechanisms of skeletal fragility with diabetes. As diabetes is a complex disorder, rodent models can first be used to determine the effects of individual components such as insulin resistance, hyperglycemia, diabetic complications (kidney disease, renal failure), etc., individually, on bone material properties and mechanical behavior [52,53,58,59]. Subsequently, studies using larger animal models such as the New Zealand white rabbit or keeshond dog for DM1, and the streptozotocin-treated pig for DM2, can be utilized to determine the spatial variations of tissue material properties with diabetes in animals with similar Haversian microstructures to those of human bone [59].

Finally, many diabetic drug treatments have direct effects on bone and may impact fracture resistance. The thiazolidinediones (TZDs) decrease osteoblast differentiation and are associated with bone loss and a higher risk for fracture, particularly in females [52]. The skeletal effects of other classes of drugs are less documented, although patients treated with metformin or sulfonylurea may have reduced fracture risk due to positive effects on osteoblast differentiation and activity [52]. Similar to the aims for this thesis, determining the relationships between tissue material properties, microcracking resistance, and mechanical performance at higher length scales with diabetes and treatments will enable a better understanding of normal and pathological bone function with this disease and may support the development of new and improved therapies for prevention and treatment.

BIBLIOGRAPHY

[1] Akkus O, Adar F, Schaffler MB. Age-related changes in physicochemical properties of mineral crystals are related to impaired mechanical function of cortical bone. Bone 2004;34:443 - 453.

[2] Gupta HS, Stachewicz U, Wagermaier W. Mechanical modulation at the lamellar level in osteonal bone. Scanning Electron Microscopy 2006;12:1913-1921.

[3] Rho JY, Roy ME, Tsui TY, Pharr GM. Elastic properties of microstructural components of human bone tissue as measured by nanoindentation. Journal of Biomedical Materials Research 1999;45:48-54.

[4] Rho JY, Zioupos P, Currey JD, Pharr GM. Microstructural elasticity and regional heterogeneity in human femoral bone of various ages examined by nano-indentation. Journal of Biomechanics 2002;35:189-198.

[5] Donnelly E, Chen DX, Boskey AL, Baker SP, van der Meulen MCH. Contribution of mineral to bone structural behavior and tissue mechanical properties. Calcified Tissue International 2010;87:450-460.

[6] Miller LM, Little W, Schirmer A, Sheik F, Busa B, Judex S. Accretion of Bone Quantity and Quality in the Developing Mouse Skeleton. Journal of Bone and Mineral Research 2007;22.

[7] Tarnowski CP, Ignelzi MA, Morris MD. Mineralization of developing mouse calvaria as revealed by Raman microspectroscopy. Journal of Bone and Mineral Research 2002;17:1118-26.

[8] Busa B, Miller LM, Rubin CT, Qin Y-X, Judex S. Rapid establishment of chemical and mechanical properties during lamellar bone formation. Calcified Tissue International 2005;77:386-94.

[9] Havill LM, Mahaney MC, Czerwinski SA, Carey KD, Rice K, Rogers J. Bone mineral density reference standards in adult baboons (Papio hamadryas) by sex and age. Bone 2003;33:877-888.

[10] Havill LM, Levine SM, Newman DE, Mahaney MC. Osteopenia and osteoporosis in adult baboons (Papio hamadryas). Journal of Medical Primatology 2008;37:146-153.

[11] Bellino FL. Nonhuman Primate Models of Menopause Workshop. Biology of Reproduction 2002;68:10-18.

[12] Martin L., Carey K., Comuzzie A. Variation in menstrual cycle length and cessation of menstruation in captive raised baboons. Mechanisms of Ageing and Development 2003;124:865-871.

[13] Wang X, Shen X, Li X, Agrawal CM. Age-related changes in the collagen network and toughness of bone. Bone 2002;31:1-7.

[14] Wang X, Puram S. The Toughness of Cortical Bone and Its Relationship with Age. Annals of Biomedical Engineering 2004;32:123-135.

[15] Drake MT, Clarke BL, Khosla S. Bisphosphonates: mechanism of action and role in clinical practice. Mayo Clinic Proceedings 2008;83:1032-45.

[16] Roelofs AJ, Thompson K, Gordon S, Rogers MJ. Molecular mechanisms of action of bisphosphonates: current status. Clinical Cancer Research 2006;12:6222s-6230s.

[17] Roelofs AJ, Thompson K, Ebetino FH, Rogers MJ, Coxon FP. Bisphosphonates : Molecular Mechanisms of Action and Effects on Bone Cells , Mono- cytes and Macrophages. Current Pharmaceutical Design 2010;16:2950-2960.

[18] Reszka AA, Rodan GA. Mechanism of action of bisphosphonates. Current Osteoporosis Reports 2003;1:45-52.

[19] Reszka AA, Rodan GA. Nitrogen-containing bisphosphonate mechanism of action. Mini Reviews in Medicinal Chemistry 2004;4:711-9.

[20] Rogers MJ, Crockett JC, Coxon FP, Mönkkönen J. Biochemical and molecular mechanisms of action of bisphosphonates. Bone 2010;49:34-41.

[21] Allen MR, Iwata K, Sato M, Burr DB. Raloxifene enhances vertebral mechanical properties independent of bone density. Bone 2006;39:1130-5.

[22] Allen MR, Burr DB. Changes in vertebral strength-density and energy absorption-density relationships following bisphosphonate treatment in beagle dogs. Osteoporosis International 2008;19:95-9.

[23] Allen MR, Iwata K, Phipps R, Burr DB. Alterations in canine vertebral bone turnover, microdamage accumulation, and biomechanical properties following 1-year treatment with clinical treatment doses of risedronate or alendronate. Bone 2006;39:872-9.

[24] Wenzel TE, Schaffler MB, Fyhrie DP. In vivo trabecular microcracks in human vertebral bone. Bone 1996;19:89-95.

[25] Chapurlat RD, Arlot M, Burt-pichat B, Chavassieux P, Roux JP, Portero-muzy N, et al. Microcrack Frequency and Bone Remodeling in Postmenopausal Osteoporotic Women on

Long-Term Bisphosphonates: A Bone Biopsy Study. Journal of Bone and Mineral Research 2007;22:1502-1509.

[26] Cremers S, Papapoulos S. Pharmacology of bisphosphonates. Bone 2011;49:42-49.

[27] Weiss HM, Pfaar U, Schweitzer A, Wiegand H, Skerjanec A, Schran H. Biodistribution and Plasma Protein Binding of Zoledronic Acid. Drug Metabolism and Disposition 2008;36:2043-2049.

[28] Tang SY, Allen MR, Phipps R, Burr DB, Vashishth D. Changes in non-enzymatic glycation and its association with altered mechanical properties following 1-year treatment with risedronate or alendronate. Osteoporosis International 2009;20:887-94.

[29] Gourion-Arsiquaud S, Allen MR, Burr DB, Vashishth D, Tang SY, Boskey AL. Bisphosphonate treatment modifies canine bone mineral and matrix properties and their heterogeneity. Bone 2010;46:666-672.

[30] Allen MR, Gineyts E, Leeming DJ, Burr DB, Delmas PD. Bisphosphonates alter trabecular bone collagen cross-linking and isomerization in beagle dog vertebra. Osteoporosis International 2008;19:329-337.

[31] Allen MR, Reinwald S, Burr DB. Alendronate reduces bone toughness of ribs without significantly increasing microdamage accumulation in dogs following 3 years of daily treatment. Calcified Tissue International 2008;82:354-60.

[32] Gallacher SJ, Dixon T. Impact of treatments for postmenopausal osteoporosis (bisphosphonates, parathyroid hormone, strontium ranelate, and denosumab) on bone quality: a systematic review. Calcified Tissue International 2010;87:469-84.

[33] Mullins LP, Bruzzi MS, McHugh PE. Measurement of the microstructural fracture toughness of cortical bone using indentation fracture. Journal of Biomechanics 2007;40:3285-8.

[34] Bushby A, Ferguson V, Boyde A. Nanoindentation of bone: comparison of specimens tested in liquid and embedded in polymethylmethacrylate. Journal of Materials Research 2004;19:249-259.

[35] Hengsberger S, Kulik A, Zysset P. Nanoindentation discriminates the elastic properties of individual human bone lamellae under dry and physiological conditions. Bone 2002;30.

[36] Rho J, Pharr G. Effects of drying on the mechanical properties of bovine femur measured by nanoindentation. Journal of Materials Science1 1999;10:485-488.

[37] Ritchie RO. The conflicts between strength and toughness. Nature Materials 2011;10:817-22.

[38] Saito M, Marumo K, Soshi S, Kida Y, Ushiku C, Shinohara A. Raloxifene ameliorates detrimental enzymatic and nonenzymatic collagen cross-links and bone strength in rabbits with hyperhomocysteinemia. Osteoporosis International 2010;21:655-66.

[39] Pinkerton JV, Dalkin AC. Combination therapy for treatment of osteoporosis: A review. American Journal of Obstetrics and Gynecology 2007;197:559-65.

[40] MacLeay JM, Olson JD, Enns RM, Les CM, Toth CA, Wheeler DL, et al. Dietary-induced metabolic acidosis decreases bone mineral density in mature ovariectomized ewes. Calcified Tissue International 2004;75:431-437.

[41] Macleay JM, Sullivan E, Jackinsky S, Les C, Turner A. Ovine modeling of dietary induced metabolic acidosis and bone loss. International Congress Series 2007;1297:282-285.

[42] Macleay JM, Olson JD, Turner AS. Effect of dietary-induced metabolic acidosis and ovariectomy on bone mineral density and markers of bone turnover. Journal of Bone and Mineral Metabolism 2004;22:561-568.

[43] MacLeay JM, Olson JD, Enns RM, Les CM, Toth CA, Wheeler DL, et al. Dietary-induced metabolic acidosis decreases bone mineral density in mature ovariectomized ewes. Calcified Tissue International 2004;75:431-437.

[44] O'Brien FJO, Taylor D, Lee TC. The effect of bone microstructure on the initiation and growth of microcrack. Journal of Orthopaedic Research 2005;23.

[45] Mohsin S, O'Brien FJ, Lee TC. Osteonal crack barriers in ovine compact bone. Journal of Anatomy 2006;208:81-9.

[46] O'Brien FJ, Hardiman DA, Hazenberg JG, Mercy MV, Mohsin S, Taylor D, et al. The behaviour of microcracks in compact bone. European Journal of Morphology 2005;42:71-9.

[47] Busse B, Hahn M, Soltau M, Zustin J, Püschel K, Duda GN, et al. Increased calcium content and inhomogeneity of mineralization render bone toughness in osteoporosis: mineralization, morphology and biomechanics of human single trabeculae. Bone 2009;45:1034-43.

[48] Lorenzetti S, Carretta R, Müller R, Stüssi E. A new device and method for measuring the elastic modulus of single trabeculae. Medical Engineering & Physics 2011;33:993-1000.

[49] Townsend PR, Rose RM, Radin EL. Buckling studies of single human trabeculae. Journal of Biomechanics 1975;8:199-201.

[50] Szabó ME, Taylor M, Thurner PJ. Mechanical properties of single bovine trabeculae are unaffected by strain rate. Journal of Biomechanics 2011;44:962-7.

[51] Kurra S, Siris E. Diabetes and bone health : the relationship between diabetes and osteoporosis-associated fractures. Diabetes/Metabolism Research and Reviews 2011;27:430-435.

[52] Merlotti D, Gennari L, Dotta F, Lauro D, Nuti R. Mechanisms of impaired bone strength in type 1 and 2 diabetes. Nutrition, metabolism, and cardiovascular diseases : NMCD 2010;20:683-90.

[53] Vestergaard P, Rejnmark L, Mosekilde L. Diabetes and its complications and their relationship with risk of fractures in type 1 and 2 diabetes. Calcified Tissue International 2009;84:45-55.

[54] Vestergaard P. Discrepancies in bone mineral density and fracture risk in patients with type 1 and type 2 diabetes--a meta-analysis. Osteoporosis International 2007;18:427-44.

[55] Browne DL, Mccrae FC, Shaw KM. Musculoskeletal disease in diabetes. Practical Diabetes International 2001;18:62-64.

[56] Saito M, Marumo K. Collagen cross-links as a determinant of bone quality: a possible explanation for bone fragility in aging, osteoporosis, and diabetes mellitus. Osteoporosis International 2010;21:195-214.

[57] Nyman JS, Even JL, Jo C-H, Herbert EG, Murry MR, Cockrell GE, et al. Increasing duration of type 1 diabetes perturbs the strength-structure relationship and increases brittleness of bone. Bone 2011;48:733-40.

[58] von Herrath M, Nepom G. Animal models of human type 1 diabetes. Nature Immunology 2009;10.

[59] Rees DA, Alcolado JC. Animal models of diabetes mellitus. Diabetic Medicine 2005;22:359-70.

APPENDIX

ADDITIONAL OVINE CORTICAL DATA AND FIGURES

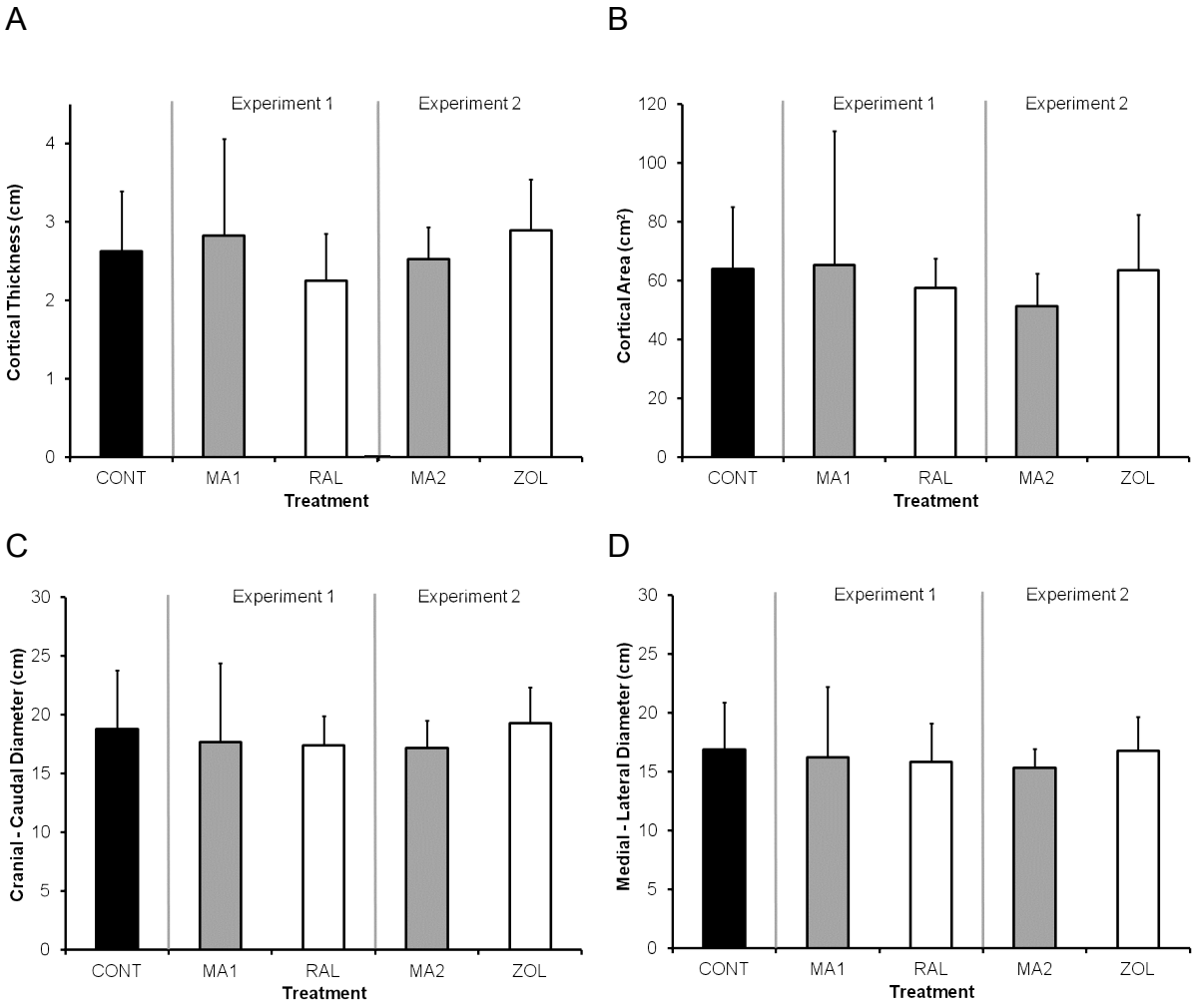

Figure A1 (A) *Cortical thickness, (B) cranial-caudal diameter, (C) medial-lateral diameter, and (D) area of mid-diaphyseal sections. No differences were found between treatment groups due to relatively large variations between sheep.*

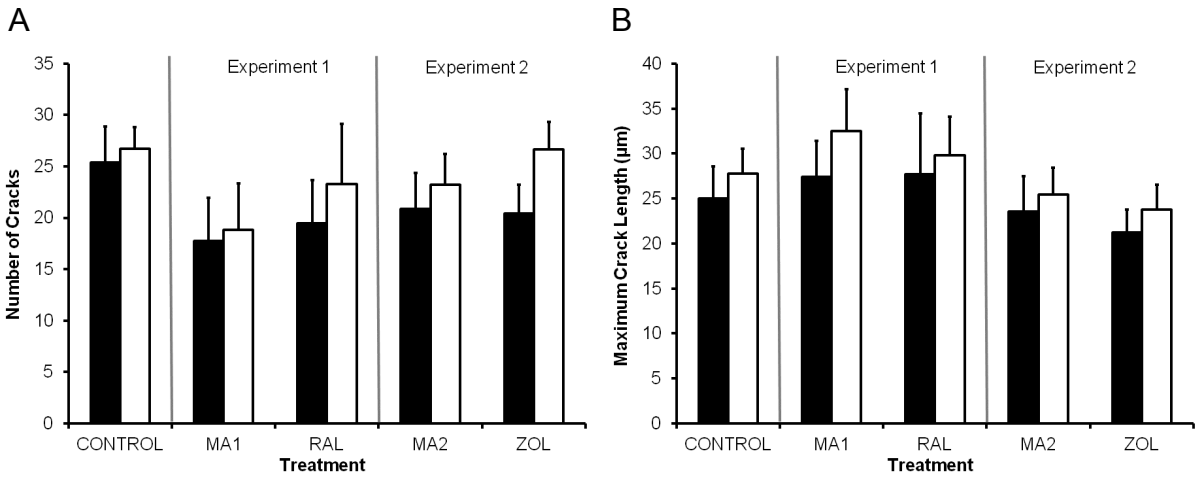

Figure A2 (A) *Number of cracks and (B) maximum crack length due to indentation fracture*

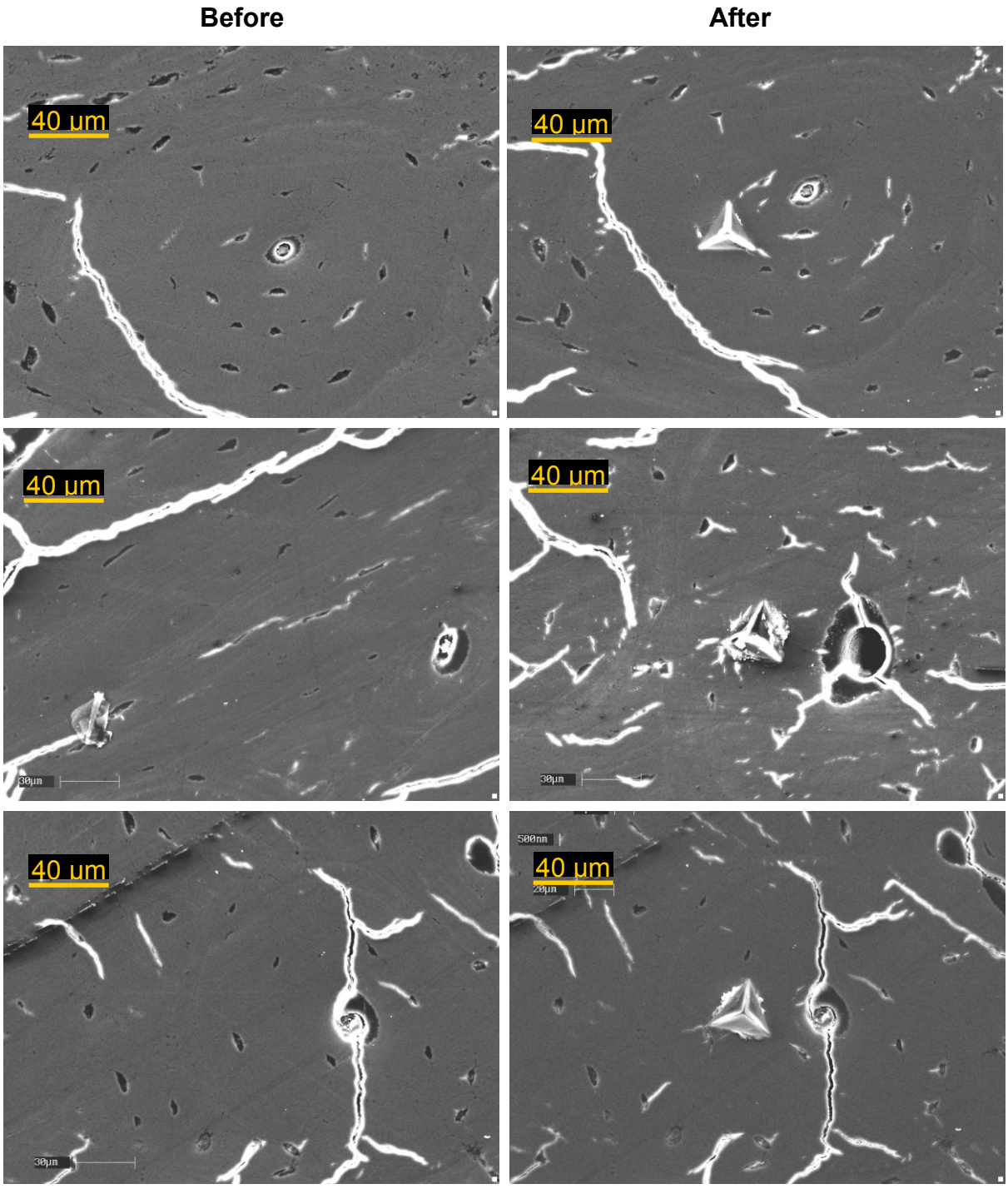

Figure A3 *Representative SEM images taken before and after indentation fracture in osteons of cortical bone from Control (normal diet) sheep.*

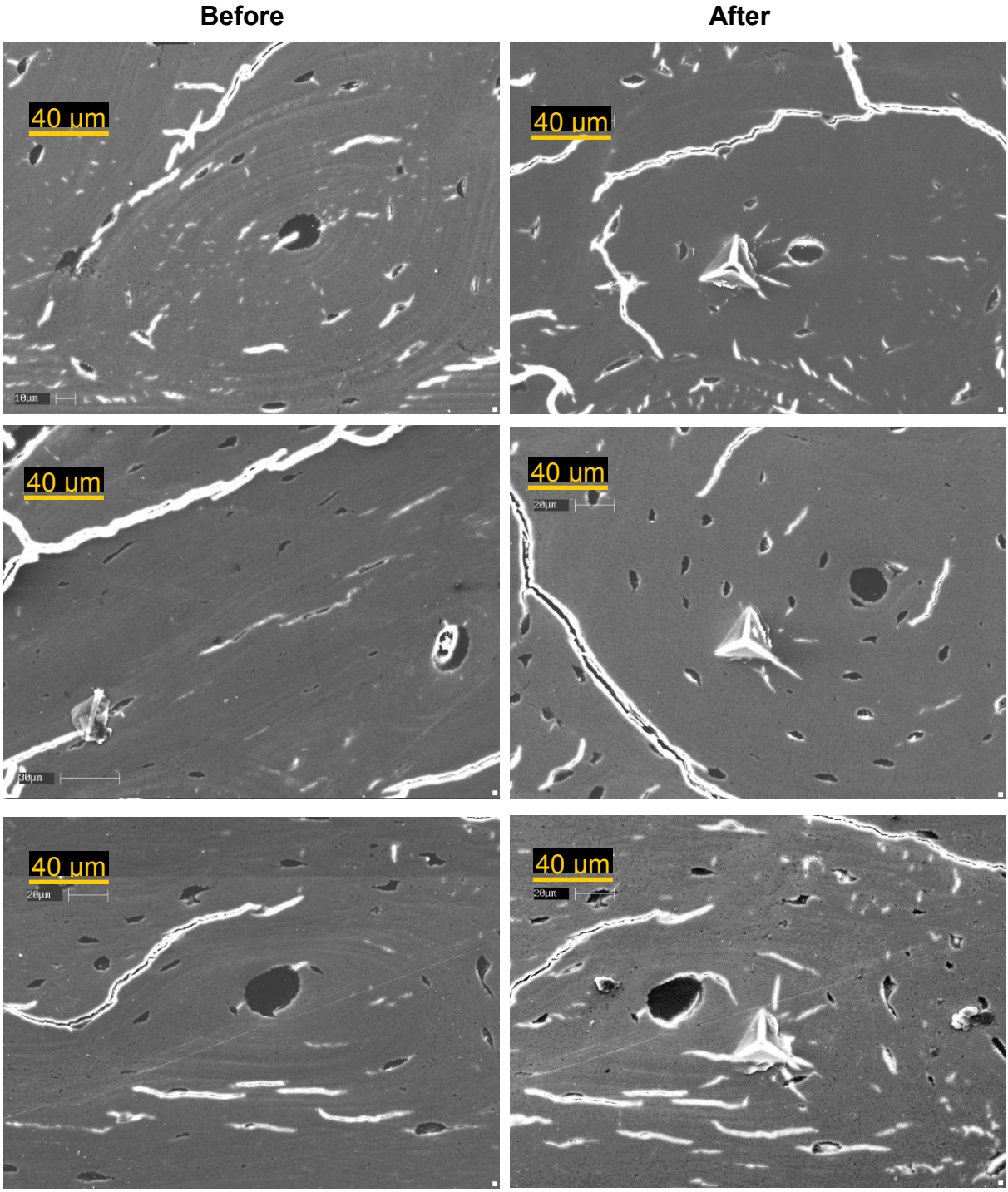

Figure A4 *Representative SEM images taken before and after indentation fracture in osteons of cortical bone from MA1 sheep.*

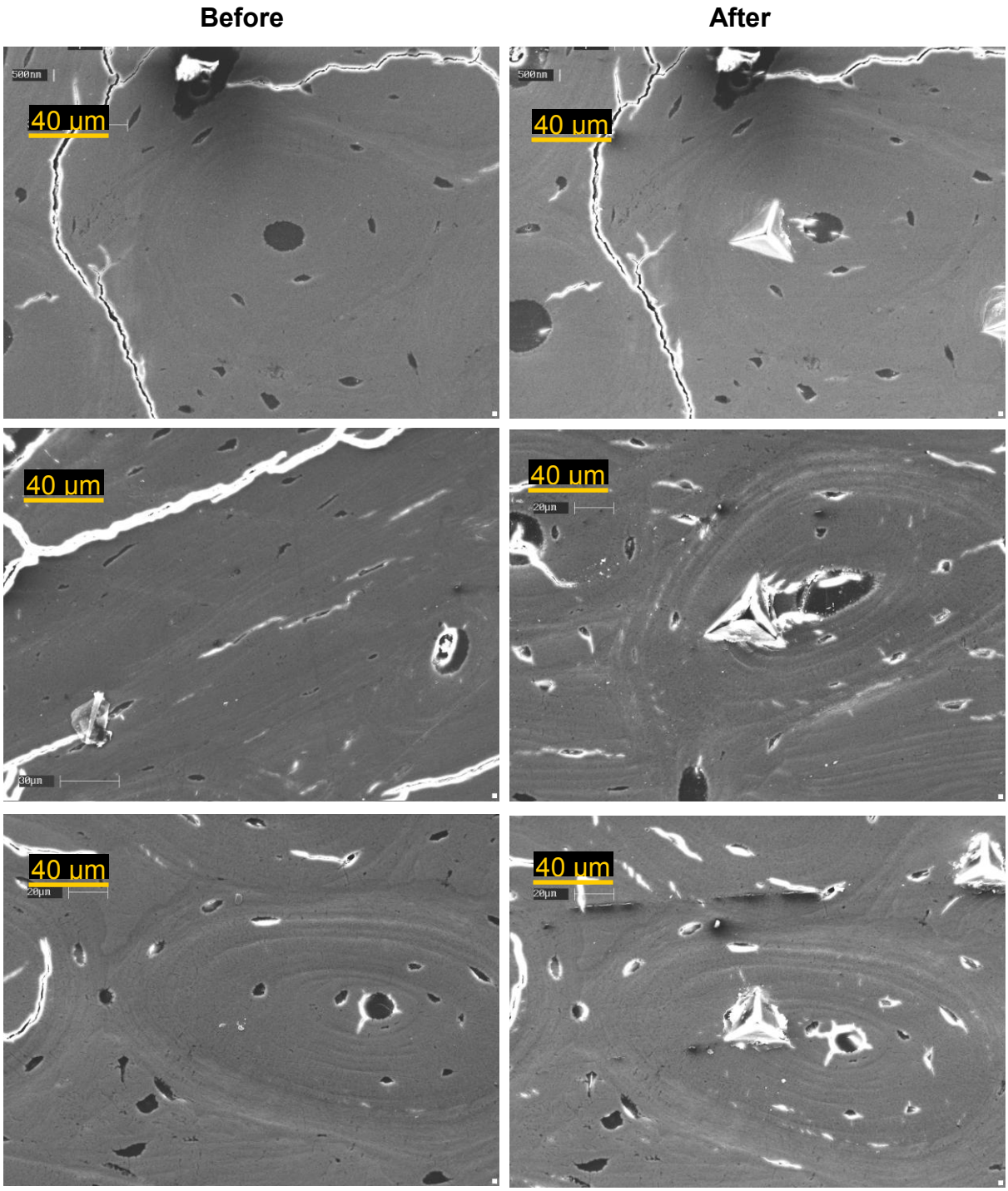

Figure A5 *Representative SEM images taken before and after indentation fracture in osteons of cortical bone from raloxifene treated sheep.*

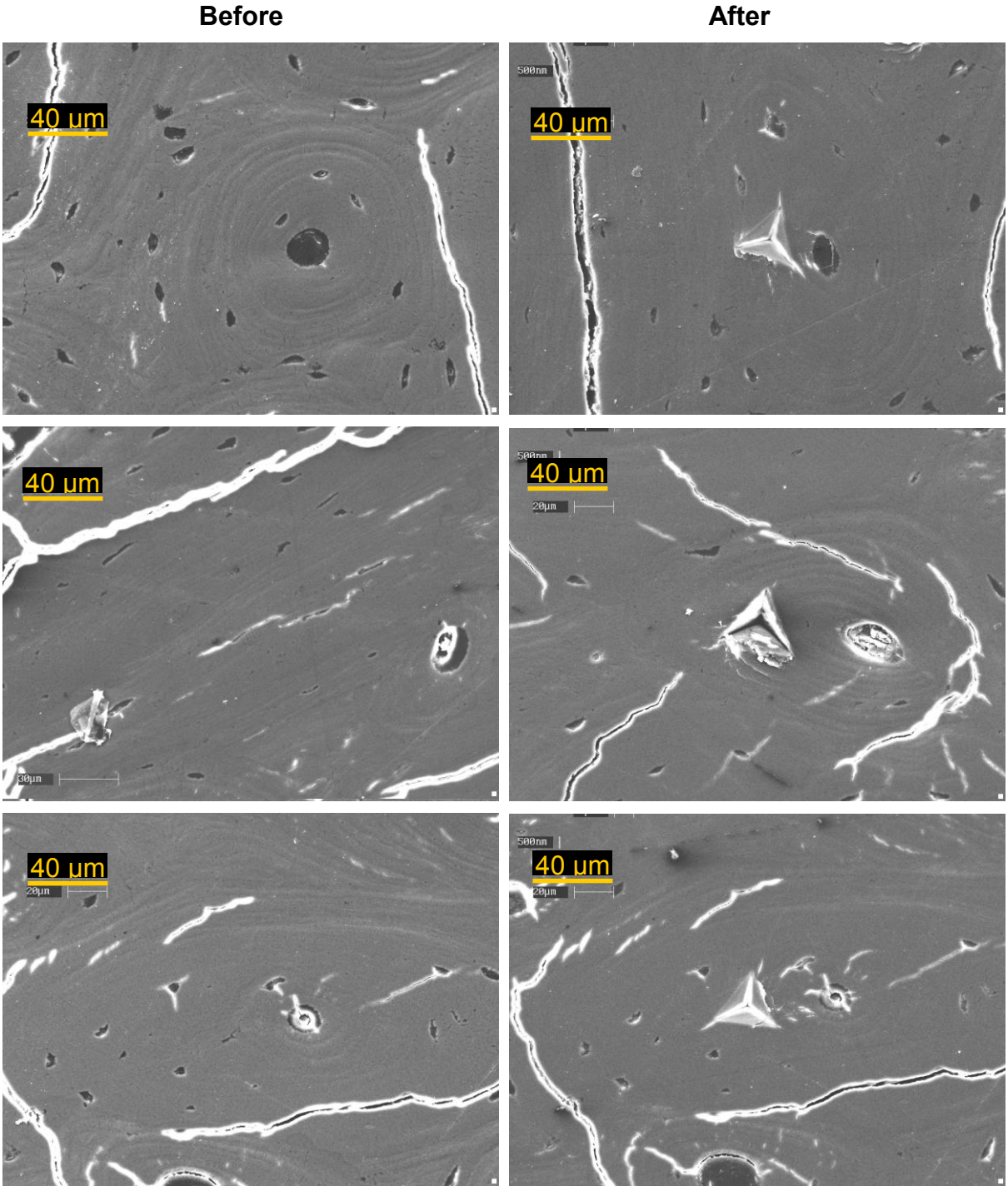

Figure A6 *Representative SEM images taken before and after indentation fracture in osteons of cortical bone from MA2 sheep.*

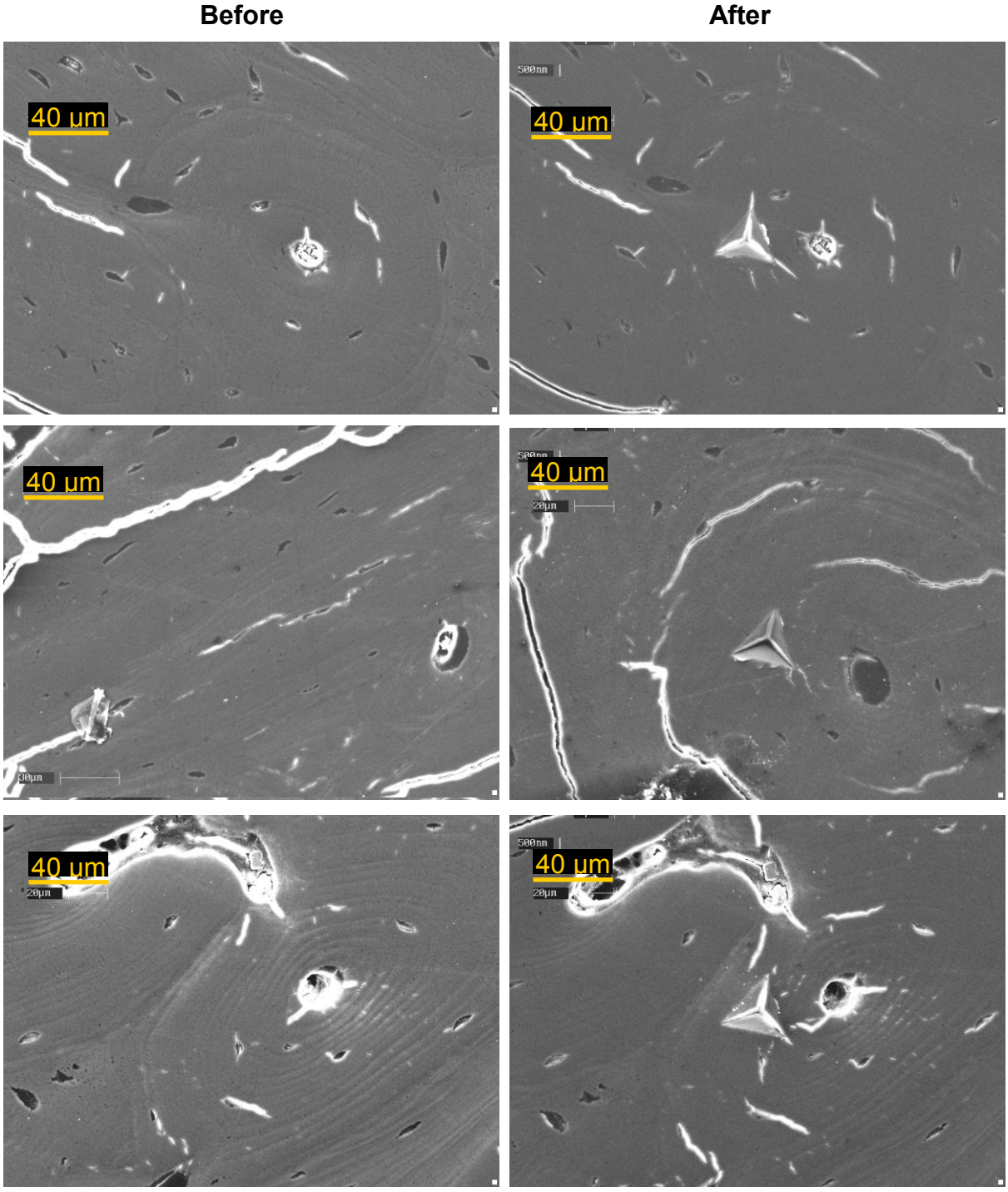

Figure A7 *Representative SEM images taken before and after indentation fracture in osteons of cortical bone from zoledronate treated sheep.*

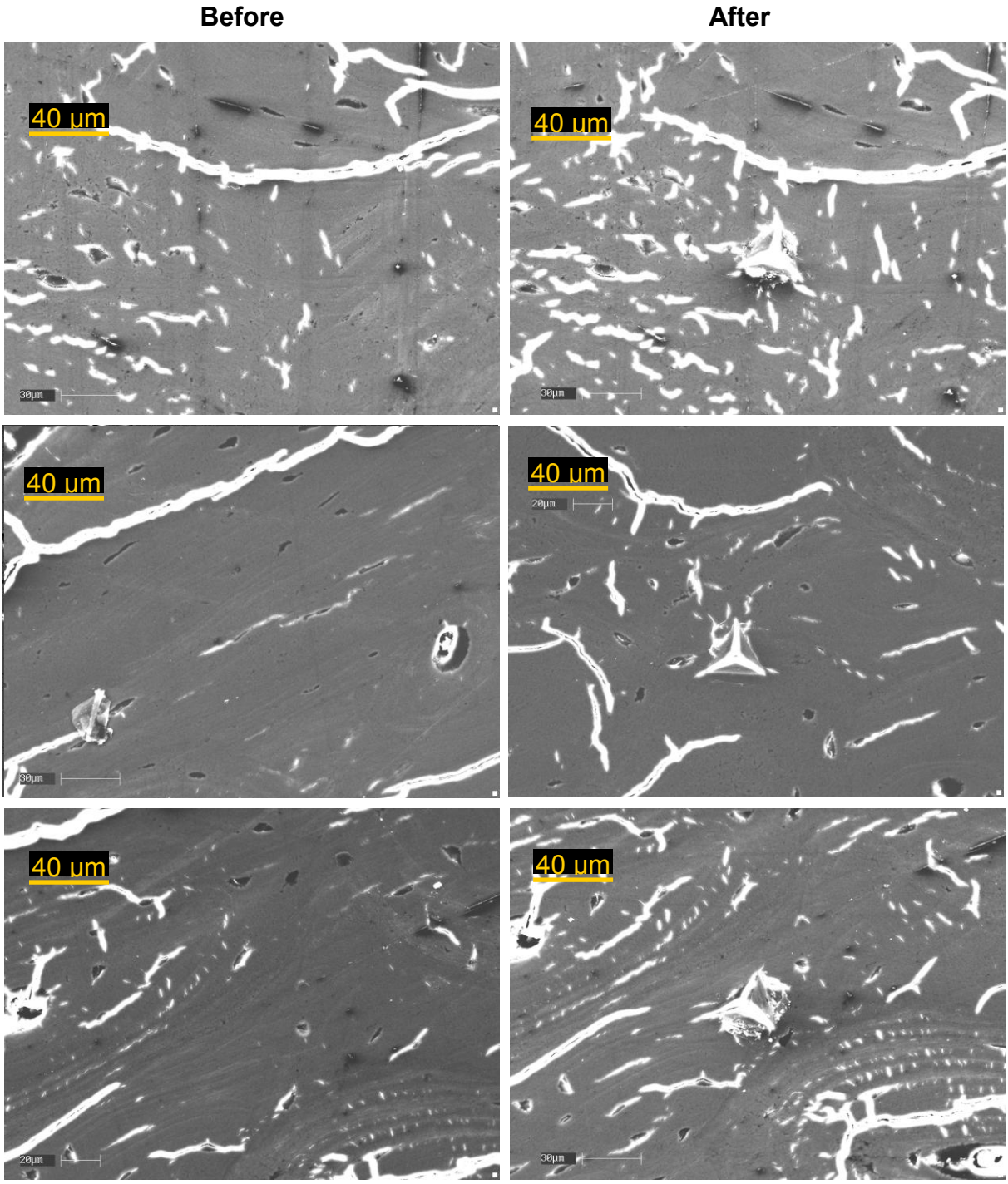

Figure A8 *Representative SEM images taken before and after indentation fracture in interstitial tissue of cortical bone from Control (normal diet) sheep.*

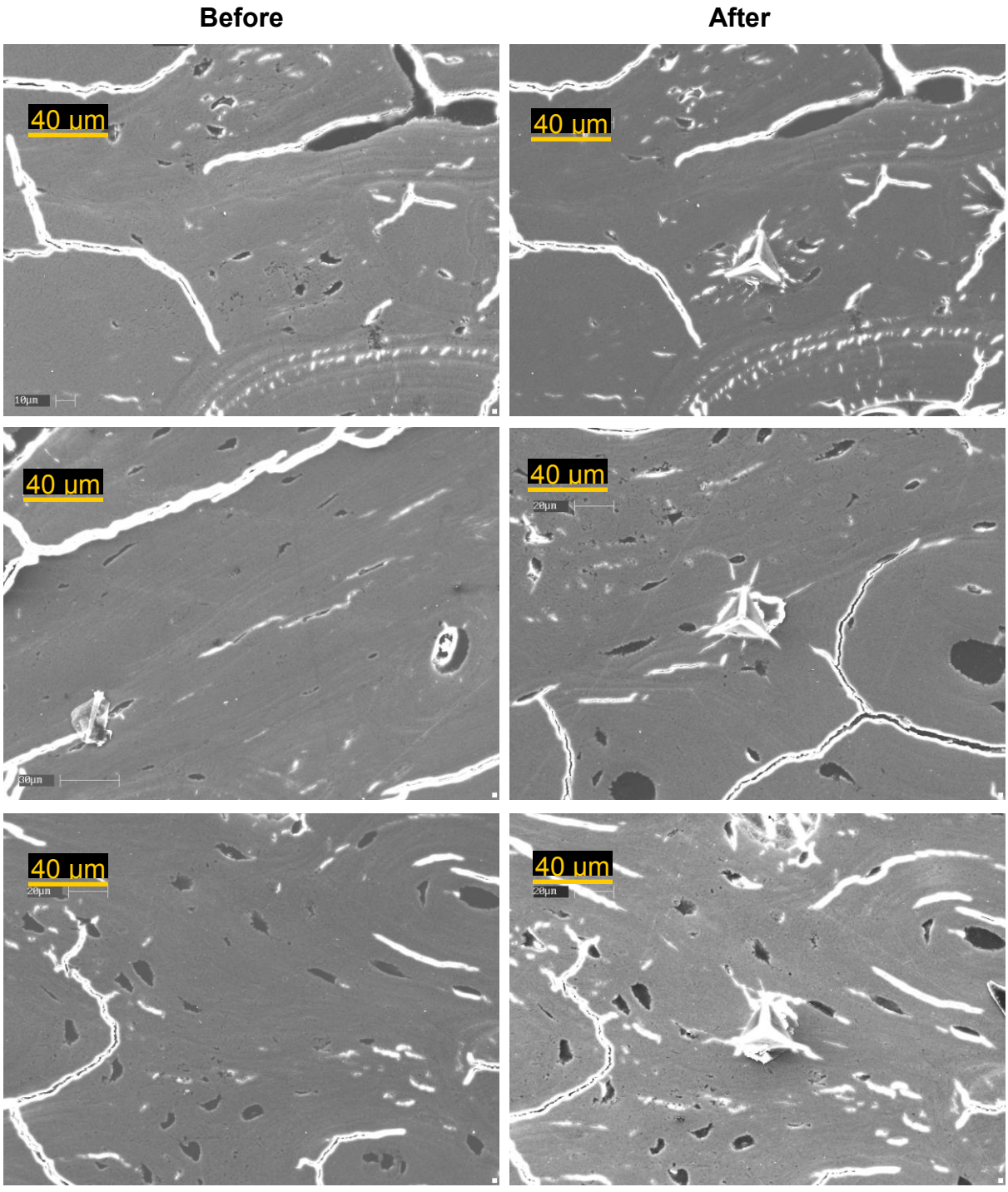

Figure A9 *Representative SEM images taken before and after indentation fracture in interstitial tissue of cortical bone from MA1 sheep.*

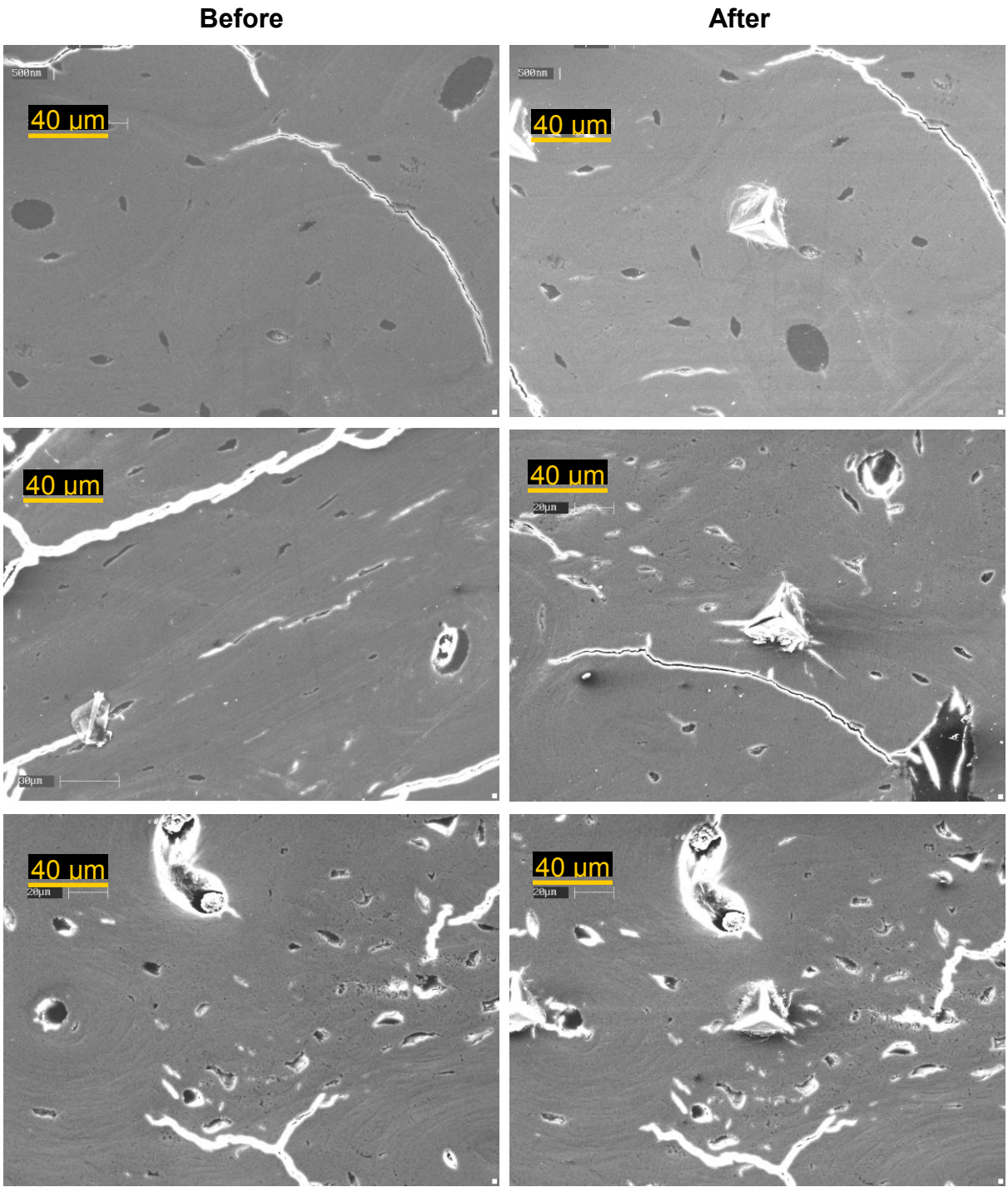

Figure A10 *Representative SEM images taken before and after indentation fracture in interstitial tissue of cortical bone from raloxifene treated sheep.*

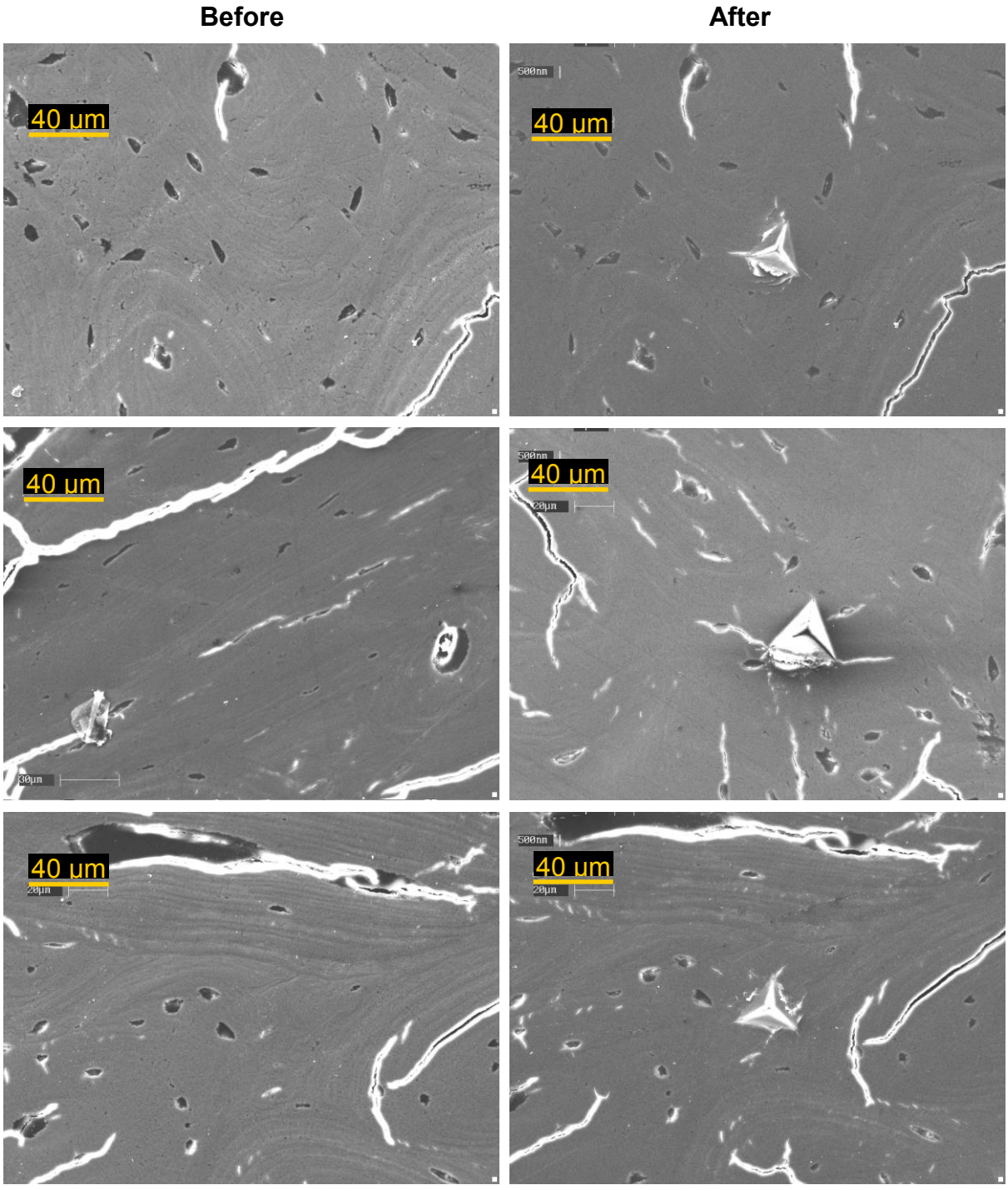

Figure A11 *Representative SEM images taken before and after indentation fracture in interstitial tissue of cortical bone from MA2 sheep.*

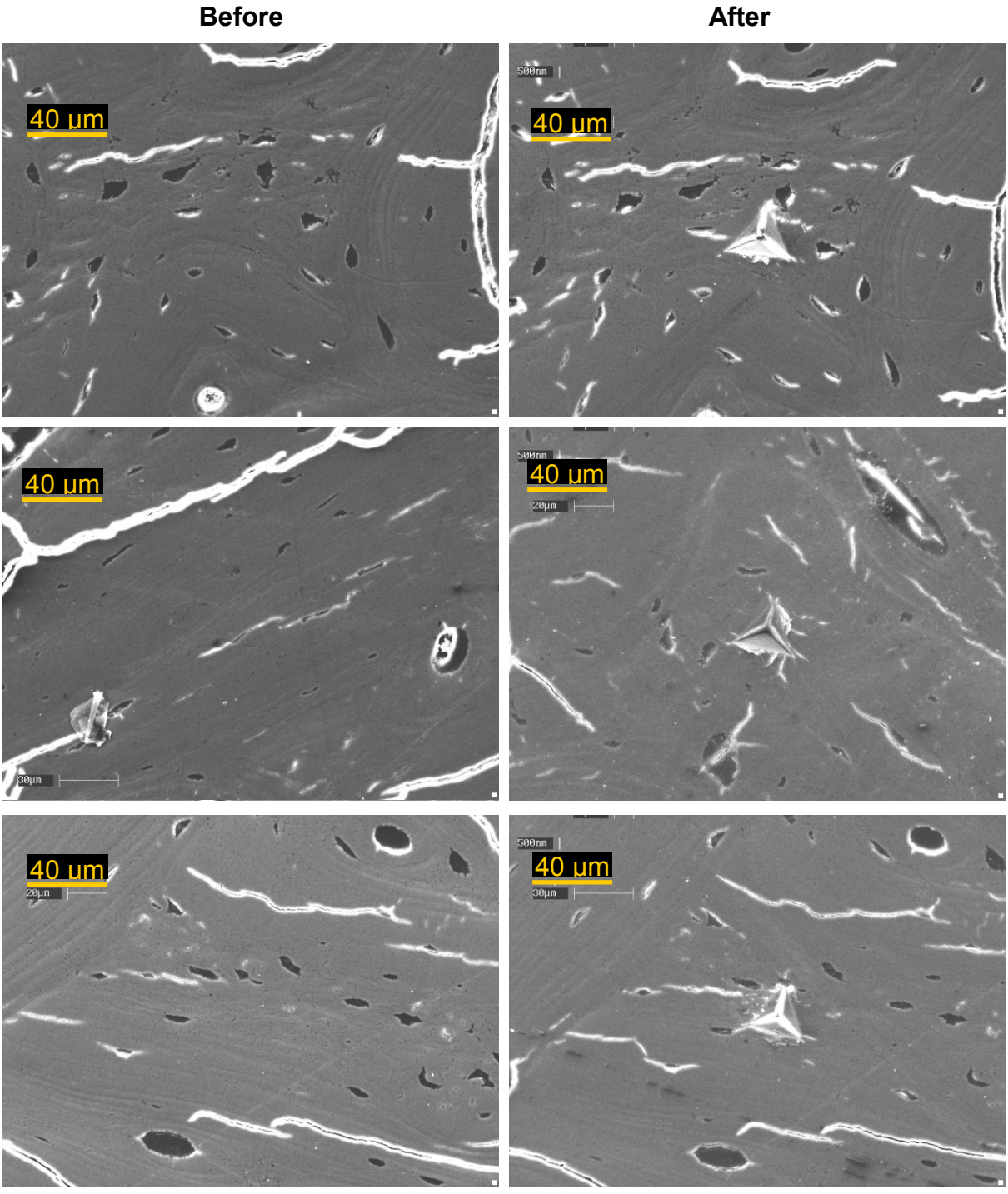

Figure A12 *Representative SEM images taken before and after indentation fracture in interstitial tissue of cortical bone from zoledronate treated sheep.*